Title

Development of Regenerable Antimicrobial and Antifouling Materials for Food Packaging and Water Disinfection Applications

Author

Ma, Yue

Publication Date

2021

Peer reviewed|Thesis/dissertation

Development of Regenerable Antimicrobial and Antifouling Materials for Food Packaging and Water Disinfection Applications

By

YUE MA

DISSERTATION

Submitted in partial satisfaction of the requirements for the degree of

DOCTOR OF PHILOSOPHY

in

Biological Systems Engineering

in the

OFFICE OF GRADUATE STUDIES

of the

UNIVERSITY OF CALIFORNIA

DAVIS

Approved:

_____

Gang Sun, Chair

_____

Nitin Nitin

_____

Juliana Maria Leite Nobrega de Moura Bell

Committee in Charge

2021

ACKNOWLEDGMENT

My deepest gratitude goes first and foremost to my advisor, Professor Gang Sun, for his unwavering patience and guidance throughout my graduate studies. He provided me with valuable suggestions and multiple choices but allowed me to express my opinions and respected my decisions, which benefited me to grow as an independent and professional researcher. There is no doubt that Prof. Sun is an awesome educator. The numerous scientific knowledge and rigorous research attitude will benefit me during the rest of my life.

I would like to express my deep and sincere gratitude to my QE committee: Profs. Nitin Nitin (Chair), Ning Pan, Zhiliang (Julia) Fan, Ameer Taha, and Charli Li, for their erudite information, insightful comments, and valuable support. Also, I appreciate Dr. Nitin Nitin and Dr. Juliana Maria Leite Nobrega de Moura Bell for serving as my dissertation committee members.

Many thanks to all my friends and labmates in Dr. Gang Sun's group, who have generously shared their valuable advice and knowledge to help my research. Peixin Tang and Zheng Zhang provided me with many constructive suggestions on organic chemical reactions and scholarly discussions about the reaction mechanisms. Cunyi Zhao, Jiahan Zou, and Huitao Ling helped me to better analyze and polish engineering models. Thank Bofeng Pan and Hunter Bolt for their friendliness and support, which are also indispensable for my research. Dr. Yang Si was a former postdoc in the group. He helped me for a smooth start of this project during the first two years of my Ph.D. Building on the expertise I learned from him, I led and participated in many projects related to antimicrobial materials. I also appreciate Julianna Perez, Lucinda Amador, and Jiaying Li, who helped me conduct and collect the experimental data as undergraduate researchers. Without their effort, I can hardly finish this dissertation with such high efficiency and qualify.

My sincere gratitude also goes to all my collaborators. In particular, I would like to gratefully acknowledge Dr. Kang Huang, Dr. Thais De Melo Ramos, Jiyoon Yi, and Nicharee Wisuthiphaet from Prof. Nitin's research group. I appreciated their willingness to help and fruitful discussions about the design of bacteria-related experiments.

Moreover, I would like to acknowledge the Biological Systems Engineering Graduate Group at University of California, Davis for providing me graduate admission fellowships and the Jastro Shields Research awards. I also appreciate the financial funding from the Center for Produce Safety and the National Institute of Food and Agriculture of United States Department of Agriculture, which supported my Ph.D. research.

Lastly, the most important person that I would like to acknowledge is my lovely family, my dady Liehua Ma and mommy Xiaoqin Ma. Thanks for all their efforts and sacrifices to ensure that I receive a good education. Thanks for the constant company with me to share all the difficult and happy times together. I would never be here without the support of my family.

Development of Regenerable Antimicrobial and Antifouling Materials for Food Packaging and Water Disinfection Applications

ABSTRACT

The frequent outbreaks of foodborne and waterborne diseases have become a serious public health issue, which is related to the presence of microbial biofilms on surfaces of materials. Current research activities aiming at reducing or eliminating the biofilm formation could be mainly divided into two major approaches: an active approach of "attacking", by killing the microbes once they are attached to the material surface; and a passive approach of "defending", creating resistance to microbial attachment or releasing the attached one. In this dissertation, a dual-functional structure was initially proposed: rechargeable biocidal moieties immobilized at the inner layer, and antifouling moieties serving as a protective layer located on the outside of the surface. With a such unique surface structure, once microorganisms approach the designed surfaces, (i) the antifouling moieties could reduce the non-specific adsorption of the microorganisms and make them difficult to adhere; (ii) any live bacteria attached on the surface could be immediately killed by the incorporated biocidal moieties; (iii) any resulting cell debris and other biofoulants could be easily washed off with mild hydrodynamic force applied; furthermore, (iv) the consumed biocidal activity could be regenerated by either chlorination or photoirradiation. Overall, I designed and successfully developed three types of rechargeable biocidal and antifouling functional materials, which exhibited great potentials in food packaging, water filtration, and medical application areas.

Specifically, in this dissertation, chapter 1 briefly introduces processes and mechanisms of microbial biofilm formation, two major strategies responding to avoid and reduce the formation of biofilm, and typical chemicals with rechargeable biocidal or antifouling functions applied in recent years.

In chapter 2, a new antibiofilm concept combining both rechargeable antimicrobial and antifouling functions was proposed. An N-halamine precursor, N,N-diallylmelamine (DAM), and a zwitterionic monomer, [2-(methacryloyloxy)ethyl]dimethyl-(3-sulfopropyl)ammonium hydroxide (SBMA), were covalently bonded onto poly(vinyl alcohol-co-ethylene) (PVA-co-PE) and generated a double-layer structure. The outside surface embedding with resisting and releasing functions and the inner layer with regenerable biocidal activities work constructively to limit the biofilm development.

In chapter 3, a new synthesized zwitterionic polymer, sulfonated polyethyleneimine (PEI-S), was chemically bonded with an N-halamine grafted PVA-co-PE nanofibrous membrane. The obtained PEI-S@BNF nanofibrous membrane with the super-high specific surface area did effectively magnify the interfacial effect. Two engineering models were constructed to explain the resisting and releasing mechanisms via typical isothermal adsorption and release experiments. Additionally, the final product, PEI-S@BNF nanofibrous membrane, showed great potential to be applied as a water filtration material.

In chapter 4, instead of N-halamine, a photo-induced biocide, benzophenonetetracarboxylic dianhydride (BPTCD) was incorporated onto the PVA-co-PE nanofibrous membranes, providing a photo-driven regenerable biocidal function. After combined with antifouling moieties, the obtained SBMA@EVOH also exhibited a desirable antibiofilm effect, which proved the universality of such proposed bifunctional antibiofilm strategy.

In chapter 5, a N-halamine-based chlorine rechargeable antimicrobial composite fabric (HCF) was fabricated via an industrial scalable dip-coating method. An imide/amide halamine grafted cotton fabric (DMH-g-cotton) served as a reinforcement component and a reservoir of active chlorine. And an amine halamine polymer (PVA-co-PE-g-DAM) as a coating component could reduce the

loss of active chlorine, realizing long-term killing performance. With such a unique combination, the designed HCF could be considered as a potential active food-contact material that could effectively reduce microbial cross-contamination, prolong the food lifetime, decrease food spoilage, and ensure food safety.

The final chapter describes all achievements related to the proposed multifunctional double-layer surface structure, which could significantly reduce the biofouling effect via resisting, killing, and releasing pathways, and a practical demonstration of biocidal functional composite fabric applied as a food-contact material.

List of Figures

and SBMA@HAF films, (g) DSC curves and (h) TGA curves of HAF, HAF+BPTCD, and SBMA@HAF films, and (i) Tensile stress-strain curves of HAF, HAF+BPTCD, and SBMA@HAF films.

Figure 2.3 Active chlorine contents of SBMA@HAF films and HAF films as a function of (a) chlorination time and (b) pH condition of chlorination solutions. (c) The change of active chlorine content against storage time. (d) The active chlorine content of SBMA@HAF films and HAF films with 10 times of chlorination-quenching cycle tests.

Figure 2.4 Antimicrobial activities of control films (unchlorinated SBMA@HAF films), chlorinated HAF and SBMA@HAF films against: (a) *E. coli* and (d) *L. innocua*, respectively. The right images exhibit viable bacteria on agar plates after 15-min exposure. Three repeated chlorination-decontamination tests of chlorinated SBMA@HAF films against: (b) *E. coli* and (e) *L. innocua,* FE-SEM images of (c) *E. coli* and (f) *L. innocua* before and after exposing to control films and chlorinated SBMA@HAF films for15 mins.

Figure 2.5 (a) FE-SEM images of HAF (left) and SBMA@HAF (right) films. FE-SEM images of unchlorinated HAF (left) and SBMA@HAF (right) films after incubating with (b) *E. coli* and (c) *L. innocua* suspensions, respectively; SG stained fluorescence microscopy images of unchlorinated HAF (left) and SBMA@HAF (right) film surfaces after incubating with (d) *E. coli* and (e) *L. innocua* suspensions, respectively. (f) Bacterial cell density of *E. coli* and *L. innocua* attached on the unchlorinated surfaces after incubating with bacteria suspensions for 24 h (resisting).

Figure 2.6 Releasing behavior of unchlorinated HAF and SBMA@HAF films against (a) *E. coli* and (e) *L. innocua* via the plate-counting method. The insert images exhibit the plate-counting

results 15 min after releasing. (b) FE-SEM images and (d) SG-stained fluorescence microscopy images of *E. coli* 15 min before and after releasing on unchlorinated HAF and SBMA@HAF films. (f) FE-SEM images and (h) SG-stained fluorescence microscopy images of *L. innocua* 15 min before and after releasing on unchlorinated HAF and SBMA@HAF films. Bacterial cell density of (c) *E. coli* and (g) *L. innocua* on the unchlorinated surfaces before and after releasing procedure.

Figure 3.1 (a) Sulfonation reaction of the PEI. (b) FT-IR spectra and (d) TGA curves of PEI and PEI-S. (c) EDX spectrum and elemental compositions of the PEI-S.

Figure 3.2 (a) Scheme of the manufacturing process, rechargeable biocidal, and antifouling performances of as-prepared PEI-S@BNF membrane. (b) SEM images, (e) water contact angle (WCA), (f) DSC spectra (insert of calculated non-freezable water ratio) of PEI-S@BNF membranes after 0h, 0.5h, 1h, 2h, 4h, and 24 h of GA crosslinking. (c) FT-IR spectra of PEI-S, BNF, and PEI-S@BNF-2h, (d) SEM-EDX results of PEI-S@BNF-2h membranes.

Figure 3.3 (a-e) Fiber diameter distributions of BNF, PEI-S@BNF-0.5 h, -1h, -2 h, -4 h, respectively. (f) FT-IR spectra and (g) TGA curves of the PEI-S@BNFs with a temperature range of 100-550□. (h) Tensile stress-strain curves of the BNF, BNF-Cl, PEI-S@BNF-2h, and PEI-S@BNF-2h-Cl membranes.

Figure 3.4 Active chlorine contents of PEI-S@BNF-xh as a function of (a) chlorination time, (b) pH of chlorination solutions, and (c) storage time. (d) Active chlorine contents of PEI-S@BNF-2h membranes with 7 chlorine charging-quenching cycle tests. Time-dependent biocidal activities of the control membrane and the chlorinated PEI-S@BNF-2h membranes against *E. coli* and *L. innocua* with a COD condition of (e) 0 and (f) 1000 mg L^{-1}, respectively. Biocidal activity of chlorinated PEI-S@BNF-2h versus (g) storage time and (h) chlorine charging-quenching cycles

(COD = 0 mg L^{-1}). SEM images of (i, j) *E. coli* and (k, l) *L. innocua* after exposing to (i, k) the control and (j, l) the chlorinated PEI-S@BNF-2h membrane, respectively.

Figure 3.5 (a) Kinetic and (b) isotherm BSA adsorption profiles of the unchlorinated BNF and the unchlorinated PEI-S@BNF-2h membrane at room temperature. Widefield bioluminescence images of the unchlorinated BNF and the unchlorinated PEI-S@BNF-2h tested by (c) touch-assay and (d) incubate assay, respectively. SEM images of (e, f) the unchlorinated BNF and (j, h) the unchlorinated PEI-S@BNF membranes after incubating with *E. coli* suspension for 24 h.

Figure 3.6 The linear fittings of isothermal adsorption kinetics of BSA protein by pseudo 1^{st} order and Pseudo 2^{nd} order kinetic models on (a) BNF and (b) PEI-S@BNF-2h. The linear fittings of BSA adsorption isotherms by Langmuir model and Freundlich model on (d) BNF and (e) PEI-S@BNF-2h. Tables of (c) adsorption kinetic parameters and (f) adsorption isotherm parameters.

Figure 3.7 (a) Schematic illustration of the loaded BSA distribution on the membrane divided into three areas. Cumulative BSA releasing rates of the unchlorinated BNF and the unchlorinated PEI-S@BNF-2h with (b) t_0 = 0 min and (c) t_0 = 3 min, respectively. (d) Time-dependent microbial releasing performance of the unchlorinated BNF and the unchlorinated PEI-S@BNF-2h assessed by a plate counting method. (e) Widefield bioluminescence images and (f) SEM images of the unchlorinated PEI-S@BNF-2h (i, ii) before and (v, vi) after 30 min of release, and the unchlorinated BNF (iii, iv) after 30 min of release.

Figure 3.8 The BSA protein release profiles at (a) stage I and (b) stage □ and □ fitting by the Ritger-Peppas model. (c) Table of n values.

Figure 4.5 Antimicrobial activity against *E. coli* of relevant NFMs under (a) UVA irradiation and (c) dark condition after 2-hours UVA irradiation. Five cycles of antimicrobial tests of BPTCD EVOH and SBMA@EVOH NFMs under (b) UVA irradiation (1h contact time) and UVA (2h) charged NFMs under (d) dark condition (2h contact time). Field emission scanning electron microscopy (FE-SEM) images of (e) SBMA@EVOH NFMs after antimicrobial test, *E. coli* after exposure to (f) EVOH, (g) BPTCD EVOH, and (h) SBMA@EVOH NFMs under UVA condition for 1 hour.

Figure 4.6 Changes of BSA protein adsorption capacities of relevant NFMs as a function of (a) adsorption time, and (b) initial BSA concentration at room temperature, respectively. (c) SG-stained fluorescence widefield microscopy images and (d) FE-SEM images uncharged BPTCD EVOH (i and ii), and uncharged SBMA@EVOH (v and vi) NFMs after incubating with *E. coli* suspension under dark condition.

Figure 4.7 The linear fitting of isothermal adsorption kinetics of BSA protein by pseudo-1st-order and Pseudo-2nd-order kinetic models on (a) EVOH, (b) BPTCD EVOH, and (c) SBMA@EVOH NFMs (C_0 = 2 mg/mL). (d) Table of adsorption kinetic parameters.

Figure 4.8 The nonlinear fitting of BSA adsorption isotherms by Langmuir model and Freundlich model on (a) EVOH, (b) BPTCD EVOH, and (c) SBMA@EVOH NFMs, respectively. (d) Table of adsorption isotherm parameters.

Figure 4.9 (a) Releasing behavior of uncharged EVOH, BPTCD EVOH, and SBMA@EVOH NFMs against *E. coli* under dark condition via the plate-counting method. (b) SG-stained fluorescence widefield microscopy images and (c) FE-SEM images of BPTCD EVOH before (i

and ii) and after (iii and iv) 2-hour *E. coli* releasing, and SBMA@EVOH NFMs after (v and vi) 2-hour *E. coli* releasing under dark condition.

Figure 5.1 (a) Potential grafting reaction pathways of DMDMH to Cotton fabric, and the (b) graft polymerization reaction of PVA-co-PE with DAM; DCP is dicumyl peroxide.

Figure 5.2 (a) Scheme of the design, processing, and rechargeable biocidal function of the halamine compositive fabric. The top inset image shows chlorination of N-halamine precursors and decontamination of N-halamine structures, and the bottom inset image exhibits the potential active chlorine transfer between imide-, amide, and amine-halamine structures. (b) Optical images of an HCF-2.5 fabric after bending, folding, rolling, and twisting. (c) SEM images of cotton fabrics coated with i) 0 %, ii)1%, iii) 2.5%, iv) 5%, and v) 7.5% of halamine polymer solutions. (d) FT-IR spectra, (e) wicking properties and air permeabilities, (f) abrasion performances, and (g) tensile stress-strain curves of the halamine composite fabrics.

Figure 5.3 Optical image of an HCF-2.5 fabric in a size of 60 × 60 cm, and optical image of the DMH-g-Cotton, HCF-1, HCF-2.5, HCF-5, and HCF-7.5 after 200 abrasion cycles.

Figure 5.4 Active chlorine contents of the halamine compositive fabrics as a function of (a) pH values of chlorination solution and (b) chlorination time. Active chlorine contents of the DMH-g-Cotton and HCF-2.5 versus (c) storage times and (d) chlorine charging/ quenching cycles. (e) Summary of the active chlorine contents of various washing cycles coated with different concentrations of halamine polymer solution, and (f) the relationship between active chlorine content and the weight ratio of coating polymer over the fabric.

Figure 5.5 Biocidal activity of chlorinated HCF-2.5 against *E. coli* ((a) COD = 0 and (c) COD = 1000 and *L. innocua* ((b) COD = 0 and (d) COD = 1000). (e) Five cycle antimicrobial tests of

chlorinated HCF-2.5 against *E. coli* and *L. innocua* and the biocidal activity of the chlorinated DMH-g-Cotton and the chlorinated HCF-2.5 against *E. coli* (f) and *L. innocua* (g) as a function of storage time. (h) Antimicrobial behaviors of the chlorinated DMH-g-Cotton after coating with 7.5 wt% of PVA-co-PE (control) and PVA-co-PE-g-DAM (sample) polymers. SEM images of the (i, j) *E. coli* and (k, l) *L. innocua* after exposing to the (i, k) unchlorinated and the (k, l) chlorinated HCF-2.5 (scale bar = 500 nm).

Figure 5.6 Measurement of the leakage of nucleic acid from *E. coli* and *L. innocua*.

Figure 5.7 (a) Scheme of the experimental process for stimulating leaf-to-leaf cross-contamination. (b) The population of the living bacteria transferred from leaf As to relevant fabrics and leaf Bs. (c) Optical photographs showing the spoilage process of the strawberries by using the cotton fabric and the HCF-2.5-Cl as the packaging pads.

Table of Contents

Chapter 1. Introduction and Literature Review

1.1 Introduction

The frequent outbreaks of foodborne diseases have become a major public health concern, resulting in significant morbidity and mortality rates.[1,2] This issue was highlighted in a report published by the United States Centers for Disease Control and Prevention (CDC): from 2013 to 2017, a total of 428 outbreaks, 4912 illnesses, 1036 hospitalizations, and 59 deaths related to the foodborne bacteria (*Escherichia* and *Listeria*) have been reported.[3] Significantly, according to a study reported by the National Institute of Health (NIH), around 80% of the microbial infections are related to the presence of the microbial biofilm on surfaces of materials, which is considered as a severe microbial contamination pathway threatening public health security.[4,5] Biofilm is a community of microorganisms irreversibly associating with a solid surface and embedding with a self-produced hydrated matrix of extracellular polymeric substances (EPSs), including polysaccharides, proteins, lipids, and extracellular DNA (eDNA), which could facilitate the survival of microorganisms by providing an adverse environment.[6-9] Biofilms are ubiquitous and problematic, not only in the food industry but also in the water treatment facilities.[10-13]

Based on a World Health Organization (WHO) report, 1.2 billion people lack access to safe drinking water, 2.6 billion have little or no sanitized water, and millions of people die annually due to waterborne microbial infections.[14-16] Membrane technologies, such as ultrafiltration (UF), reverse osmosis (RO), and nanofiltration (NF) membranes, have been wildly applied to achieve water disinfection as the microorganisms are intercepted by the membranes based on the size-sieving effect.[17-21] Compared with the conventional strategies, which rely on the a direct and irreversible addition of disinfectants to the wastewater, membrane technologies could avoid the formation of the harmful disinfection byproducts and enhance the reliability of the water

disinfection.[22,23] However, during the filtration process, membrane surfaces are constantly in contact with the feeding water containing a high concentration of microorganisms, which tend to foul the filter membrane driven by the non-specific interactions. Such accumulated biofouling effect finally results in the formation of the biofilm, reducing the permeate fluxes and shortening the shelf life of the filtration membrane.[18,20]

The biofilm formation and maturation are sequential dynamic and complex processes, which could be briefly described by a five-stage biofilm formation model: (1) an initial reversible attachment of planktonic bacteria approaching the solid surface driven by hydrophobic interactions, electrostatic interactions, and Van der Waals forces; (2) a transition stage from the reversible to irreversible attachments due to the production of EPS and anchoring effect of bacterial appendages, such as pili, flagella, and adhesion proteins; (3) the formation of a microcolony where multilayer appear implying the early development of biofilm architecture; (4) the development from microcolonies to a matured biofilm, forming characteristic "mushroom" structure; and (5) the dispersion of bacteria cells from the biofilms into the surrounding bulk environment, which facilitates the spreading of bacterial contaminants.[6,24,25] An established biofilm with high tolerance against exogenous stress is difficult to be eradicated due to the physiochemical diffusion barrier generated by the extracellular polymeric matrix, altered microbial metabolic state, and expression of specific resistance genes.[26,27] Therefore, the best strategy to treat bacterial biofilm is to prevent their formation at the early stages.

1.2 Overview of Antibiofilm Strategies

In general, there are two major approaches to prevent the formation of a biofilm: an active approach, which is to "attack", by killing the microbial once they are attached to the material

surface; and a passive approach, which is to "defend", by resisting the microbial attachment or releasing the attached one.[28,29]

1.2.1 Antimicrobial agents

The bacteria killing mechanism of antimicrobial agents in materials, in general, could be divided into two types: releasing killing and contact killing.[29] In a typical releasing killing mode, the antimicrobial agents are gradually released to the intermediates and kill the microbes.[30.31] Since the consumption of antimicrobial agents is chemically irreversible, the major concern with such an approach is the long-term durability of antimicrobial function. In contrast, the contact killing mode is usually realized via covalently bonding between the antimicrobial agents and the micorbes attached on active surfaces [21,30] Once the microbe attaches to the active surface, it can be killed by the local bonded antimicrobial agents. As long as the inactivated microbe could be removed from the surface, in theory, the antimicrobial agents could be exposed to the bulk environment again, and the antimicrobial function could be reactivated. Therefore, compared with the releasing kill mode, the contact killing mode exhibits better long-term durability.[29]

Commonly used antimicrobial agents are classified into three categories based on their material types.

(1) Inorganic antimicrobial agents: metal-based antimicrobial agents are widely applied in various areas because they could be easily incorporated with a substrate via either deposition or adsorption. Compared with copper- and tin-based complexes, silver-based antimicrobial agents with a relatively safer profile in living bodies have been wildly applied in the food area.[29,32] Specifically, silver nanoparticles (Ag NPs)-based coating surfaces, with a large specific surface area, have been wildly studied. [33-35] These Ag NPs were physically trapped by the 3D structure of the coating

matrix and gradually oxidized to silver cation (Ag+), providing an antimicrobial activity. However, the retention of the Ag NPs incorporated surface could be weak due to the absence of strong chemical linkages, limiting the antimicrobial functions for a long-term application. In general, these silver-based antimicrobial coating materials could only work for limited durations under certain laboratory-test conditions.[36,37] Therefore, more intensive studies in this area are focusing on improving the antimicrobial efficacy and long-term durability of the Ag NPs via introducing encapsulation and controllable release techniques.[38-40]

Besides metal-based materials, some nanoscale carbon-based materials, including graphene, graphene oxides, reductive graphene oxides, and carbon nanotubes, also exhibited antimicrobial performance by anchoring the bacterial cells via some weak interactions and generating ROS to trigger oxidative stress of cells.[41-43] However, the detailed killing mechanisms against microbes by these materials are still unclear.[41] Usually, they serve as a supporting carrier and combine with highly effective antimicrobial agents to improve the stability of the resulted nanocomposites and also provide a synergetic antimicrobial killing effect.[44,45]

(2) Biological antimicrobial compounds: They come from living bodies, mainly including enzymes, peptides, and bacteriophages.[46-50] Compared with the metal-based antimicrobial agents, biological antimicrobial compounds could be covalently bonded to the substrates via various surface reactions, thereby increasing the long-term durability.[49,50] However, antimicrobial performances of this type of antimicrobial agents are usually restricted by environmental factors, such as pH, temperature, and concentration of salts.[51,52]

(3) Organic antimicrobial agents: natural-produced essential oils with antimicrobial activity have received great interest due to their low toxicity, pharmacological activity, and economic viability.[53] The major antimicrobial compounds in the essential oils are chemically derived terpenes $(C_5H_8)_n$,

and terpenoids, which are aromatic and aliphatic acid esters and phenolic compounds.[54,55] Depending on different types of essential oils and microbes, the microbial killing mechanisms are different. While the underlying principle relies on the hydrophobicity of the essential oils, which enables them to partition with the lipids present in the cell membrane, resulting in increased cell permeability and eventually death of the microbe due to leakage of critical molecules and ions.[55,56]

In addition, numerous types of organic antimicrobial agents have been developed artificially.[57-60] The widely applied organic antibiotics, such as penicillin and amoxicillin, kill the bacteria via targeting bacterial cell wall synthesis, DNA-directed RNA polymerase, DNA gyrase, DNA replication, folic acid metabolism, and protein synthesis, which can hardly completely inactive bacteria in a short time.[61] More importantly, bacteria are capable of developing resistance against these killing mechanisms via adjusting the metabolism behaviors.[62] Directly destroying the bacterial cell structures could be a more effective killing pathway to inactive drug-resistant bacteria and slow down drug resistance evolution. For example, quaternary ammonium compounds (QACs), with positively charged structure NR_4^+ (R refers to an alkyl, an aryl group or aralkyl groups), could generate strong electrostatic interactions with the negatively charged microbial cell walls, leading to bacterial cell wall lysis, protein denaturation, disrupting cell wall permeability, and finally completely inactivating the targeted microbes.[41,63-65] QACs exhibited higher kill efficiency against negatively charged microbes than others. In contrast, oxidative biocides, including halogen-based and reactive oxygen species (ROS)-based antimicrobial agents, exhibited strong killing activity against a broad spectrum of microbes, which could kill 5 log of the bacteria within 30 seconds and are defined as disinfectants/sanitizers by the United States Environmental Protection Agency (EPA).[66] These biocides directly damage the bacterial cellular structures at both biochemical and molecular levels, realizing the fast-killing performance and effectively limiting

biofilm formation via redox reactions.[66,67] However, all of these biocide incorporated surfaces pose a common problem: the bacterial cells or generated cell debris may physically block the active surfaces due to the non-specific contamination and adsorption, leading to the reduction of their antimicrobial performance and benefiting the biofilm formation.

1.2.2 DLVO theory

Biofilm formation is a typical biofouling process, which refers to the microorganism accumulation on the wet surface.[25] Embedding surfaces with antifouling function can be the other strategy responding to the biofilm challenge. Unlike antimicrobial surfaces, instead of inactivating microbes, antifouling surfaces reduced the microbial contamination based on two mechanisms: resisting (prevent the reversible bacteria adhesion in aqueous media) and releasing (remove the previously attached live/dead bacteria under a wet condition).[29] A DLVO theory, named after four scientists, Derjaguin, Landau, Verwey, and Overbeek, was well studied to estimate whether the adsorption of biofoulants to a specific surface is a favorable process, which provides theoretical support to predict the resisting performance of the functional surface toward various types of the biofoulants.[68,69] According to the DLVO theory, the balance between the Lifshitz-van der Waals (LW) attractive interaction and the electrostatic double-layer (EL) repulsive interaction determines the adsorption behavior of the specific biofoulants (assuming the biofoulants are smooth spheres). The total interaction energy (ΔE^{TOT}) between a biofoulant and a solid surface can be explained as the sum of these corresponding interaction terms:

$$\Delta E^{TOT} = \Delta E^{LW} + \Delta E^{EL} \qquad \text{Equation (1.1)}$$

when ΔE^{TOT} is negative, the biofoulants will adhere to the solid surface.

The LW interaction between a sphere with a radius of R and a flat surface could be calculated based on equation (1.2):

$$\Delta E^{LW} = -\frac{A \times R}{6D} \qquad \text{Equation (1.2)}$$

Where D is the distance between the spherical biofoulant and the surface. A is the Hamaker constant related to the properties of the involved materials, including solid surface, biofoulant, and intermedium.

The electrostatic double-layer interaction term could be expressed as equation (1.3):

$$\Delta E^{EL} = RZe^{-kD} \qquad \text{Equation (1.3)}$$

Where Z is the interaction constant, which is a function of surface potential (ψ) and dielectric permittivity of solution (ε), D is the distance between the sphere and the surface, k is the debye parameter, and k^{-1} is the debye length.

1.2.3 Hydrophobic antifouling polymer

According to the Gibbs free energy law, the adhesion process of high-surface energy biofoulants to hydrophobic surfaces is unfavorable since the potential coverage would further increase the surface energy of the coated substance. [29,70] However, in reality, some biofoulants do adhere to the hydrophobic surfaces but could be easily removed compared with regular surfaces, which could be explained and predicted by the DLVO theory (discussed in section 1.2.2). Usually, these antifouling hydrophobic surfaces are chemically composed of fluorocarbon and silicon long-chains, which have low surface energy (< 30 Mn/m).[71,72] Depending on the antifouling mechanisms, these functional surfaces could be divided into two types. (1) Omniphobic surfaces, displaying a robust repelling function against any kind of liquid with a high static water contact

angle (> 150º) and a low sliding angle (< 5º), are highly desirable for the antifouling application to reduce microbial contamination and biofilm formation.[71,73] The underlying design principle is the introduction of multi-scale roughness structures onto the low-surface-energy surfaces. With the increased roughness structure, more air pockets could be entrapped by the 3D morphology of the surfaces, benefiting the generation of a stable Cassie state.[74,75] Therefore, the contact area between the biofoulant liquids and the surfaces is significantly reduced, enabling liquid droplets to roll off with ease.[71,76,77] Slippery porous lubricant-infused surfaces (SLIPS) are a newly developed class of omniphobic surfaces by infusing the low-surface-energy liquid into a porous low-surface-energy surface.[78-80] For example, a silicon oil-infused nano-wrinkled poly(tetrafluoroethlene) (PTFE, Teflon, 20 nM/m) surface with a high water contact angle of 160º, exhibited high resistance to bacteria adhesion up to 99% within 24 h incubation. However, the major challenge for such SLIPS is the weak durability of the lubricant layer, which was usually subjected to gradual leakage through diffusion and shear stress of the fluid.[79] (2) The other type of hydrophobic antifouling surface is based on the steric hindrance effect of flexible polymer long chain. For example, the PDMS surface with a surface energy of 19.8 mN/m, showed significant mobility of the polymer chains accounting for a higher level of surface entropy. The potential biofoulants adsorption tends to compress the polymer chains and restrict the chain movements, leading to an increase of the system Gibbs free energy. Therefore, the overall biofouling process is thermodynamically unfavorable.[29,81,82] This principle is also applicable to the hydrophilic polymer chain for constructing an antifouling surface.[83,84]

1.2.4 Hydrophilic antifouling polymer

Unlike the hydrophobic strategy, most hydrophilic polymers exhibit good microbial resisting and releasing performances owning to their strong hydration capability. These hydrophilic surfaces

possess a robust interaction with surrounding water molecules, generating a dense hydration layer, which provides strong repulsive hydration forces to resist the biofoulants adsorption.[85-87] Poly(ethylene glycol) (PEG) is one of the most popular hydrophilic polymers for antifouling applications.[84,88] With the abundant existences of ether groups, PEG could build up a strong hydration layer via hydrogen bonds, which was responsible for its high resistance of more than 99 % of bacteria from the non-specific adsorption.[89] Additionally, this microbial resisting function could be optimized by adjusting the PEG chain length and density to achieve a maximized surface entropy and the strongest hydration ability.[84,90,91] However, the chemical stability of PEG is insufficient as it is subject to auto-oxidation, limiting the long-term applicability of it.[92,93]

Zwitterionic polymers, carrying both positive and negative charges while maintaining the overall net charge of zero, are wildly applied to construct the other type of hydrophilic antifouling surface.[94] Different from nonionic antifouling polymer, which forms the hydration layer via hydrogen bonds, the zwitterionic polymers provide a strong hydration effect via electrostatic interaction of each cationic and anionic component to ionic solvent. In addition, since the net charge of the zwitterion structure is nearly zero with a homogenous charge distribution, itself would not interact with the charged biofoulants.[86,95,96] A report indicated that poly(carboxybetaine methacrylate) (poly CBMA), a commercially available zwitterionic polymer reduced the formation of *Pseudomonas aeruginosa* (*P. aeruginosa*) biofilm by 95 % and maintained such high antifouling performance for 10 days, which exhibited significantly superior antifouling performance over other reported PEG coatings (only delay biofilm formation for 1 day).[97] Despite the improvement of the antifouling performance, usually, chemically linkages with substances are required for the zwitterionic polymers due to their high solubility in an aqueous environment.[98,99]

1.3 Refreshable Biocidal Structures

1.3.1 N-Halamine structures

As shown in Figure 1.1, N-halamine is a group of compounds containing one or more nitrogen-halogen (N-X) covalent bonds formed by the halogenation of the amine, amide, and imide groups.[100] N-halamine materials with robust regenerable biocidal performances have been investigated in broad application areas, such as food packaging materials, water disinfection, medical applications, and personal protective textiles.[101-104] The major antibacterial mechanism of the N-halamine materials is contact killing, which means oxidative halogens (with the oxidative state of +1) directly transfer from the active halamine structures to the proteins and polysaccharides of the microorganisms, leading to the damage and collapse of cell structures.[100] However, in an aqueous solution, N-halamine materials could also inactivate microorganisms via releasing killing mode. The oxidative halogen atoms of the halamine structures could dissociate into the water, following with diffusion over to the microorganisms.[105] Such dissociation rate is related to the halamine structures, following the order of imide > amide > amine halamines. On the contrary, the antimicrobial activity of the halamines is in an inverse trend: imide > amide >> amine halamines.[100,106] During the killing process, the active N-halamine structures are consumed and converted to amine, amide, or imide groups, which could be rehalogenated and converted back to active halamine structures again by exposing to chlorine solutions.[102,103] According to the chemical structure, N-halamines can be generally classified as cyclic and acyclic. Theoretically, both classes have great biocidal activity and could always be regenerated. However, the latter, with potential hydrolysis of amide groups, exhibits weaker chemical stability. A dehydrohalogenation process could easily occur in halamine structures containing α-hydrogen in the presence of water, light, and heat (Figure 1.2), resulting in a loss of N-halamine precursor structures and a limitation of regeneration of the biocidal activity. Therefore, cyclic N-halamines, such as 2,4□diamino□6□

diallylamino□1,3,5□triazine (DAM),[103] 2,2,5,5-tetramethylimidazolidin-4-one (TMIO),[106] and 5,5 dimethylhydantoin (DMH),[107] with the absence of an α-hydrogen are more desirable due to the better long-term stability (Figure1.3).

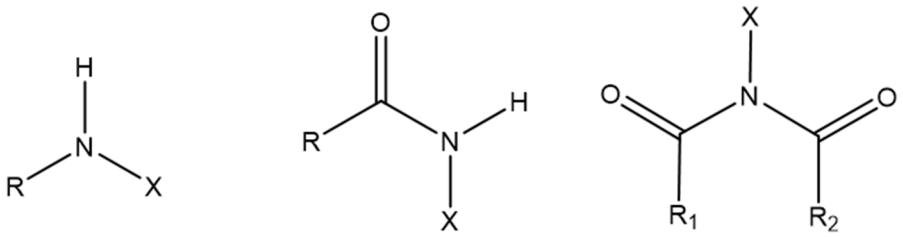

Figure 1.1. General structures of an amine, amide, and imide halamine compounds, respectively. X = Cl or Br, or I. R, and R could be any organic or inorganic group.

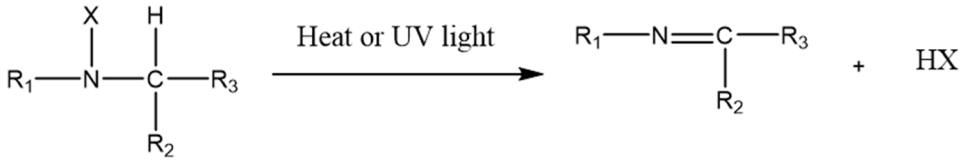

Figure 1.2. The dehydrohalogenation reaction of the N-halamine structure with the existence of an α-hydrogen

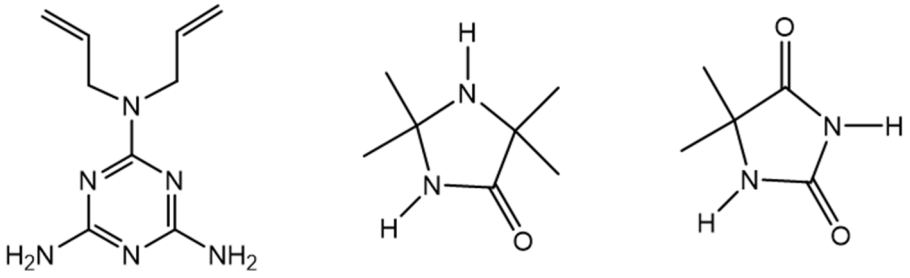

Figure 1.3. The chemical structures of DAM, TMIO, and DMH, which are the amine-, amide, and imide halamine precursors, respectively.

1.3.2 Benzophenone structures

Benzophenones (BPs) are a group of aromatic ketones, with the main structure of two benzene rings linked by a carbonyl group (Figure 1.4a). Depending on different substituents on the two benzene rings, a wide range of BP derivatives have been identified with different physiochemical properties.[108] However, the photosensitization mechanisms of these BP derivatives are similar, which are called photosensitizers. As shown in Figure 1.4b, a photosensitizer in the ground state (S_0) could be excited to a singlet state (S_1 to S_n, mixed) by absorbing protons to overcome the energy bandgap. The photoexcited BPs could undergo an intersystem crossing (ISC) pathway, generating a high population in the triplet excited state (T_1 to T_n), donated as 3BP*. After that, the 3BP* could absorb a hydrogen atom and yield a quinone radical (BP-H·), further reacting with surrounding oxygen species and generating reactive oxygen species (ROS).[109,110] These ROS would attack surrounding microbes, leading to cell damage and death. Numerous research activities have been conducted and proved the promising antimicrobial performance of the photoexcited BPs.[111] For example, 4-hydroxybenzophenone incorporated cotton fabric could realize a noticeable log scale reduction of both *Staphylococcus aureus* (*S. aureus*) and *Escherichia coli* (*E. coli*) under UVA light irradiation.[112,113] Similar results could be observed on benzophenone-blended polymer films, including polystyrene (PS), polyethylene (PE), polypropylene (PP), and polyvinyl alcohol (PVA) as polymer matrixes.[114-116] Additionally, BPs are applied as a typical photo initiator under UV light. Some polymer substrates contain weak C-H or N-H bonds, which could serve as hydrogen donors and react with 3BP*, resulting in both quinone radical (BP-H·) and a polymeric radical. These polymeric radicals would initiate graft polymerization of the potential monomers onto the polymer substrates. [117,118]

3,3′,4,4′-benzophenonetetracarboxylic dianhydride (BPTCD), as a BP derivative, has attracted much attention due to its unique chemical structure. The anhydride groups on the two benzene

rings could serve as a reaction site to chemically bond with the potential polymer substances while maintaining the photoactive BP structure intact. A research study successfully immobilized the BPTCD onto the nanofibrous cellulose membrane via an esterification reaction.[117] The covalently bonded BPTCD with a shortened distance to the cellulose matrix exhibited a promising efficiency to abstract hydrogen atoms from the cellulose chain, generating polymeric radical and further initiating the graft reaction. More interestingly, in an anaerobic environment, the quinone radical structure of BPTCD (BPTCD-H·) could be rearranged and process a second hydrogen extraction, forming a metastable structure (LAT-BPTCD) with photoactivity stored. Once LAT-BPTCD structures expose to the oxygen condition, this stored photoactive could readily be released with ROS generation even under dark conditions.[112, 119] The detailed mechanism will be discussed in chapter 4.

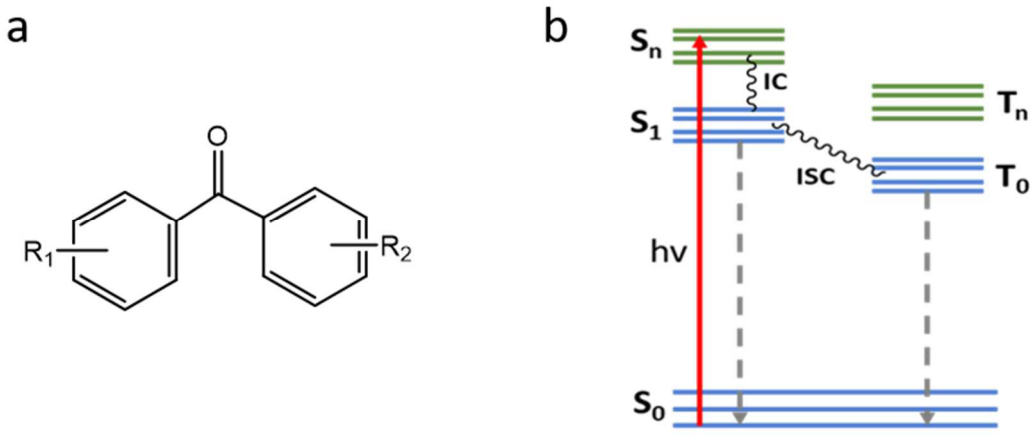

Figure 1.4. (a) Chemical structure of benzophenone derivatives, and (b) Jablonski diagram of the photochemical process of the benzophenones.

1.4 Antifouling Approach

1.4.1 Zwitterionic structures

The zwitterionic polymer is biologically inspired by zwitterionic phosphatidylcholine headgroups of the phospholipid bilayer, which is defined as a polymer that carries the equimolar number of the homogenously distributed cationic and anionic groups along their polymer chain.[94,120] As shown in Figure 1.5, depending on whether the charged groups are located on the same or different pendant side chains, zwitterionic polymers could be divided into polybetaines and polyampholytes, respectively, and both of them exhibit great antifouling performance against various biofoulants.[120] Usually, these polyzwitterions, with high water solubility, can hardly survive in an aqueous media for a long time. Copolymerization of zwitterionic monomers containing alkene groups with some hydrophobic monomers via a general free radical polymerization could be a solution responding to this challenge.[121] So far, various zwitterionic copolymers with a unique amphiphilic performance and great antifouling ability, have been developed, such as poly(acrylonitrile-random-sulfobetaine methacrylate)[122], poly(trifluoroethyl methacrylate-random-sulfobetaine methacrylate)[121], and poly(carboxybetaine) (PCB)–poly(lactic-co-glycolic acid) (PLGA).[123]

However, the synthesized zwitterionic copolymeric materials by step growth method can rarely be applied on a large-scale due to the low functional efficacy. Most of the zwitterionic moieties are distributed inside the bulk polymer, therefore they can hardly interact with surrounding water molecules and generate a hydration layer via electrostatic interactions. Also, these polymer chains do not perform in an ideal “brush up” configuration, which has limited the steric hindrance effect, resulting in reduced antifouling efficiency.[124] Therefore, directly incorporating zwitterion structure onto stable substrate surfaces could be a more effective means to maximize the antifouling effect. Surface grafting, providing good long-term stability via constructing robust chemical bonds between polymers and substances, is one of the most popular techniques.[94] Typically, the grafting process could be divided into two types, "grafting to" and "grafting from". The "grafting to" refers

to the direct graft end-functionalized polymer chain onto the solid surface, while the "grafting from" means graft polymerization of the monomers from surfaces. Many polybetaines, such as poly(sulfobetaine methacrylate) (PSBMA), poly(carboxybetaine methacrylate) (PCBMA), and poly(2-methacryloyloxyethyl phosphorylcholine) (PMPC) have been successfully grafted onto various solid surfaces via a "grafting from" polymerization reaction due to the existence of the alkene structure of their monomers.[119,125-128] However, "grafting to" methods were hardly reported due to the significant steric hindrance of polymer, limiting the reaction efficiency and grafting density. [94,129]

1.4.2 Antifouling mechanisms of zwitterionic material

Two major antifouling mechanisms are underlaying the zwitterionic materials in an aqueous condition: hydration effect and steric hindrance effect. The latter has been introduced in section 1.2.3.

Strong hydration is considered as a key feature of zwitterionic materials to resist non-specific biofoulants adsorption. [85-87,130] Compared with the nonionic antifouling polymer, such as PEG and its derivatives, the zwitterionic structure could generate a denser and thicker hydration shell, which serves as an effective barrier to prevent the surface from the direct contact of the biofoulants.[131] For PEG, each repeating unit could only integrate with one water molecule via hydrogen bonds. However, each repeating unit of zwitterionic polymer carries one cationic and one anionic group, which could integrate with at most eight water molecules via electrostatic interaction.[85,124] Additionally, He et al. and Kondo et al. studied the structural and dynamic properties of the water molecules near the zwitterionic structure by using molecular dynamic simulation (MD) and sum frequency generation spectroscopy. [132,133] The results showed that these water molecules exhibited less mobility and wider dipole orientation distribution than those near other hydrophilic antifouling

materials. The limited water mobility benefited for maintaining the conformation of the hydration layer undamaged, therefore, providing a strong and stable repulsive force against the biofoulants. Moreover, the wide dipole orientation distribution could decrease the attractive interaction with any charged biofoulants. [29]

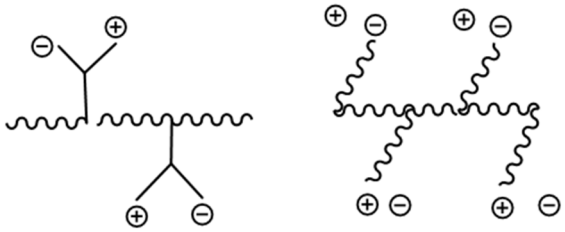

Figure 1.5. A simplistic model of polybetaines (left) and polyampholytes (right)

1.5 Research Objectives

In this study, three types of rechargeable biocidal and antifouling materials for food packaging, water disinfection, and medical applications were successfully designed and fabricated. The coexistence of the functional moieties on the surface may lead to the respective compromise of their functions. For example, the biocidal moieties tend to kill the bacteria, while the antifouling moieties tend to repel them. To minimize such compromising effects, the biocidal moieties are immobilized at the inner layer, and the antifouling moieties serve as a protective layer locating on the outside of the surface. As shown in Figure 1.6, once the microorganisms are approaching the designed surfaces, (i) the antifouling moieties could reduce the non-specific adsorption of the microorganisms and make them difficult to adhere; (ii) any live bacteria attached to the surface could be immediately killed by the incorporated biocidal moieties; (iii) any resulting cell debris and other biofoulants could be easily washed off with mild hydrodynamic force applied; furthermore, (iv) the consumed biocidal activity could be regenerated by either chlorination or photoirradiation.

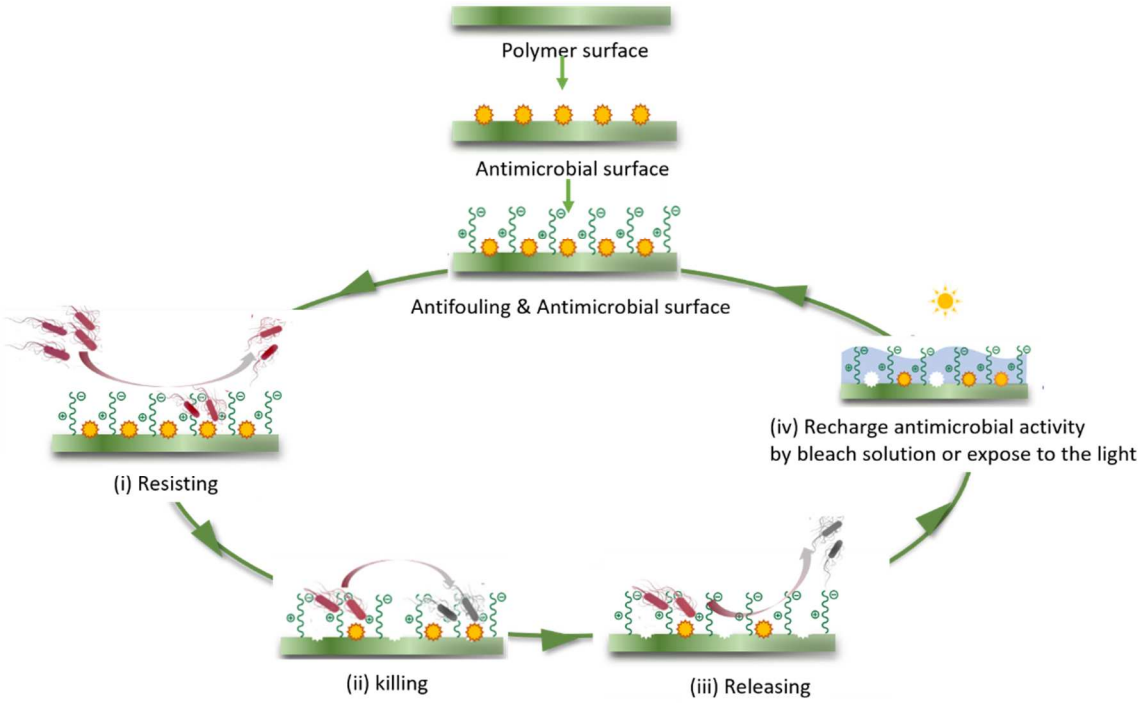

Figure 1.6. Scheme of the bacterial-resisting, biocidal, debris-releasing, and recharging functions of the proposed double-layer surface with the incorporated antimicrobial (inner layer) and antifouling (out layer) components.

The specific objectives of my dissertation include:

(1) Proof of concept: to investigate a rechargeable biocidal and antifouling plastic film and establish a characterization system to evaluate each function;

(2) Mechanism analysis: to investigate and analyze the antifouling mechanisms with the existence of biocidal moieties via modeling;

(3) Application exploration: changing different functional moieties and proofing the universality of the proposed model.

(4) A practical case demonstration: to investigate the antimicrobial effect of an N-halamine-based fabric serving as a food-contact material on prepackaged strawberries.

In the first part, I developed a chlorine rechargeable biocidal and antifouling material by chemically grafting both N,N-diallylmelamine (DAM), a halamine precursor, and [2-(methacryloyloxy)ethyl]dimethyl-(3-sulfopropyl)ammonium hydroxide (SBMA), a zwitterionic monomer, onto poly(vinyl alcohol-co-ethylene) (PVA-co-PE) plastic film to prove the proposed concept. The obtained polymer product named SBMA@HAF exhibited the highest active chlorine content at an optimized chlorination condition, which could be quantitively measured by an established iodometric titration method. Two typical pathogenic foodborne bacteria, Gran-negative *Escherichia coli O157: H7* and Gram-positive *Listeria innocua* were used to evaluate the biocidal ability of the chlorinated SBMA@HAF films. The antifouling function of the designed SBMA@HAF film was investigated based on the microbial resisting and releasing tests. The other physiochemical properties of the SBMA@HAF film could be confirmed by FT-IR, SEM-EDX, UV-vis, DSC, and fluorescence microscope.

With a fully proven concept in the first part, I further investigated the resisting and releasing mechanisms of the antifouling moieties with the existence of the N-halamine structures via conducting typical isothermal protein adsorption and releasing experiments, respectively. Nanofibrous membrane with the superhigh specific surface area could effectively magnify the interfacial effect, being considered as a good matrix. A rechargeable biocidal PVA-co-PE-g-DAM nanofibrous membrane (BNF membrane) could be prepared by applying the electrospinning technique. A zwitterionic polymer (PEI-S), serving as an antifouling agent, was introduced onto the BNF membrane through an optimized chemical cross-linking process. The final product, named PEI-S@BNF membrane, was tested by the same evaluation system of the SBMA@HAF film, including active chlorine contents, biocidal efficiency, microbial resisting/releasing performance, and other physicochemical properties. Additionally, some engineering models were

applied to explain the resisting and releasing functions of the antifouling moieties. The final product, PEI-S@BNF nanofibrous membrane, showed great potential to be applied as a water filtration material.

Besides the N-halamine structure, the proposed antibiofilm strategy should also work for other biocidal matrixes. As a continuous study, instead of halamine structure, a photosensitizer, benzophenonetetracarboxylic dianhydride (BPTCD), which could produce reactive oxygen species (ROS), was incorporated onto the PVA-co-PE nanofibrous membrane, serving as a biocidal component. After combining with the antifouling moieties, the resulted product, SBMA@EVOH nanofibrous membrane, was also tested by the established evaluation system. This photo-induced bifunctional material could prove the universality of the proposed double-layer surface with the antimicrobial moieties locating in the inner layer while the antifouling moieties locating in the outside layer and extend the potential application areas.

Finally, practical applications of a designed material with a regenerable antimicrobial function were carried out. An industrial scalable dip-coating methodology for fabricating a chlorine rechargeable antimicrobial halamine composite fabrics (HCFs) was developed. A previously developed imide/amide halamine grafted cellulose fabric (DMH-g-Cotton) served as a reinforcement component and a reservoir of active chlorine, and an amine-halamine polymer 2,4-diamino-6-diallylamino-1,3,5-triazine grafted poly(vinyl alcohol-co-ethylene), (PVA-co-PE-g-DAM), was applied as a coating component to construct such HCFs. Besides the physiochemical properties and antimicrobial activities of as-prepared HCFs, the practical incorporation of HCFs as a biocidal food pad was also established. The results showed that the shelf life of prepackaged strawberries could be significantly prolonged due to the durable and rechargeable antimicrobial

function of the HCFs, demonstrating the great potentials of the N-halamine-based material in the practical food processing areas.

1.6 References

2. Rumbo, C.; Tamayo-Ramos, J. A.; Caso, M. F.; Rinaldi, A.; Romero-Santacreu, L.; Quesada, R.; Cuesta-López, S., Colonization of electrospun polycaprolactone fibers by relevant pathogenic bacterial strains. *ACS Applied Materials & Interfaces* **2018,** *10* (14), 11467-11473.
3. Heiranian, M.; Farimani, A. B.; Aluru, N. R., Water desalination with a single-layer MoS2 nanopore. *Nature Communications* **2015,** *6* (1), 1-6.
4. Data from National Outbreak Reporting System (NORS) of Centers for Disease Control and Prevention (CDC). Available at https://wwwn.cdc.gov/norsdashboard/, accessed: December 2020.
5. Khatoon, Z.; McTiernan, C. D.; Suuronen, E. J.; Mah, T.-F.; Alarcon, E. I., Bacterial biofilm formation on implantable devices and approaches to its treatment and prevention. *Heliyon* **2018,** *4* (12), e01067.
6. Gupta, P.; Sarkar, S.; Das, B.; Bhattacharjee, S.; Tribedi, P., Biofilm, pathogenesis and prevention—a journey to break the wall: a review. *Archives of Microbiology* **2016,** *198* (1), 1-15.
7. Zhao, X.; Zhao, F.; Wang, J.; Zhong, N., Biofilm formation and control strategies of foodborne pathogens: food safety perspectives. *RSC Advances* **2017,** *7* (58), 36670-36683.
8. Vu, B.; Chen, M.; Crawford, R.; Ivanova, E., Bacterial extracellular polysaccharides involved in biofilm formation. *Molecules* **2009,** *14* (7), 2535-2554.
9. Hall-Stoodley, L.; Costerton, J. W.; Stoodley, P., Bacterial biofilms: from the natural environment to infectious diseases. *Nature Reviews Microbiology* **2004,** *2* (2), 95.
10. Donlan, R. M.; Costerton, J. W., Biofilms: survival mechanisms of clinically relevant microorganisms. *Clinical Microbiology Reviews* **2002,** *15* (2), 167-193.

11. Mukherjee, M.; Hu, Y.; Tan, C. H.; Rice, S. A.; Cao, B., Engineering a light-responsive, quorum quenching biofilm to mitigate biofouling on water purification membranes. *Science Advances* **2018,** *4* (12), eaau1459.
12. Vitzilaiou, E.; Stoica, I. M.; Knøchel, S., Microbial biofilm communities on reverse osmosis membranes in whey water processing before and after cleaning. *Journal of Membrane Science* **2019,** *587*, 117174.
13. Zhang, P.; Qu, Y.; Feng, Y.; Liu, J., The influence of the filtration membrane air-cathode biofilm on wastewater treatment. *Bioresource Technology* **2018,** *256*, 17-21.
14. Al Ashhab, A.; Sweity, A.; Bayramoglu, B.; Herzberg, M.; Gillor, O., Biofouling of reverse osmosis membranes: effects of cleaning on biofilm microbial communities, membrane performance, and adherence of extracellular polymeric substances. *Biofouling* **2017,** *33* (5), 397-409.
15. Rotzetter, A.; Kellenberger, C.; Schumacher, C.; Mora, C.; Grass, R.; Loepfe, M.; Luechinger, N.; Stark, W. J., Combining phosphate and bacteria removal on chemically active filter membranes allows prolonged storage of drinking water. *Advanced Materials* **2013,** *25* (42), 6057-6063.
16. Wang, Y.; El-Deen, A. G.; Li, P.; Oh, B. H.; Guo, Z.; Khin, M. M.; Vikhe, Y. S.; Wang, J.; Hu, R. G.; Boom, R. M., High-performance capacitive deionization disinfection of water with graphene oxide-graft-quaternized chitosan nanohybrid electrode coating. *ACS Nano* **2015,** *9* (10), 10142-10157.
17. Kroll, S.; Brandes, C.; Wehling, J.; Treccani, L.; Grathwohl, G.; Rezwan, K., Highly efficient enzyme-functionalized porous zirconia microtubes for bacteria filtration. *Environmental Science & Technology* **2012,** *46* (16), 8739-8747.

18. Katsoufidou, K.; Yiantsios, S.; Karabelas, A., A study of ultrafiltration membrane fouling by humic acids and flux recovery by backwashing: experiments and modeling. *Journal of Membrane Science* **2005,** *266* (1-2), 40-50.
19. Khan, A.; Sherazi, T. A.; Khan, Y.; Li, S.; Naqvi, S. A. R.; Cui, Z., Fabrication and characterization of polysulfone/modified nanocarbon black composite antifouling ultrafiltration membranes. *Journal of Membrane Science* **2018,** *554*, 71-82.
20. Mondal, S.; Wickramasinghe, S. R., Produced water treatment by nanofiltration and reverse osmosis membranes. *Journal of Membrane Science* **2008,** *322* (1), 162-170.
21. Shtreimer Kandiyote, N.; Avisdris, T.; Arnusch, C. J.; Kasher, R., Grafted polymer coatings enhance fouling inhibition by an antimicrobial peptide on reverse osmosis membranes. *Langmuir* **2018,** *35* (5), 1935-1943.
22. Jiang, C.; Tian, L.; Hou, Y.; Niu, Q. J., Nanofiltration membranes with enhanced microporosity and inner-pore interconnectivity for water treatment: Excellent balance between permeability and selectivity. *Journal of Membrane Science* **2019,** *586*, 192-201.
23. Zazouli, M. A.; Kalankesh, L. R., Removal of precursors and disinfection byproducts (DBPs) by membrane filtration from water; a review. *Journal of Environmental Health Science and Engineering* **2017,** *15* (1), 25.
24. Postigo, C.; Emiliano, P.; Barceló, D.; Valero, F., Chemical characterization and relative toxicity assessment of disinfection byproduct mixtures in a large drinking water supply network. *Journal of Hazardous Materials* **2018,** *359*, 166-173.
25. Sadekuzzaman, M.; Yang, S.; Mizan, M.; Ha, S., Current and recent advanced strategies for combating biofilms. *Comprehensive Reviews in Food Science and Food Safety* **2015,** *14* (4), 491-509.

26. Zander, Z. K.; Becker, M. L., Antimicrobial and antifouling strategies for polymeric medical devices. *ACS Macro Letters* **2018**, *7*,1,16-25.

27. Davies, D., Understanding biofilm resistance to antibacterial agents. *Nature Reviews Drug Discovery* **2003,** *2* (2), 114-122.

28. Mah, T.-F. C.; O'Toole, G. A., Mechanisms of biofilm resistance to antimicrobial agents. *Trends in Microbiology* **2001,** *9* (1), 34-39.

29. Cao, Z.; Mi, L.; Mendiola, J.; Ella-Menye, J. R.; Zhang, L.; Xue, H.; Jiang, S., Reversibly switching the function of a surface between attacking and defending against bacteria. *Angewandte Chemie International Edition* **2012,** *51* (11), 2602-2605.

30. Song, B.; Zhang, E.; Han, X.; Zhu, H.; Shi, Y.; Cao, Z., Engineering and application perspectives on designing an antimicrobial surface. *ACS Applied Materials & Interfaces* **2020,** *12* (19), 21330-21341.

31. Li, Z.; Lee, D.; Sheng, X.; Cohen, R. E.; Rubner, M. F., Two-level antibacterial coating with both release-killing and contact-killing capabilities. *Langmuir* **2006,** *22* (24), 9820-9823.

32. Qian, W.; Qiu, J.; Su, J.; Liu, X., Minocycline hydrochloride loaded on titanium by graphene oxide: An excellent antibacterial platform with the synergistic effect of contact-killing and release-killing. *Biomaterials Science* **2018,** *6* (2), 304-313.

33. Sharma, V. K.; Yngard, R. A.; Lin, Y., Silver nanoparticles: green synthesis and their antimicrobial activities. *Advances in Colloid and Interface Science* **2009,** *145* (1-2), 83-96.

34. Xia, Q.; Yang, L.; Hu, K.; Li, K.; Xiang, J.; Liu, G.; Wang, Y., Chromium cross-linking based immobilization of silver nanoparticle coating on leather surface with broad-spectrum antimicrobial activity and durability. *ACS Applied Materials & Interfaces* **2018,** *11* (2), 2352-2363.

35. Gunell, M.; Haapanen, J.; Brobbey, K. J.; Saarinen, J. J.; Toivakka, M.; Mäkelä, J. M.; Huovinen, P.; Eerola, E., Antimicrobial characterization of silver nanoparticle-coated surfaces by "touch test" method. *Nanotechnology, Science and Applications* **2017,** *10*, 137.

36. Mei, L.; Teng, Z.; Zhu, G.; Liu, Y.; Zhang, F.; Zhang, J.; Li, Y.; Guan, Y.; Luo, Y.; Chen, X., Silver nanocluster-embedded zein films as antimicrobial coating materials for food packaging. *ACS Applied Materials & Interfaces* **2017,** *9* (40), 35297-35304.

37. Ertem, E.; Gutt, B.; Zuber, F.; Allegri, S.; Le Ouay, B.; Mefti, S.; Formentin, K.; Stellacci, F.; Ren, Q. Core-shell silver nanoparticles in endodontic disinfection solutions enable long-term antimicrobial effect on oral biofilms. *ACS Applied Materials & Interfaces* **2017,** *9* (40), 34762-34772.

38. Wu, J.; Yu, C.; Li, Q. Novel regenerable antimicrobial nanocomposite membranes: Effect of silver loading and valence state. *Journal of Membrane Science* **2017,** *531*, 68-76.

39. Damm, C.; Münstedt, H.; Rösch, A., Long-term antimicrobial polyamide 6/silver-nanocomposites. *Journal of Materials Science* **2007,** *42* (15), 6067-6073.

40. Wu, J.; Zheng, Y.; Song, W.; Luan, J.; Wen, X.; Wu, Z.; Chen, X.; Wang, Q.; Guo, S., In situ synthesis of silver-nanoparticles/bacterial cellulose composites for slow-released antimicrobial wound dressing. *Carbohydrate Polymers* **2014,** *102*, 762-771.

41. Sathiyaseelan, A.; Saravanakumar, K.; Mariadoss, A. V. A.; Wang, M.-H., Biocompatible fungal chitosan encapsulated phytogenic silver nanoparticles enhanced antidiabetic, antioxidant and antibacterial activity. *International Journal of Biological Macromolecules* **2020,** *153*, 63-71.

42. Zhu, J.; Hou, J.; Zhang, Y.; Tian, M.; He, T.; Liu, J.; Chen, V., Polymeric antimicrobial membranes enabled by nanomaterials for water treatment. *Journal of Membrane Science* **2018,** *550*, 173-197.

43. Perreault, F.; De Faria, A. F.; Elimelech, M., Environmental applications of graphene-based nanomaterials. *Chemical Society Reviews* **2015,** *44* (16), 5861-5896.

44. Schiffman, J. D.; Elimelech, M., Antibacterial activity of electrospun polymer mats with incorporated narrow diameter single-walled carbon nanotubes. *ACS Applied Materials & Interfaces* **2011,** *3* (2), 462-468.

45. Zhu, J.; Wang, J.; Uliana, A. A.; Tian, M.; Zhang, Y.; Zhang, Y.; Volodin, A.; Simoens, K.; Yuan, S.; Li, J., Mussel-inspired architecture of high-flux loose nanofiltration membrane functionalized with antibacterial reduced graphene oxide–copper nanocomposites. *ACS applied materials & interfaces* **2017,** *9* (34), 28990-29001.

46. Gunawan, P.; Guan, C.; Song, X.; Zhang, Q.; Leong, S. S. J.; Tang, C.; Chen, Y.; Chan-Park, M. B.; Chang, M. W.; Wang, K., Hollow fiber membrane decorated with Ag/MWNTs: toward effective water disinfection and biofouling control. *ACS Nano* **2011,** *5* (12), 10033-10040.

47. Yu, Q.; Ista, L. K.; López, G. P., Nanopatterned antimicrobial enzymatic surfaces combining biocidal and fouling release properties. *Nanoscale* **2014,** *6* (9), 4750-4757.

48. Wu, T.; Huang, J.; Jiang, Y.; Hu, Y.; Ye, X.; Liu, D.; Chen, J., Formation of hydrogels based on chitosan/alginate for the delivery of lysozyme and their antibacterial activity. *Food Chemistry* **2018,** *240*, 361-369.

49. Nandi, N.; Gayen, K.; Ghosh, S.; Bhunia, D.; Kirkham, S.; Sen, S. K.; Ghosh, S.; Hamley, I. W.; Banerjee, A., Amphiphilic peptide-based supramolecular, noncytotoxic, stimuli-responsive hydrogels with antibacterial activity. *Biomacromolecules* **2017,** *18* (11), 3621-3629.

50. Costa, F.; Carvalho, I. F.; Montelaro, R. C.; Gomes, P.; Martins, M. C. L., Covalent immobilization of antimicrobial peptides (AMPs) onto biomaterial surfaces. *Acta Biomaterialia* **2011,** *7* (4), 1431-1440.
51. Huang, K.; Nitin, N., Edible bacteriophage based antimicrobial coating on fish feed for enhanced treatment of bacterial infections in aquaculture industry. *Aquaculture* **2019,** *502*, 18-25.
52. Czeslik, C.; Winter, R., Effect of temperature on the conformation of lysozyme adsorbed to silica particles. *Physical Chemistry Chemical Physics* **2001,** *3* (2), 235-239.
53. Lu, J.; Su, T.; Thirtle, P.; Thomas, R.; Rennie, A.; Cubitt, R., The denaturation of lysozyme layers adsorbed at the hydrophobic solid/liquid surface studied by neutron reflection. *Journal of Colloid and Interface Science* **1998,** *206* (1), 212-223.
54. Auddy, B.; Ferreira, M.; Blasina, F.; Lafon, L.; Arredondo, F.; Dajas, F.; Tripathi, P.; Seal, T.; Mukherjee, B., Screening of antioxidant activity of three Indian medicinal plants, traditionally used for the management of neurodegenerative diseases. *Journal of ethnopharmacology* **2003,** *84* (2-3), 131-138.
55. Guleria, S.; Tiku, A.; Gupta, S.; Singh, G.; Koul, A.; Razdan, V., Chemical composition, antioxidant activity and inhibitory effects of essential oil of Eucalyptus teretecornis grown in north-western Himalaya against Alternaria alternata. *Journal of Plant Biochemistry and Biotechnology* **2012,** *21* (1), 44-50.
56. Chouhan, S.; Sharma, K.; Guleria, S., Antimicrobial activity of some essential oils—present status and future perspectives. *Medicines* **2017,** *4* (3), 58.

57. Yang, X.-N.; Khan, I.; Kang, S. C., Chemical composition, mechanism of antibacterial action and antioxidant activity of leaf essential oil of Forsythia koreana deciduous shrub. *Asian Pacific journal of tropical medicine* **2015,** *8* (9), 694-700.

58. Qi, R.; Guo, R.; Zheng, F.; Liu, H.; Yu, J.; Shi, X., Controlled release and antibacterial activity of antibiotic-loaded electrospun halloysite/poly (lactic-co-glycolic acid) composite nanofibers. *Colloids and Surfaces B: Biointerfaces* **2013,** *110*, 148-155.

59. Wu, H.-X.; Tan, L.; Tang, Z.-W.; Yang, M.-Y.; Xiao, J.-Y.; Liu, C.-J.; Zhuo, R.-X., Highly efficient antibacterial surface grafted with a triclosan-decorated poly (n-hydroxyethylacrylamide) brush. *ACS Applied Materials & Interfaces* **2015,** *7* (12), 7008-7015.

60. Devlieghere, F.; Vermeulen, A.; Debevere, J., Chitosan: antimicrobial activity, interactions with food components and applicability as a coating on fruit and vegetables. *Food Microbiology* **2004,** *21* (6), 703-714.

61. Elena, P.; Miri, K., Formation of contact active antimicrobial surfaces by covalent grafting of quaternary ammonium compounds. *Colloids and Surfaces B: Biointerfaces* **2018,** *169*, 195-205.

62. Kohanski, M. A.; Dwyer, D. J.; Collins, J. J., How antibiotics kill bacteria: from targets to networks. *Nature Reviews Microbiology* **2010,** *8* (6), 423-435.

63. Zampieri, M.; Enke, T.; Chubukov, V.; Ricci, V.; Piddock, L.; Sauer, U., Metabolic constraints on the evolution of antibiotic resistance. *Molecular Systems Biology* **2017,** *13* (3), 917.

64. Yang, M.-R.; Chen, K.-S.; Tsai, J.-C.; Tseng, C.-C.; Lin, S.-F., The antibacterial activities of hydrophilic-modified nonwoven PET. *Materials Science and Engineering: C* **2002,** *20* (1-2), 167-173.

65. Zhang, X.; Wang, Z.; Chen, M.; Liu, M.; Wu, Z., Polyvinylidene fluoride membrane blended with quaternary ammonium compound for enhancing anti-biofouling properties: effects of dosage. *Journal of Membrane Science* **2016,** *520*, 66-75.

66. Chen, J.; Wang, F.; Liu, Q.; Du, J., Antibacterial polymeric nanostructures for biomedical applications. *Chemical Communications* **2014,** *50* (93), 14482-14493.

67. Available at https://www.epa.gov/pesticide-registration/what-are-antimicrobial-pesticides, accessed: December 2020.

68. Product Performance Test Guidelines Ocspp 810.2300: Sanitizers for Use on Hard Surfaces Efficacy Data Recommendations. Available at https://www.regulations.gov/document?D=EPA-HQ-OPPT-2009-0150-0022, accessed: December 2020.

69. Verwey, E. J. W., Theory of the stability of lyophobic colloids. *The Journal of Physical Chemistry* **1947,** *51* (3), 631-636.

70. Liu, Y.; Zhao, Q., Influence of surface energy of modified surfaces on bacterial adhesion. *Biophysical Chemistry* **2005,** *117* (1), 39-45.

71. Kohli, R.; Mittal, K. L., Developments in surface contamination and cleaning, Vol. 1: Fundamentals and applied aspects. *William Andrew: USA*, **2015.**

72. Imani, S. M.; Maclachlan, R.; Rachwalski, K.; Chan, Y.; Lee, B.; McInnes, M.; Grandfield, K.; Brown, E. D.; Didar, T. F.; Soleymani, L., Flexible hierarchical wraps repel drug-resistant gram-negative and positive bacteria. *ACS Nano* **2020,***14*, 454-465.

73. Zhang, H.; Chiao, M., Anti-fouling coatings of poly (dimethylsiloxane) devices for biological and biomedical applications. *Journal of Medical and Biological Engineering* **2015,** *35* (2), 143-155.

74. Tuteja, A.; Choi, W.; Mabry, J. M.; McKinley, G. H.; Cohen, R. E., Robust omniphobic surfaces. *Proceedings of the National Academy of Sciences* **2008,** *105* (47), 18200-18205.

75. Lafuma, A.; Quéré, D., Superhydrophobic states. *Nature Materials* **2003,** *2* (7), 457-460.

76. Shirtcliffe, N. J.; McHale, G.; Newton, M. I.; Chabrol, G.; Perry, C. C., Dual-scale roughness produces unusually water-repellent surfaces. *Advanced Materials* **2004,** *16* (21), 1929-1932.

77. Chhatre, S. S.; Choi, W.; Tuteja, A.; Park, K.-C.; Mabry, J. M.; McKinley, G. H.; Cohen, R. E., Scale dependence of omniphobic mesh surfaces. *Langmuir* **2010,** *26* (6), 4027-4035.

78. Nguyen, T. P. N.; Boukherroub, R.; Thomy, V.; Coffinier, Y., Micro-and nanostructured silicon-based superomniphobic surfaces. *Journal of Colloid and Interface Science* **2014,** *416*, 280-288.

79. Vogel, N.; Belisle, R. A.; Hatton, B.; Wong, T.-S.; Aizenberg, J., Transparency and damage tolerance of patternable omniphobic lubricated surfaces based on inverse colloidal monolayers. *Nature Communications* **2013,** *4* (1), 1-10.

80. Ware, C. S.; Smith-Palmer, T.; Peppou-Chapman, S.; Scarratt, L. R.; Humphries, E. M.; Balzer, D.; Neto, C., Marine antifouling behavior of lubricant-infused nanowrinkled polymeric surfaces. *ACS Applied Materials & Interfaces* **2018,** *10* (4), 4173-4182.

81. Kamei, J.; Yabu, H., On‐Demand liquid transportation using bioinspired omniphobic lubricated surfaces based on self‐organized honeycomb and pincushion films. *Advanced Functional Materials* **2015,** *25* (27), 4195-4201.

82. Zhang, R.; Liu, Y.; He, M.; Su, Y.; Zhao, X.; Elimelech, M.; Jiang, Z., Antifouling membranes for sustainable water purification: strategies and mechanisms. *Chemical Society Reviews* **2016,** *45* (21), 5888-5924.

83. S. I. Jeon, J. H. Lee, J. D. Andrade and P. G. De Gennes, Protein—surface interactions in the presence of polyethylene oxide: I. Simplified theory. *Journal of Colloid and Interface Science*, **1991,** *142*, 149-158.

84. Kenausis, G. L.; Vörös, J.; Elbert, D. L.; Huang, N.; Hofer, R.; Ruiz-Taylor, L.; Textor, M.; Hubbell, J. A.; Spencer, N. D., Poly (L-lysine)-g-poly (ethylene glycol) layers on metal oxide surfaces: attachment mechanism and effects of polymer architecture on resistance to protein adsorption. *The Journal of Physical Chemistry B* **2000,** *104* (14), 3298-3309.

85. Michel, R.; Pasche, S.; Textor, M.; Castner, D. G., Influence of PEG architecture on protein adsorption and conformation. *Langmuir* **2005,** *21* (26), 12327-12332.

86. Wu, J.; Lin, W.; Wang, Z.; Chen, S.; Chang, Y., Investigation of the hydration of nonfouling material poly (sulfobetaine methacrylate) by low-field nuclear magnetic resonance. *Langmuir* **2012,** *28* (19), 7436-7441.

87. Shao, Q.; Jiang, S., Molecular understanding and design of zwitterionic materials. *Advanced Materials* **2015,** *27* (1), 15-26.

88. Leng, C.; Sun, S.; Zhang, K.; Jiang, S.; Chen, Z., Molecular level studies on interfacial hydration of zwitterionic and other antifouling polymers in situ. *Acta Biomaterialia* **2016,** *40*, 6-15.

89. Xing, C.-M.; Meng, F.-N.; Quan, M.; Ding, K.; Dang, Y.; Gong, Y.-K., Quantitative fabrication, performance optimization and comparison of PEG and zwitterionic polymer antifouling coatings. *Acta Biomaterialia* **2017,** *59*, 129-138.

90. Chapman, R. G.; Ostuni, E.; Liang, M. N.; Meluleni, G.; Kim, E.; Yan, L.; Pier, G.; Warren, H. S.; Whitesides, G. M., Polymeric thin films that resist the adsorption of proteins and the adhesion of bacteria. *Langmuir* **2001,** *17* (4), 1225-1233.

91. Gref, R.; Lück, M.; Quellec, P.; Marchand, M.; Dellacherie, E.; Harnisch, S.; Blunk, T.; Müller, R., 'Stealth'corona-core nanoparticles surface modified by polyethylene glycol (PEG): influences of the corona (PEG chain length and surface density) and of the core composition on phagocytic uptake and plasma protein adsorption. *Colloids and Surfaces B: Biointerfaces* **2000,** *18* (3-4), 301-313.

92. Su, Y.-L.; Cheng, W.; Li, C.; Jiang, Z., Preparation of antifouling ultrafiltration membranes with poly (ethylene glycol)-graft-polyacrylonitrile copolymers. *Journal of Membrane Science* **2009,** *329* (1-2), 246-252.

93. Hucknall, A.; Rangarajan, S.; Chilkoti, A., In pursuit of zero: polymer brushes that resist the adsorption of proteins. *Advanced Materials* **2009,** *21* (23), 2441-2446.

94. Giroto, J. A.; Teixeira, A. C.; Nascimento, C. A.; Guardani, R., Degradation of poly (ethylene glycol) in aqueous solution by photo-Fenton and H2O2/UV processes. *Industrial & Engineering Chemistry Research* **2010,** *49* (7), 3200-3206.

95. Jiang, S.; Cao, Z., Ultralow-fouling, functionalizable, and hydrolyzable zwitterionic materials and their derivatives for biological applications. *Advanced Materials* **2010,** *22* (9), 920-932.

96. Ma, Y.; Li, J.; Si, Y.; Huang, K.; Nitin, N.; Sun, G., Rechargeable antibacterial N-halamine films with antifouling function for food packaging applications. *ACS Applied Materials & Interfaces* **2019,** *11* (19), 17814-17822.

97. Cao, Z.; Jiang, S., Super-hydrophilic zwitterionic poly (carboxybetaine) and amphiphilic non-ionic poly (ethylene glycol) for stealth nanoparticles. *Nano Today* **2012,** *7* (5), 404-413.

98. Cheng, G.; Li, G.; Xue, H.; Chen, S.; Bryers, J. D.; Jiang, S., Zwitterionic carboxybetaine polymer surfaces and their resistance to long-term biofilm formation. *Biomaterials* **2009,** *30* (28), 5234-5240.

99. Wang, W.; Lu, Y.; Zhu, H.; Cao, Z., Superdurable coating fabricated from a double-sided tape with long term "zero" bacterial adhesion. *Advanced Materials* **2017,** *29* (34), 1606506.

100. Wang, G.; Wang, L.; Lin, W.; Wang, Z.; Zhang, J.; Ji, F.; Ma, G.; Yuan, Z.; Chen, S., Development of robust and recoverable ultralow-fouling coatings based on poly (carboxybetaine) ester analogue. *ACS Applied Materials & Interfaces* **2015,** *7* (31), 16938-16945.

101. Hui, F.; Debiemme-Chouvy, C., Antimicrobial N-halamine polymers and coatings: a review of their synthesis, characterization, and applications. *Biomacromolecules* **2013,** *14* (3), 585-601.

102. Ren, T.; Qiao, M.; Huang, T.-S.; Weese, J.; Ren, X., Efficacy of N-halamine compound on reduction of microorganisms in absorbent food pads of raw beef. *Food Control* **2018,** *84*, 255-262.

103. Si, Y.; Li, J.; Zhao, C.; Deng, Y.; Ma, Y.; Wang, D.; Sun, G., Biocidal and rechargeable N-halamine nanofibrous membranes for highly efficient water disinfection. *ACS Biomaterials Science & Engineering* **2017,** *3* (5), 854-862.

104. Si, Y.; Cossu, A.; Nitin, N.; Ma, Y.; Zhao, C.; Chiou, B. s.; Cao, T.; Wang, D.; Sun, G., Mechanically robust and transparent N-halamine grafted PVA-co-PE films with renewable antimicrobial activity. *Macromolecular Bioscience* **2017,** *17* (3), 1600304.

105. Sun, Y.; Sun, G., Durable and regenerable antimicrobial textile materials prepared by a continuous grafting process. *Journal of Applied Polymer Science* **2002,** *84* (8), 1592-1599.

106. Sun, X.; Cao, Z.; Porteous, N.; Sun, Y., An N-halamine-based rechargeable antimicrobial and biofilm controlling polyurethane. *Acta Biomaterialia* **2012,** *8* (4), 1498-1506.

107. Qian, L.; Sun, G., Durable and regenerable antimicrobial textiles: Synthesis and applications of 3-methylol-2, 2, 5, 5-tetramethyl-imidazolidin-4-one (MTMIO). *Journal of Applied Polymer Science* **2003,** *89* (9), 2418-2425.

108. Chen, Z.; Sun, Y., N-halamine-based antimicrobial additives for polymers: preparation, characterization, and antimicrobial activity. *Industrial & Engineering Chemistry Research* **2006,** *45* (8), 2634-2640.

109. Surana, K.; Chaudhary, B.; Diwaker, M.; Sharma, S., Benzophenone: a ubiquitous scaffold in medicinal chemistry. *MedChemComm* **2018,** *9* (11), 1803-1817.

110. Yi, S.; Zou, Y.; Sun, S.; Dai, F.; Si, Y.; Sun, G., Rechargeable photoactive silk-derived nanofibrous membranes for degradation of reactive red 195. *ACS Sustainable Chemistry & Engineering* **2018,** *7* (1), 986-993.

111. Si, Y.; Zhang, Z.; Wu, W.; Fu, Q.; Huang, K.; Nitin, N.; Ding, B.; Sun, G., Daylight-driven rechargeable antibacterial and antiviral nanofibrous membranes for bioprotective applications. *Science Advances* **2018,** *4* (3), eaar5931.

112. Fang, F. C., Antimicrobial reactive oxygen and nitrogen species: concepts and controversies. *Nature Reviews Microbiology* **2004,** *2* (10), 820-832.

113. Hong, K. H.; Sun, G., Antimicrobial and chemical detoxifying functions of cotton fabrics containing different benzophenone derivatives. *Carbohydrate Polymers* **2008,** *71* (4), 598-605.

114. Hong, K. H.; Sun, G., Photoactive antibacterial cotton fabrics treated by 3, 3′, 4, 4′-benzophenonetetracarboxylic dianhydride. *Carbohydrate Polymers* **2011,** *84* (3), 1027-1032.

115. Hong, K. H.; Sun, G., Poly (styrene-co-vinylbenzophenone) as photoactive antimicrobial and self-decontaminating materials. *Journal of Applied Polymer Science* **2008,** *109* (5), 3173-3179.

116. Jang, J.; Go, W.-S., Continuous photo grafting of HEMA onto polypropylene fabrics with benzophenone photoinitiator. *Fibers and Polymers* **2008,** *9* (4), 375-379.

117. Hong, K. H.; Sun, G., Photoinduced antimicrobial polymer blends with benzophenone as a functional additive. *Journal of Applied Polymer Science* **2009,** *112* (4), 2019-2026.

118. Hong, K. H.; Liu, N.; Sun, G., UV-induced graft polymerization of acrylamide on cellulose by using immobilized benzophenone as a photo-initiator. *European Polymer Journal* **2009,** *45* (8), 2443-2449.

119. Amaly, N.; Ma, Y.; El-Moghazy, A. Y.; Sun, G., Copper Complex formed with Pyridine Rings Grafted on Cellulose Nanofibrous Membranes for Highly Efficient Lysozyme Adsorption. *Separation and Purification Technology* **2020,** 117086.

120. Ma, Y.; Zhang, Z.; Nitin, N.; Sun, G., Integration of photo-induced biocidal and hydrophilic antifouling functions on nanofibrous membranes with demonstrated reduction of biofilm formation. *Journal of Colloid and Interface Science* **2020,** *578*,779-787.

121. Laschewsky, A., Structures and synthesis of zwitterionic polymers. *Polymers* **2014,** *6* (5), 1544-1601.

122. Ozcan, S.; Kaner, P.; Thomas, D.; Cebe, P.; Asatekin, A., Hydrophobic antifouling electrospun mats from zwitterionic amphiphilic copolymers. *ACS Applied Materials & Interfaces* **2018,** *10* (21), 18300-18309.

123. Bengani, P.; Kou, Y.; Asatekin, A., Zwitterionic copolymer self-assembly for fouling resistant, high flux membranes with size-based small molecule selectivity. *Journal of Membrane Science* **2015,** *493*, 755-765.

124. Cao, Z.; Yu, Q.; Xue, H.; Cheng, G.; Jiang, S., Nanoparticles for drug delivery prepared from amphiphilic PLGA zwitterionic block copolymers with sharp contrast in polarity between two blocks. *Angewandte Chemie International Edition* **2010,** *49* (22), 3771-3776.

125. He, M.; Gao, K.; Zhou, L.; Jiao, Z.; Wu, M.; Cao, J.; You, X.; Cai, Z.; Su, Y.; Jiang, Z., Zwitterionic materials for antifouling membrane surface construction. *Acta Biomaterialia* **2016,** *40*, 142-152.

126. Zhang, Z.; Chen, S.; Chang, Y.; Jiang, S., Surface grafted sulfobetaine polymers via atom transfer radical polymerization as superlow fouling coatings. *The Journal of Physical Chemistry B* **2006,** *110* (22), 10799-10804.

127. Zhang, Z.; Vaisocherová, H.; Cheng, G.; Yang, W.; Xue, H.; Jiang, S., Nonfouling behavior of polycarboxybetaine-grafted surfaces: structural and environmental effects. *Biomacromolecules* **2008,** *9* (10), 2686-2692.

128. Zhang, Z.; Chao, T.; Chen, S.; Jiang, S., Superlow fouling sulfobetaine and carboxybetaine polymers on glass slides. *Langmuir* **2006,** *22* (24), 10072-10077.

129. Chen, S.; Zheng, J.; Li, L.; Jiang, S., Strong resistance of phosphorylcholine self-assembled monolayers to protein adsorption: insights into nonfouling properties of zwitterionic materials. *Journal of the American Chemical Society* **2005,** *127* (41), 14473-14478.

130. Li, Q.; Imbrogno, J.; Belfort, G.; Wang, X. L., Making polymeric membranes antifouling via "grafting from" polymerization of zwitterions. *Journal of Applied Polymer Science* **2015,** *132* (21).

131. Chen, S.; Li, L.; Zhao, C.; Zheng, J., Surface hydration: Principles and applications toward low-fouling/nonfouling biomaterials. *Polymer* **2010,** *51* (23), 5283-5293.

132. Leng, C.; Hung, H.-C.; Sun, S.; Wang, D.; Li, Y.; Jiang, S.; Chen, Z., Probing the surface hydration of nonfouling zwitterionic and PEG materials in contact with proteins. *ACS Applied Materials & Interfaces* **2015,** *7* (30), 16881-16888.

133. He, Y.; Hower, J.; Chen, S.; Bernards, M. T.; Chang, Y.; Jiang, S., Molecular simulation studies of protein interactions with zwitterionic phosphorylcholine self-assembled monolayers in the presence of water. *Langmuir* **2008,** *24* (18), 10358-10364.

134. Kondo, T.; Nomura, K.; Gemmei-Ide, M.; Kitano, H.; Noguchi, H.; Uosaki, K.; Saruwatari, Y., Structure of water at zwitterionic copolymer film–liquid water interfaces as examined by the sum frequency generation method. *Colloids and Surfaces B: Biointerfaces* **2014,** *113*, 361-367.

Chapter 2. Rechargeable Antibacterial N-halamine Films with Antifouling Function for Food Packaging Applications

Abstract

Pathogenic microbial contamination from microbial adhesion and subsequent formation of biofilm on surfaces of plastic food packaging materials is a major source of outbreaks of foodborne infections. Conventional strategies in controlling the contaminations are significantly limited either by biofouling of material surfaces or by irreversible consumption of sanitizing agents. Herein, we report a robust methodology to create chlorine rechargeable biocidal poly(vinyl alcohol-co-ethylene) films (SBMA@HAF films) with antifouling function via chemically incorporating both N-halamine (HAF) and zwitterionic (SBMA) moieties. The promise of the design exhibits three features to defend bacteria contaminations: (i) zwitterionic moieties can effectively reduce bacteria adhesion onto the films, (ii) N-halamine with rechargeable biocidal activity can rapidly kill any attached microorganisms, and (iii) any inactivated bacteria debris can be easily released to avoid potential biofilm formation by the superhydrophilic zwitterions. The resulting SBMA@HAF films exhibit integrated properties of high transparency, robust mechanical property, great hydrophilicity, ease of chlorine recharging (>250 ppm), long-term stability, high biocidal efficacy (>99.9999% via contact killing), and promising antifouling functions, enabling the SBMA@HAF films to serve as an ideal biocidal material for food packaging applications.

Objectives

- Proof of concept: covalently combine the chlorine rechargeable halamine and super hydrophilic zwitterion structures onto a plastic film (SBMA@HAF).
- Characterize the physiochemical performances of the obtained SBMA@HAF, including transparency, thermal performance, mechanical property, and hydrophilicity.
- Investigate the optimal chlorination condition, stability, and rechargeability of the loaded active chlorine.

- Apply the contact-killing method to evaluate the killing efficiency of the chlorinated product film.
- Establish standard bacterial resisting and releasing experimental protocols.

2.1 Introduction

Pathogenic microbial contamination and infections through surface contacts of solid materials constitute the forefront of public health concerns.[1,2] This issue was highlighted in a recent review on biofilm related outbreaks and a total of 2536 confirmed listeriosis cases with the highest proportion (8.0 %) of deaths reported in 2016.[3] The conventional strategies responding to this challenge are based on the addition of antimicrobials directly and irreversibly to the food washing water or packaging materials, causing an immediate reduction in the pathogen population.[4,5,6] However, the immediate antibacterial functions usually suffer from significant decline during uses due to the irreversible consumption of the active agents from the materials.[7,8] A rechargeable, especially chlorine rechargeable, antimicrobial material is needed to provide a durable and long-term biocidal function since chlorine water is the most commonly used produce sanitizing agent. Additionally, microbial adhesion onto surfaces and subsequent formation of biofilms are other critical issues for waterborne disease breakout.[9,10,11] These antimicrobials which are useful for planktonic bacteria have limited effect on cleaning biofouling and preventing the formation of biofilm.[12,13] Therefore, more powerful, effective, and durable biocidal and antifouling polymeric materials are highly desirable.

We envision that an ideal material for food packaging applications should possess the following characters: refreshable biocidal activity that can quickly kill microbial pathogens and can be recharged during washing or cleaning processes, and anti-biofouling function that can prevent adhesion of bacterial cells.[14,15] N-halamines, as the forefront of advanced biocidal materials,

possess robust activity to kill bacteria, ease recharging activity, long-term stability, and low toxicity with mild environmental concern.[16,17] N-halamine incorporated polymeric materials would be, in this regard, a great promise to meet the requirements for the production of antibacterial food contact materials.[18,19] However, even though N-halamine can provide the desired rapid and efficient bactericidal functions, the generated bacteria debris can adhere to the surfaces of the halamine materials.[20,21] The attached bacteria debris, combined with adherent bacteria and extracellular polymeric substances (EPS), can form a dense biofilm-biofouling effect, which will physically block the active halamine sites in contact with microorganisms, consequently hindering the biocidal effect.[18,22,23]

Therefore, the addition of a layer of antifouling structures on top of the halamine polymer was considered as an option to reduce the adhesion of the debris. In fact, many attempts to buildi promising antifouling surfaces on polymeric material surfaces have been conducted, including the uses of various chemicals, such as irgarol,[21] diuron,[24] copper/zinc pyrithione,[25,26] and 4,5-dichloro-2-n-octyl-4-iso-thiazolin-3-one (DCOIT)[27]. However, the uses of these agents usually cause severe negative environmental impacts due to their toxicity.[28] Alternatively, zwitterionic compounds, carrying both cationic and anionic groups in one single molecule, can reduce adhesion of biomolecules and microorganisms onto the material surface due to electrostatically induced hydration.[29,30] Zwitterionic polymers, such as polycarboxybetaine, polyphosphorylcholine, and polysulfobetaine, have been wildly reported to have good antifouling performance, great biocompatibility, and environmental friendliness, which are considered as a promising candidate for constructing antifouling materials.[31,32,33]

Herein, we report the development of a novel chlorine rechargeable biocidal and antifouling material by chemically grafting both N,N-diallylmelamine (DAM), a halamine precursor, and [2-

(methacryloyloxy)ethyl]dimethyl-(3-sulfopropyl)ammonium hydroxide (SBMA), a zwitterionic monomer, onto poly(vinyl alcohol-co-ethylene) (PVA-co-PE). The polymer product (PVA-co-PE-DAM-SBMA, also named as SBMA@HAF films) possesses both intrinsically rechargeable N-halamine and chemically bonded zwitterionic moieties and can provide powerful chlorine rechargeable biocidal activity and antifouling efficiency. The produced films exhibited features of: (i) reduced adhesion of microorganisms onto surfaces of the films due to the superhydrophilic effect of the zwitterionic moieties, (ii) chlorine rechargeable biocidal activity to any attached microorganisms due to the existence of N-halamine groups, and (iii) quick release of killed microorganisms to avoid formation of biofilms due to the existence of the zwitterions.

2.2 Experimental Sections

2.2.1 Materials

[2-(Methacryloyloxy)ethyl]dimethyl-(3-sulfopropyl)ammonium hydroxide (SBMA), 3,3',4,4'-benzophenone tetracarboxylic dianhydride (BPTCD), polyphosphoric acid (PPA), tetrahydrofuran (THF), 0.1 N iodine standard solution, 0.1 N sodium thiosulfate standard solution, 1 × M9 minimal salts medium, hydrochloric acid, sodium hydroxide, SYBR® green dye (SG dye), methanol, acetone were purchased from Sigma-Aldrich (Louis, MO, USA) and used without further purification. Luria-Bertani (LB) broth, LB agar, Tryptic soy broth (TSB), and Tryptic soy agar (TSA) were purchased from Thermo Fisher Scientific (Waltham, MA, USA). A Clorox bleach solution with a free chlorine content of 6.0 % was produced by Clorox Co., Ltd. (Oakland, CA, USA). Phosphate buffer saline (PBS) was obtained from USB Co., Ltd. (Cleveland, OH, USA).

2.2.2 Immobilization of photoinitiator

BPTCD (5 wt %) and PPA (1 wt %) were dissolved in THF with continuous stirring at 50°C, and then, HAF films, produced according to a previously reported procedure,[18] were completely immersed into the as-prepared solution. After 5 minutes, the HAF films were taken out and dried at ambient temperature for 1 hour. The obtained HAF films were cured at 120°C for 3 minutes. Then, the BPTCD-reacted HAF films (HAF+BPTCD films) were washed with deionized water and acetone alternately to remove nonchemically bonded BPTCD and stored in dark conditions.

2.2.3 Preparation of SBMA@HAF films

SBMA@ HAF films were obtained via a photoinduced graft polymerization. HAF+BPTCD films were soaked into 3 wt % of SBMA solution (100% methanol as a solvent) for 1 hour. A vacuum oven was employed to remove the solvent, and the obtained films were exposed to a UVA (365 nm) light for 10 minutes per each side of the film at room temperature. The resulted SBMA@HAF films were washed with acetone and vacuum dried.

2.2.4 Chlorination of SBMA@HAF films

A chlorination solution containing 1 wt% of active chlorine was prepared by diluting the Clorox bleach solution. The pH of the chlorination solutions were adjusted via the addition of hydrochloric acid or sodium hydroxide. In a typical chlorination process, the SBMA@HAF films were immersed completely in a chlorination solution with gentle shaking for the desired time. Subsequently, the films were washed with a large quantity of deionized water to remove any free active chlorine and then dried in the air. For a chlorine rechargeability test, the sample films were first charged with chlorination solution for 1 hour, and then the active chlorine on the films was quenched by an excess amount of sodium thiosulfate solution (0.001 N) for 1 hour. To determine the content of active chlorine, an established iodometric titration method was adopted. Typically,

0.500 g of chlorine charged SBMA@HAF films were immersed into 15.00 mL of 0.001 N sodium thiosulfate solution ($Na_2S_2O_3$). All active chlorine on the sample films could be quenched by $Na_2S_2O_3$, and the residual $Na_2S_2O_3$ was titrated by a 0.001 N iodine standard solution. The active chlorine content (ppm) of the SBMA@HAF films was calculated according to the equation: $34.45 \times (V_o - V_s)N \times 500 / m_s$, where V_o and V_s are the volume (mL) of the iodine solution consumed in titration without and with chlorine charged SBMA@HAF films, respectively. m_s is the weigh (g) of the charged SBMA@HAF films. Data are expressed as the mean ± SD of three replicates. 2.2.5

Incubation of bacterial cultures

Bactericidal experiments were performed on two typical etiological bacteria, Gram-negative *Escherichia coli* O157: H7 (ATCC 700728, *E. coli*) and Gram-positive *Listeria innocua* (ATCC 33090, *L. innocua*). A colony of *E. coli* was cultured in 10 mL of LB broth at 37ºC for 24 hours at 150 rpm. A bacterial culture with an absorbance at 600 nm of 0.4 (2×10^8 CFU mL^{-1} assessed by plate count) was used for the following experiments. *L. innocua* was grown in 10 mL of TSB and allowed to incubate at 30ºC with a shaking speed of 150 rpm until it reached an absorbance at 600nm of 1.5 (1×10^9 CFU mL^{-1} assessed by plate count) and used for the following experiments.

2.2.6 Antimicrobial assays against *E. coli* and *L. innocua*

In a typical experiment, 10 μL of the bacterial (*E. coli* or *L. innocua*) suspension was spotted on the surfaces of control samples (unchlorinated HAF@SBMA films), chlorinated HAF films or chlorinated HAF@SBMA films in a size of 1×1 cm^2, and then, the samples were incubated inside a plastic petri dish for 0, 5, 10, 15, 30, and 60 min. At each time point, the bacteria on the sample were harvested by vortexing with 1 mL PBS buffer, and the bacterial suspensions were serially diluted by 10^1, 10^2, 10^4 and 10^6 times, respectively. A standard plate count method was adopted,

whereby the diluted bacteria suspensions were plated on LB agar (*E. coli*) and TSA agar (*L. innocua*), respectively. The plates were incubated overnight at 37ºC before quantification of the number of CFU to determine the survived organisms. For the cyclic antimicrobial assays, the films contacted with the bacteria were charged with chlorination solution for 1 hour to refresh the biocidal activity.

2.2.7 Bacterial resisting and releasing behavior

For bacterial resistance test, a 1 mL bacterial (*E. coli* or *L. innocua*) suspension (10^8 CFU mL^{-1} in a 10 wt % of 1 × M9 minimal salts medium) was incubated with the unchlorinated HAF films (control films) and unchlorinated SBMA@HAF films (sample films) in a size of 1 × 1 cm^2 for 24 hours in the dark. After incubation, the films adhered with bacteria were gently rinsed for 10 seconds by 5 mL of fresh PBS buffer (to remove planktonic bacteria). Then, the obtained sample films with bacteria attached on were dried in the air and processed for the next tests.

In a typical bacterial releasing test, 10 μL of bacterial (*E. coli* or *L. innocua*) suspension (10^8 CFU ml^{-1} in water) was dropped onto the surface of unchlorinated HAF films or unchlorinated SBMA@ HAF films (1 × 1 cm^2), and the films were allowed to dry for 1 hour. (fixation of bacteria on the surface). The samples were then incubated with 1 mL of fresh PBS in test tubes for a certain duration. At each time point, the bacteria released from the film samples were harvested by vortexing the sample for 10 seconds, and the suspension was serially diluted ($\times 10^1$, $\times 10^3$, and $\times 10^5$) and plated on LB agar (E. *coli*) and TSA ager (*L. innocua*) for the bacteria enumeration.2.2.8 SEM images and fluorescence microscopy

For the SEM imaging, the films attached with bacteria or free bacteria were fixed at 4ºC overnight with 2.5 wt % of glutaraldehyde. Then, the samples were rinsed with 95 wt % of ethanol.

Subsequently, the samples were soaked in 1 wt % of OsO4 solution for 30 min and dehydrated by sequential ethanol /water mixtures with increasing ethanol content of 25, 50, 75, 90, and 100%, respectively. Finally, the samples were placed on a silver tape and coated with palladium before SEM analysis.

For the fluorescence microscope imaging, following the releasing and resisting tests, 10 μL of SG fluorescence DNA dye with a concentration of 5 μg mL^{-1}, a cell-permeant dye, were spotted on the surface of the control films (HAF films) and sample films (unchlorinated SBMA@HAF films), and then incubated in dark for 15 min at room temperature. Finally, the films were placed on a microscope slide and examined using a laser scanning confocal microscope (Olympus FV1000) with an FITC (ex 490 nm/em 525 nm) filter.

2.2.9 Characterizations of films

Field emission scanning electron microscopy (FE-SEM) images and Energy-dispersive X ray (EDX) scanning electron microscopy mappings were examined by a Philips FEI XL30. FT-IR spectra were collected with a Nicolet 6700 spectrometer in the range of 750-2000 cm^{-1}. DSC spectra were conducted via a Shimadazu DSC-60 differential scanning calorimeter with a heating rate of 5^{o}C min^{-1}. UV-vis transmittance spectra were processed with a Thermo Scientific Evolution 600 spectrophotometer. Surface wettability of films was assessed by measuring the static water contact angles (10 μL) using a goniometer Kino SL200B. Tensile-strain tests were performed using Intron 5565 testing system equipped with 5000-N load cells.

2.2.10 Statistical analysis and quantitative data analysis

Statistical analysis was performed using the SPSS Statistics software (version 24, IBM SPSS, Chicago, IL, USA) to evaluate the measurement sets of obtained data. All the experiments were

performed in triplicates. A one- or two-way analysis of variance was used to determine the significant differences among the values of the selected measurements ($p < 0.05$).

2.3 Results and Discussion

2.3.1 Design and preparation of SBMA@HAF films

The renewable biocidal activity has already been achieved in a previous study, and high-strength N-halamine (diallylmelamine, DAM) modified poly(vinyl alcohol-co-ethylene) films (PVA-co-PE-DAM, also named as HAF films) with renewable antimicrobial activity were prepared by using a radical graft polymerization through reactive extrusion technique.[18] We would like to take the unique halamine polymers as raw materials to chemically incorporate hydrophilic zwitterionic compounds onto the surfaces of the HAF films.

To demonstrate the speculated functions of the zwiterionic structures, a commercially available zwitterion, [2-(methacryloyloxy)ethyl]dimethyl-(3-sulfopropyl)ammonium hydroxide (SBMA), was grafted onto surfaces of the HAF films via a photo-induced radical graft polymerization process (Figure 2.1a and 2.1b). SBMA contains a vinyl group that is capable of reacting with the PVA-co-PE-DAM via free radical graft polymerization. Benzophenone tetracarboxylic dianhydride (BPTCD) is a photo-sensitizer with acid anhydride groups to react with hydroxyl groups on the HAF, obtaining HAF+BPTCD films (Figure 2.1a).[34] Under ultraviolet irradiation at 365 nm (UVA) wavelength, excited triplet BPTCD molecules could abstract hydrogen atoms from tertiary C-H bonds or amino groups on the HAF, resulting in the formation of polymeric radicals (potentially at tertiary carbon, amino groups on the melamine structures and even the carbonyl carbon on the BPTCD, respectively). Then, these radicals could initiate graft polymerization of SBMA monomers onto the surfaces of the HAF films (Figure 2.1b).

Figure 2.1c displays a schematic biocidal and antifouling behavior of SBMA@HAF films against pathogenic microbes. Once the pathogens are approaching the surfaces of the SBMA@HAF films, the grafted zwitterionic SBMA groups make the microorganism difficult to adhere; any live bacteria attached on the surface of the films could be immediately killed by the halamine groups. Furthermore, any resulting cell debris could be easily removed from the film surface in aqueous solutions, due to the super hydrophilic feature of the zwitterionic SBMA moieties on the film surfaces.

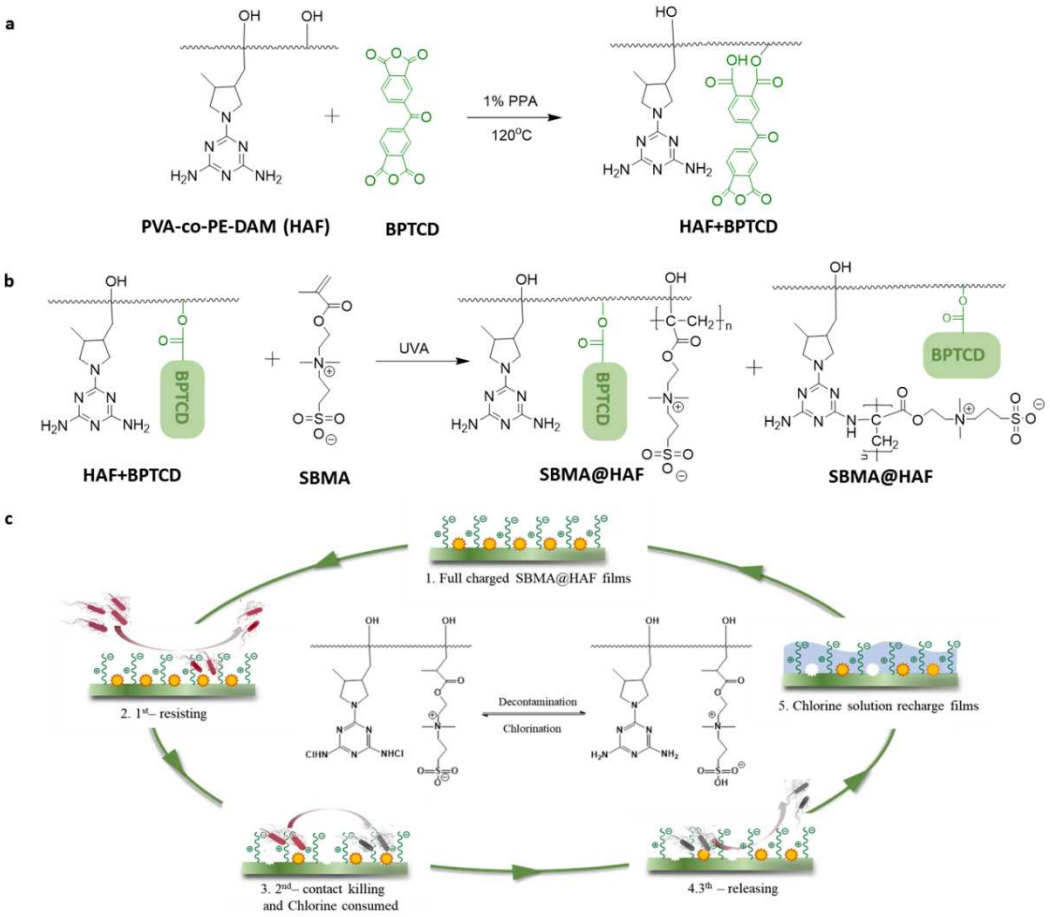

Figure 2.1. **(**a) Esterification reaction of HAF films with BPTCD. (b) Photo initiated graft polymerization reactions of HAF+BPTCD films with SBMA. (c) Schematic drawing of the resisting, biocidal, releasing, and rechargeable biocidal functions of SBMA@HAF films. The inset

image shows the chlorination of N-halamine precursors and decontamination of the N-halamine moieties of SBMA@HAF films.

2.3.2 Structural characterization and properties of SBMA@HAF films

A final product, SBMA@HAF film, was finally produced through the above described processes, the film is basically transparent and mechanically stable (Figure 2.2a). Fourier transform infrared (FT-IR) spectra provided the evidence of the successful incorporation of SBMA onto the films (Figure 2.2b). The new peaks at 1346 and 1184 cm^{-1} in the SBMA@HAF films were assigned to stretching vibrations of sulfonate groups.[35] Energy-dispersive X ray (EDX) scanning electron microscopy mapping of on the SBMA@HAF surfaces further authenticated the presence of sulfate element which is the characteristic element of the SBMA monomer (Figure 2.2c), confirming its uniform distribution on surfaces of the films. Furthermore, the elemental abundance spectra (Figure 2.2d) ascertained the presence of sulfate groups. Atomically, 1.7 % of S element could be found based on EDX quantitative analysis, indicating the high grafting efficiency of SBMA onto the PVA-co-PE-DAM films by the photo-induced radical graft polymerization reaction.

Physiochemical performances of the SBMA@HAF films, including optical, hydrophilic, thermal and mechanical properties, were evaluated to justify the potential applications of the films as food packaging or contact materials. As shown in Figure 2.2e, only a 5% decrease in transparency between HAF and SBMA@HAF films was observed over the visible wavelength range. And they remained over 80% of the original transmittance of PVA-co-PE films. Robust hydrophilicity provides benefits for good contact with common microorganisms, which could effectively enhance the biocidal ability of the SBMA@HAF films.[36,37,38] Figure 2.2f exhibited the hydrophilicity of the original PVA-co-PE and the modified films. The pristine PVA-co-PE films with numerous hydroxyl groups on the polymer chain exhibited good hydrophilicity with a water contact angle

(WCA) of 60°. After modification with DAM monomer, the hydrophilicity was further improved, and the WCA decreased to 40°, due to the presence of amino groups. The hydrophilicity of the SBMA@HAF films was further increased with a WCA reduced to 24° due to the addition of the zwitterionic groups on the surfaces of the polymer films.

Thermal stability is another important feature for food packaging materials. As shown in Figure 2.2g, the differential scanning calorimetry (DSC) analyses revealed that the typical melting points of HAF, HAF+BPTCD, and SBMA@HAF films were around 160 °C, almost unchanged from the original PVA-co-PE. A new peak appearing around 285°C could be attributed to the decomposition of grafted SBMA structure on the films, which was also proved by TGA results (Figures 2.2 h). There are two distinct weight loss stages: (1) the initial weight loss stage in the range of 280-380°C, due to the degradation of the grafted chemical structure (BPTCD, and SBMA), and (2) the second stage in the range of 380-500°C corresponding to the polymer mainchain degradation. Overall, the HAF films exhibited good thermal stability without any weight loss below 250 °C, and the SBMA@HAF films resulted in more residues at 500 °C, due to the presence of the SBMA moieties.

Moreover, strong mechanical property is one of the most important requirements of food packaging materials.[39,40] As shown in Figure 2.2i, the tensile stress-strain curves of the HAF, HAF+BPTCD, and SBMA@HAF films exhibited similar patterns with similar Young's moduli and yield points, except varied breaking strains. The increase in the breaking strain of the HAF+BPTCD films may be due to the partial loss of hydrogen bonds caused by formed ester bonds with BPTCD. After the photo-induced radical reactions with SBMA, the obtained SBMA@HAF became more brittle with a decreased breaking strain of 13% because of potential crosslinking of the polymers during the photo-induced graft polymerization.

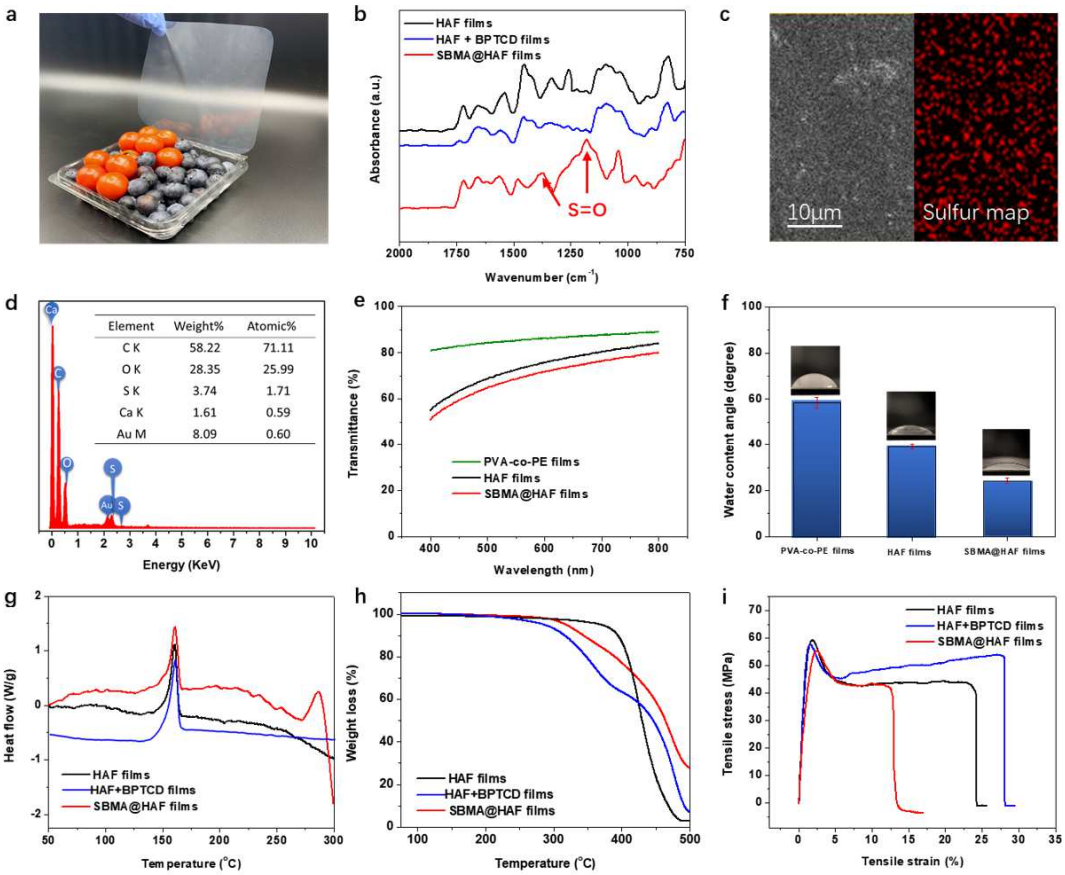

Figure 2.2. **(**a) Optical image of a SBMA@HAF film with the thickness of 0.05 mm. (b) FT-IR spectra of HAF, HAF+BPTCD and SBMA@HAF films, (c) EDX-SEM sulfur mapping and (d) EDX results of SBMA@HAF films, (e) UV-vis transmittance spectra and (f) water contact angles of PVA-co-PE film, HAF films, and SBMA@HAF films, (g) DSC curves and (h) TGA curves of HAF, HAF+BPTCD, and SBMA@HAF films, and (i) Tensile stress-strain curves of HAF, HAF+BPTCD, and SBMA@HAF films.

2.3.3 Rechargeable chlorination of SBMA@HAF films

The SBMA@HAF films possess chlorine chargeable biocidal functions, which could be implemented by soaking in a diluted household bleach solution containing about 1500 ppm of active chlorine. The active chlorine contents of the chlorinated SBMA@HAF films prepared from

varied reaction times and pH values of the chlorination solutions were determined via an iodometric titration method. Figure 2.3a demonstrated the active chlorine contents of the films as a function of chlorination times. With the increase of the time, the active chlorine contents of the SBMA@HAF exhibited two characteristic regions; a rapid increase in the first 1 hour, reaching a chlorine content of 232 ppm, and then a slow increase when chlorination time was extended to 6 hours, reaching a saturated active chlorine content of 284 ppm. With such a high active chlorine content in the films, a rapid and powerful biocidal activity could be expected from the SBMA@HAF films.

The chlorination of halamine precursors such as amine or amide bonds are affected by pH conditions of chlorination solutions. Thus, the SBMA@HAF films were chlorinated in diluted chlorine bleach solution with controlled pH conditions. Due to the structure of amino groups in PVA-co-PE-DAM, the amino groups could become $-NH_3^+$ at low pH, preventing the conversion of amino to N-halamine (NH-Cl). But on the other side, the weak hypochlorous acid (HOCl) is more effective than (-OCl) in the chlorination system to produce N-halamine (NH-Cl)[18]. As shown in Figure 2.3b, the active chlorine contents on the polymer films were highly pH dependent with a maximum value achieved at a neutral pH of 6, which is consistent with the pKa values of $-NH_3^+$ (pKa = 5.0) on melamine and HOCl (pKa = 7.53) in the solution. Under very acidic or basic conditions, only less than 150 ppm of active chlorine content was achieved on the SBMA@HAF films.

The durability of biocidal functions of the films was also evaluated for prolonged storage without chlorine recharging. As shown in Figure 2.3c, both the HAF and the SBMA@HAF films were stable and retained over 90% of original active chlorine contents after stored for fifteen days. This good stability of the N-halamine structure is mainly caused by the film structure with limited

surface areas. And the added SBMA moieties did not influence the stability of the N-halamine chemical structure. Moreover, the SBMA@HAF films demonstrated robust rechargeability of the functional N-halamine structure and biocidal activity. Repeated recharging and reducing agent quenching tests were conducted with results displayed in Figure 2.3d. For each cycle, the film was first chlorinated for 1 hour at an optimized chlorination condition and then was fully quenched with an excess amount of thiosulfate solutions (0.001 N) for 1 hour. Afterward, the film was chlorinated again under the same chlorination condition. This process was repeated ten times. The active chlorine contents of both HAF films and SBMA@HAF films were nearly unchanged up to 10 repeated quenching/recharging cycles, which could be attributed to the stable covalent bonding between N-halamine and polymer backbones that was not influenced by the addition of the SBMA moieties.

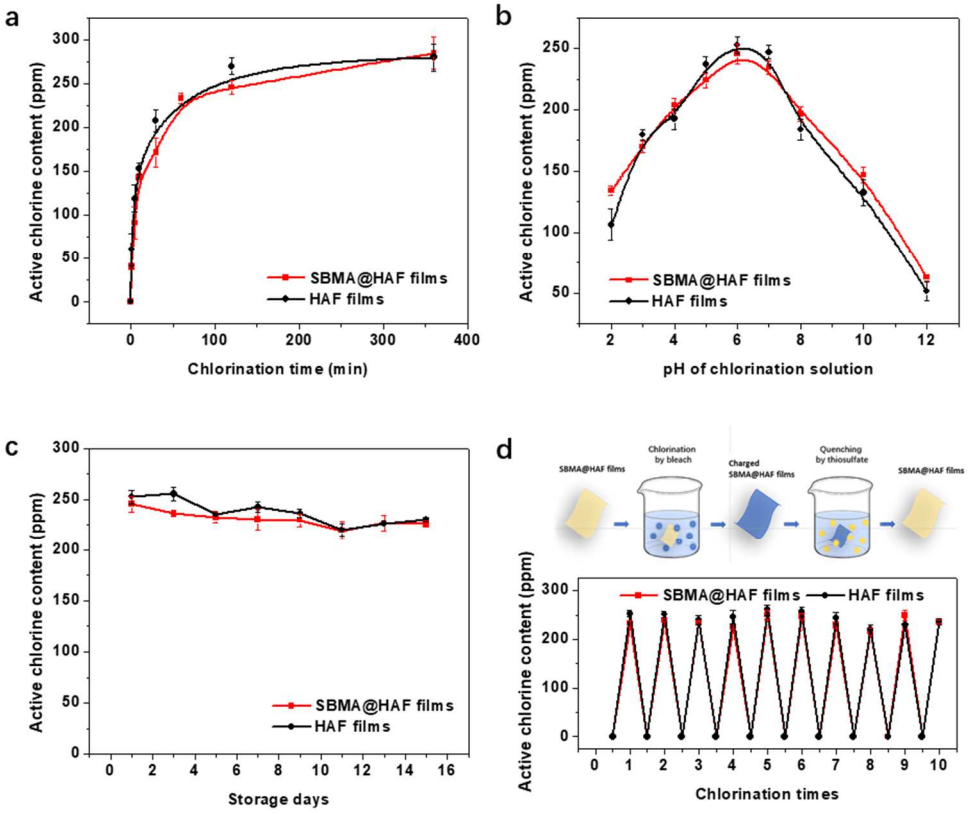

Figure 2.3. Active chlorine contents of SBMA@HAF films and HAF films as a function of (a) chlorination time and (b) pH condition of chlorination solutions. (c) The change of active chlorine content against storage time. (d) The active chlorine content of SBMA@HAF films and HAF films with 10 times of chlorination-quenching cycle tests.

2.3.4 Contact killing of bacteria

To evaluate the biocidal activity of the SBMA@HAF films, two typical pathogenic foodborne bacteria, Gram-negative *Escherichia coli* O157: H7 and Gram-positive *Listeria innocua*, were applied to challenge the films. For the contact-killing assay, control films (unchlorinated SBMA@HAF films), chlorinated HAF, and chlorinated SBMA@HAF films with a size of 1 × 1 cm^2 were loaded with 10 μL of 1 × 10^8 colony-forming units (CFU) bacteria suspensions. Figures 2.4a and 2.4d exhibit the time-dependent antimicrobial effect of the SBMA@HAF films. The control films did not provide any noticeable reduction of bacteria even after 1 hour of contact. In contrast, both chlorinated HAF and SBAM@HAF films showed 6 logs of reduction of *E. coli* and *L. innocua* within 1-hour contact. In addition, the chlorinated SBMA@HAF films achieved a 6 log reduction in 15 minutes of contact for both *E. coli* and *L. innocua*, which were nearly 3 times faster than that of the chlorinated HAF film in killing speed. As discussed before, the grafted SBMA structure increased the hydrophilicity of the films, with reduced WCA of 23^o. The improved hydrophilicity of the films ensured better contact with bacteria, resulting in faster biocidal functions of the films.

The rechargeable N-halamine structure is responsible for the renewable biocidal performance of the SBMA@HAF films against bacteria. As shown in Figures 2.4b and 2.4e, three cycles of contact killing tests revealed consistent 3-5 log reductions of *E. coli* with a 15-minutes contact each time.

And the biocidal efficacy was nearly unchanged with a 6 log reduction of *L. innocua* in these three contacts, highlighting the robust refreshable biocidal activity of the SBMA@HAF films.

The biocidal functions of the chlorinated SBMA@HAF films should result in complete inactivation of the microorganism instead of only knocking them down. To prove such a fact, we investigated the morphological changes of bacterial cells after being in contact with the chlorinated SBMA@HAF films. As shown in Figures 2.4c and 2.4f, both *E. coli* and *L. innocua,* after contacting with the control films for 15 mins, remained with their intact cell structure, with a smooth surface. However, cellular deformation and the surface collapse of bacterial cells can be clearly observed from the bacteria cells after exposure to the chlorinated SBMA@HAF films for 15 minutes. Some of the bacterial cells were lysed and become fragmented on the film surface. These results exhibited the robust biocidal function of the N-halamine films, but also brought a concern on the potential formation of biofilm by physical attachment of bacteria cell debris, which could block the active halamine surfaces and lead to biofouling on the films.

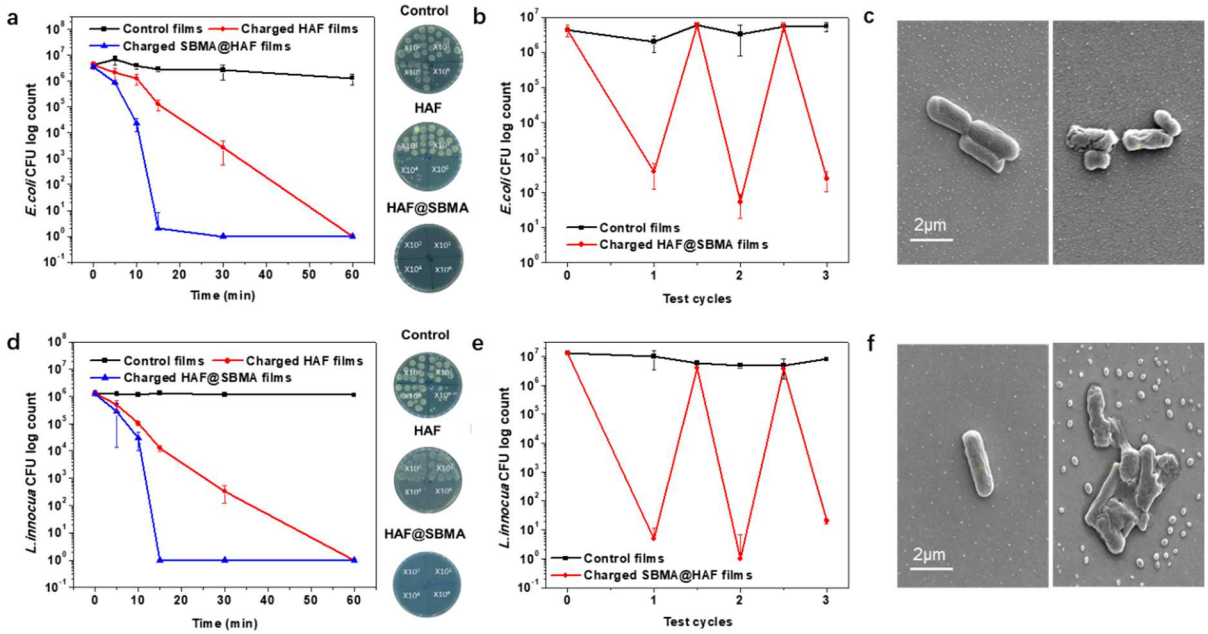

Figure 2.4. Antimicrobial activities of control films (unchlorinated SBMA@HAF films), chlorinated HAF and SBMA@HAF films against: (a) *E. coli* and (d) *L. innocua*, respectively. The right images exhibit viable bacteria on agar plates after 15-min exposure. Three repeated chlorination-decontamination tests of chlorinated SBMA@HAF films against: (b) *E. coli* and (e) *L. innocua,* FE-SEM images of (c) *E. coli* and (f) *L. innocua* before and after exposing to control films and chlorinated SBMA@HAF films for15 mins.

2.3.5 Antifouling functions of SBMA@HAF films

The grafted zwitterionic groups should bring expected resistance to bacterial adhesion and easy release of any surface attached microorganisms, which were examined by using the unchlorinated SBMA@HAF films with both *E. coli* and *L. innocua*, respectively. To test the resistance to bacteria adhesion, the films were incubated in steady bacteria suspensions for 24 h, and then rinsed with fresh PBS to remove planktonic bacteria. SEM images of the films were obtained to determine the morphology change and the distribution of bacteria on the film surfaces. Compared with the HAF film surfaces, an obvious bubble-like structure was observed on the SBMA@HAF film surface, which could be attributed to the surface modifications and superficial swelling of the hydrophilic films (Figure 2.5a). As shown in Figures 2.5b and 2.5c, numerous bacteria cells can be observed on the surface of the HAF films, while only a few of them can be observed on the surfaces of the SBMA@HAF for both *E. coli* and *L. innocua*. These observations were also supported by the results of bacterial fluorescence staining results. The bacteria in contact with films were first rinsed and stained with a cell-permeant SYBG Green (SG) dye, which can stain the nucleic acid of both living and dead bacteria cells. The quantitative data of relevant samples presented in Figure 2.5f (one-way analysis of variance (ANOVA) with $\alpha = 0.05$). The zwitterion film surface of the SBMA@HAF showed an extremely low bacterial population of $(2.4 \pm 0.3) \times 10^5$ (*E. coli*) and (4.3

± 0.2) x 10^5 (*L. innocua*) cells/cm^2 (representative images are shown in Figures 2.5d and 2.5e), a reduction of around 85 % bacterial adhesion compared with the HAF films. This is a significant difference in antifouling functions between the HAF films and the SBMA@HAF films ($p < 0.15$), which implied that the existing SBMA structures on the film surface could effectively prevent bacterial adhesion and reduce bio-film formation.

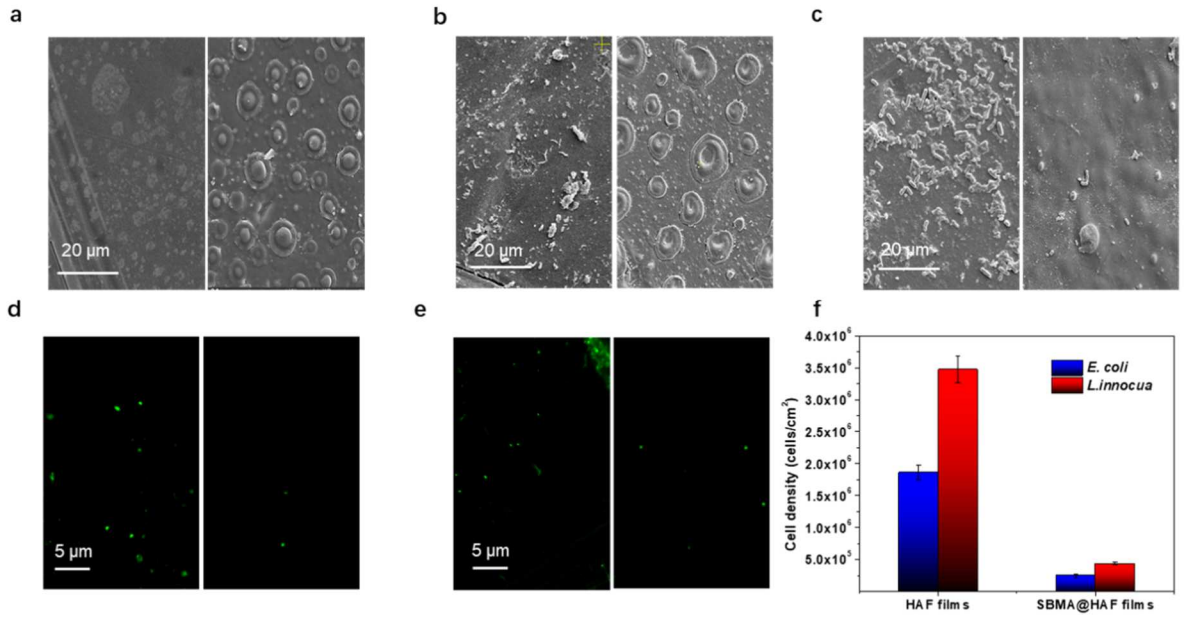

Figure 2.5. (a) FE-SEM images of HAF (left) and SBMA@HAF (right) films. FE-SEM images of unchlorinated HAF (left) and SBMA@HAF (right) films after incubating with (b) *E. coli* and (c) *L. innocua* suspensions, respectively; SG stained fluorescence microscopy images of unchlorinated HAF (left) and SBMA@HAF (right) film surfaces after incubating with (d) *E. coli* and (e) *L. innocua* suspensions, respectively. (f) Bacterial cell density of *E. coli* and *L. innocua* attached on the unchlorinated surfaces after incubating with bacteria suspensions for 24 h (resisting).

The bacterial cell releasing behavior of the SBMA@HAF films was further investigated. The film surfaces were loaded with 10 μL of 10^8 CFU ml^{-1} *E. coli* and *L. innocua* suspensions, respectively.

After incubation for certain times and vortexing, successfully released bacterial proliferations from the film samples were assessed by using agar plate counting. Figures 2.6a and 2.6e depict the time-dependent bacterial-releasing effects of both HAF and SBMA@HAF films. It was found that the HAF film showed a slower bacterial releasing speed, which required 60 mins to release 6 log CFU of bacteria. In contrast, the SBMA@HAF films showed more effective bacterial releasing behavior, achieving 6 log releasing of *E. coli* and *L. innocua* in 15-min releasing time, which was three times faster than that of the HAF films in releasing adhered bacteria. To gain straightforward insight of the bacteria-releasing function of the SBMA@HAF films, we investigated the bacterial populations on the film surfaces before/after 15 min releasing process. As shown in Figures 2.6b and 2.6f, after 15 min release test, numerous bacteria still can be observed on the HAF film surfaces. Comparatively, the SBMA@HAF films were capable of releasing most of the bacteria with little bacteria left on the surface. The bacterial fluorescence dye staining test was performed to further visibly prove the bacteria-releasing behavior of the films (quantitative data in Figure 2.6c and 2.6g one-way analysis of variance (ANOVA) with $\alpha = 0.05$); The images in Figures 2.6d and 2.6h reveal the most intense fluorescence signals on the HAF surfaces. The SBMA@HAF films showed weak fluorescence signals compared with the HAF films with 95% of the bacteria (both *E. coli* and *L. innocua*) were released from the SBMA@HAF film surface. The resulted residual bacterial populations on the film surfaces were $(4.3 \pm 2.4) \times 10^6$ (*E. coli*) and $(2.0 \pm 0.3) \times 10^7$ (*L. innocua*) cells/cm^2, respectively. In sharp contrast, the HAF films only released 75% and 50% coated *E. coli* and *L. innocua,* respectively. The significant differences between the HAF films and the SBMA@HAF films proved the success in the development of biocidal and antifouling films for food packaging applications.

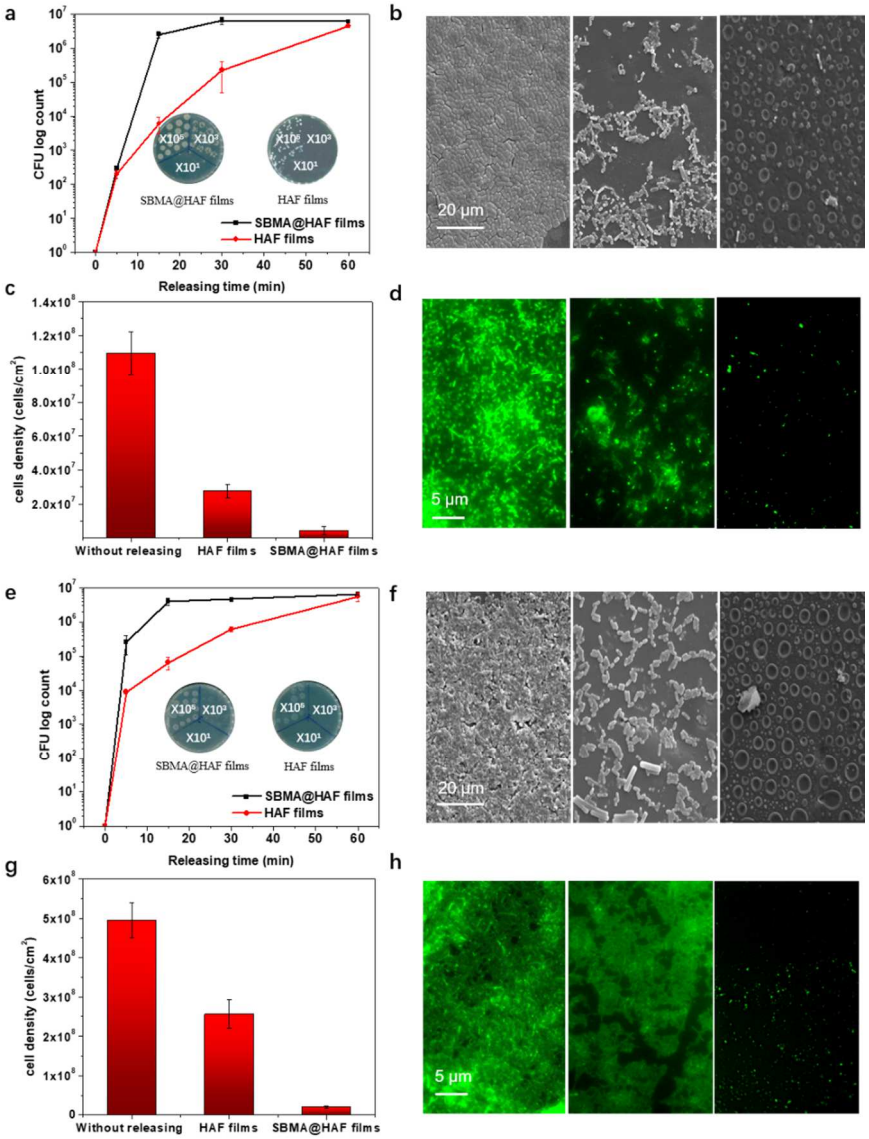

Figure 2.6. Releasing behavior of unchlorinated HAF and SBMA@HAF films against (a) *E. coli* and (e) *L. innocua* via the plate-counting method. The insert images exhibit the plate-counting results 15 min after releasing. (b) FE-SEM images and (d) SG-stained fluorescence microscopy images of *E. coli* 15 min before and after releasing on unchlorinated HAF and SBMA@HAF films. (f) FE-SEM images and (h) SG-stained fluorescence microscopy images of *L. innocua* 15 min before and after releasing on unchlorinated HAF and SBMA@HAF films. Bacterial cell density of (c) *E. coli* and (g) *L. innocua* on the unchlorinated surfaces before and after releasing procedure.

2.4 Conclusions

In summary, we demonstrated a scalable strategy for fabrication of rechargeable biocidal and antifouling materials via radical graft polymerization modifications of poly(vinyl alcohol-co-ethylene). The incorporated N-halamine moieties provided chlorine rechargeable biocidal functions, and the addition of the zwitterionic structure (SBMA) to the surface resulted in robust antifouling properties of the polymer films. With high transparency, robust mechanical property, great hydrophilicity, and rechargeable high chlorine capacity, the obtained chlorinated SBMA@HAF films exhibited good biocidal efficacy, long-term stability, and significantly antifouling performance. These attributes enabled the potential use of SBMA@HAF films to serve as a food packaging material that can meet the challenging requirements for reduced microbial contamination and improved produce safety.

2.5 References

1. Rumbo, C.; Tamayo-Ramos, J. A.; Caso, M. F.; Rinaldi, A.; Romero-Santacreu, L.; Quesada, R.; Cuesta-López, S., Colonization of electrospun polycaprolactone fibers by relevant pathogenic bacterial strains. *ACS Applied Materials & Interfaces* **2018,** *10* (14), 11467-11473.
2. Heiranian, M.; Farimani, A. B.; Aluru, N. R., Water desalination with a single-layer MoS_2 nanopore. *Nature Communications* **2015,** *6*, 8616.
3. Galiè, S.; García-Gutiérrez, C.; Miguélez, E. M.; Villar, C. J.; Lombó, F., Biofilms in the food industry: health aspects and control methods. *Frontiers in Microbiology* **2018,** *9*, 898.
4. Kashiri, M.; Cerisuelo, J. P.; Domínguez, I.; López-Carballo, G.; Muriel-Gallet, V.; Gavara, R.; Hernández-Muñoz, P., Zein films and coatings as carriers and release systems of Zataria multiflora Boiss. essential oil for antimicrobial food packaging. *Food Hydrocolloids* **2017,** *70*, 260-268.
5. Mei, L.; Teng, Z.; Zhu, G.; Liu, Y.; Zhang, F.; Zhang, J.; Li, Y.; Guan, Y.; Luo, Y.; Chen, X., Silver nanocluster-embedded zein films as antimicrobial coating materials for food packaging. *ACS Applied Materials & Interfaces* **2017,** *9* (40), 35297-35304.
6. Makaremi, M.; Pasbakhsh, P.; Cavallaro, G.; Lazzara, G.; Aw, Y. K.; Lee, S. M.; Milioto, S., Effect of morphology and size of halloysite nanotubes on functional pectin bionanocomposites for food packaging applications. *ACS Applied Materials & Interfaces* **2017,** *9* (20), 17476-17488.
7. Gaw, S. L.; Sarkar, S.; Nir, S.; Schnell, Y.; Mandler, D.; Xu, Z. J.; Lee, P. S.; Reches, M., Electrochemical approach for effective antifouling and antimicrobial surfaces. *ACS Applied Materials & Interfaces* **2017,** *9* (31), 26503-26509.
8. Bano, I.; Arshad, M.; Yasin, T.; Ghauri, M. A.; Younus, M., Chitosan: A potential biopolymer

for wound management. *International Journal of Biological Macromolecules* **2017,** *102*, 380-383.

9. Nguyen, T.-K.; Lam, S. J.; Ho, K. K.; Kumar, N.; Qiao, G. G.; Egan, S.; Boyer, C.; Wong, E. H., Rational design of single-chain polymeric nanoparticles that kill planktonic and biofilm bacteria. *ACS Infectious Diseases* **2017,** *3* (3), 237-248.
10. Yan, J.; Nadell, C. D.; Stone, H. A.; Wingreen, N. S.; Bassler, B. L., Extracellular-matrix-mediated osmotic pressure drives Vibrio cholerae biofilm expansion and cheater exclusion. *Nature Communications* **2017,** *8* (1), 327.
11. Teschler, J. K.; Zamorano-Sánchez, D.; Utada, A. S.; Warner, C. J.; Wong, G. C.; Linington, R. G.; Yildiz, F. H., Living in the matrix: assembly and control of Vibrio cholerae biofilms. *Nature Reviews Microbiology* **2015,** *13* (5), 255.
12. Cossu, A.; Si, Y.; Sun, G.; Nitin, N., Antibiofilm effect of poly (vinyl alcohol-co-ethylene)(PVA-co-PE) halamine film against *Listeria innocua* and *Escherichia coli O157: H7*. *Applied and Environmental Microbiology* **2017,** AEM. 00975-17.
13. Demir, B.; Broughton, R.; Huang, T.-S.; Bozack, M.; Worley, S., Polymeric antimicrobial N-halamine-surface modification of stainless steel. *Industrial & Engineering Chemistry Research* **2017,** *56* (41), 11773-11781.
14. Richter, A. P.; Brown, J. S.; Bharti, B.; Wang, A.; Gangwal, S.; Houck, K.; Hubal, E. A. C.; Paunov, V. N.; Stoyanov, S. D.; Velev, O. D., An environmentally benign antimicrobial nanoparticle based on a silver-infused lignin core. *Nature Nanotechnology* **2015,** *10* (9), 817.
15. Zeng, Q.; Zhu, Y.; Yu, B.; Sun, Y.; Ding, X.; Xu, C.; Wu, Y.-W.; Tang, Z.; Xu, F.-J., Antimicrobial and antifouling polymeric agents for surface functionalization of medical implants. *Biomacromolecules* ***2018,*** *19* (7), 2805-2811.

16. Demir, B.; Cerkez, I.; Worley, S.; Broughton, R.; Huang, T.-S., N-halamine-modified antimicrobial polypropylene nonwoven fabrics for use against airborne bacteria. *ACS Applied Materials & Interfaces* **2015,** *7* (3), 1752-1757.
17. Pan, N.; Liu, Y.; Fan, X.; Jiang, Z.; Ren, X.; Liang, J., Preparation and characterization of antibacterial graphene oxide functionalized with polymeric N-halamine. *Journal of Materials Science* **2017,** *52* (4), 1996-2006.
18. Si, Y.; Cossu, A.; Nitin, N.; Ma, Y.; Zhao, C.; Chiou, B. s.; Cao, T.; Wang, D.; Sun, G., Mechanically robust and transparent N□halamine grafted PVA□co□PE films with renewable antimicrobial activity. *Macromolecular Bioscience* **2017,** *17* (3), 1600304.
19. Si, Y.; Li, J.; Zhao, C.; Deng, Y.; Ma, Y.; Wang, D.; Sun, G., Biocidal and rechargeable N-halamine nanofibrous membranes for highly efficient water disinfection. *ACS Biomaterial Science Engineering* **2017,** *3* (5), 854-862.
20. Lin, J.; Jiang, F.; Wen, J.; Lv, W.; Porteous, N.; Deng, Y.; Sun, Y., Fluorinated and un-fluorinated N-halamines as antimicrobial and biofilm-controlling additives for polymers. *Polymer* **2015,** *68*, 92-100.
21. Mohr, S.; Berghahn, R. d.; Mailahn, W.; Schmiediche, R.; Feibicke, M.; Schmidt, R., Toxic and accumulative potential of the antifouling biocide and TBT successor Irgarol on freshwater macrophytes: a pond mesocosm study. *Environmental Science & Technology* **2009,** *43* (17), 6838-6843.
22. Luo, J.; Porteous, N.; Sun, Y., Rechargeable biofilm-controlling tubing materials for use in dental unit water lines. *ACS Applied Materials & Interfaces* **2011,** *3* (8), 2895-2903.
23. Mah, T.-F. C.; O'toole, G. A., Mechanisms of biofilm resistance to antimicrobial agents. *Trends in Microbiology* **2001,** *9* (1), 34-39.

24. Giacomazzi, S.; Cochet, N., Environmental impact of diuron transformation: a review. *Chemosphere* **2004,** *56* (11), 1021-1032.

25. Kobayashi, N.; Okamura, H., Effects of new antifouling compounds on the development of sea urchin. *Marine Pollution Bulletin* **2002,** *44* (8), 748-751.

26. Almond, K. M.; Trombetta, L. D., The effects of copper pyrithione, an antifouling agent, on developing zebrafish embryos. *Ecotoxicology* **2016,** *25* (2), 389-398.

27. Chen, L.; Au, D. W.; Hu, C.; Peterson, D. R.; Zhou, B.; Qian, P.-Y., Identification of molecular targets for 4, 5-Dichloro-2-n-octyl-4-isothiazolin-3-one (DCOIT) in teleosts: new insight into mechanism of toxicity. *Environmental Science & Technology* **2017,** *51* (3), 1840-1847.

28. Landmeyer, J. E.; Tanner, T. L.; Watt, B. E., Biotransformation of tributyltin to tin in freshwater river-bed sediments contaminated by an organotin release. *Environmental Science & Technology* **2004,** *38* (15), 4106-4112.

29. Jiang, S.; Cao, Z., Ultralow□fouling, functionalizable, and hydrolyzable zwitterionic materials and their derivatives for biological applications. *Advanced Material* **2010,** *22* (9), 920-932.

30. Leng, C.; Sun, S.; Zhang, K.; Jiang, S.; Chen, Z., Molecular level studies on interfacial hydration of zwitterionic and other antifouling polymers in situ. *Acta Biomaterialia* **2016,** *40*, 6-15.

31. Leng, C.; Han, X.; Shao, Q.; Zhu, Y.; Li, Y.; Jiang, S.; Chen, Z., In situ probing of the surface hydration of zwitterionic polymer brushes: structural and environmental effects. *The Journal of Physical Chemistry C* **2014,** *118* (29), 15840-15845.

32. Hong, D.; Hung, H.-C.; Wu, K.; Lin, X.; Sun, F.; Zhang, P.; Liu, S.; Cook, K. E.; Jiang, S., Achieving ultralow fouling under ambient conditions via surface-initiated arget atrp of carboxybetaine. *ACS Applied Materials & Interfaces* **2017,** *9* (11), 9255-9259.

33. Leng, C.; Huang, H.; Zhang, K.; Hung, H.-C.; Xu, Y.; Li, Y.; Jiang, S.; Chen, Z., Effect of surface hydration on antifouling properties of mixed charged polymers. *Langmuir* **2018**.

34. Si, Y.; Zhang, Z.; Wu, W.; Fu, Q.; Huang, K.; Nitin, N.; Ding, B.; Sun, G., Daylight-driven rechargeable antibacterial and antiviral nanofibrous membranes for bioprotective applications. *Science Advances* **2018,** *4* (3), eaar5931.

35. Zhou, R.; Ren, P.-F.; Yang, H.-C.; Xu, Z.-K., Fabrication of antifouling membrane surface by poly (sulfobetaine methacrylate)/polydopamine co-deposition. *Journal of Membrane Science* **2014,** *466*, 18-25.

36. Si, Y.; Yu, J.; Tang, X.; Ge, J.; Ding, B., Ultralight nanofibre-assembled cellular aerogels with superelasticity and multifunctionality. *Nature Communications* **2014,** *5*, 5802.

37. Giano, M. C.; Ibrahim, Z.; Medina, S. H.; Sarhane, K. A.; Christensen, J. M.; Yamada, Y.; Brandacher, G.; Schneider, J. P., Injectable bioadhesive hydrogels with innate antibacterial properties. *Nature Communications* **2014,** *5*, 4095.

38. Li, P.; Poon, Y. F.; Li, W.; Zhu, H.-Y.; Yeap, S. H.; Cao, Y.; Qi, X.; Zhou, C.; Lamrani, M.; Beuerman, R. W., A polycationic antimicrobial and biocompatible hydrogel with microbe membrane suctioning ability. *Nature Materials* **2011,** *10* (2), 149.

39. Marsh, K.; Bugusu, B., Food packaging—roles, materials, and environmental issues. *Journal of Food Science* **2007,** *72* (3), R39-R55.

40. Liu, R.; Chen, X.; Hayouka, Z.; Chakraborty, S.; Falk, S. P.; Weisblum, B.; Masters, K. S.; Gellman, S. H., Nylon-3 polymers with selective antifungal activity. *Journal of the American Chemical Society* **2013,** *135* (14), 5270-5273.

Chapter 3. Chlorine Rechargeable Biocidal N-Halamine Nanofibrous Membranes Incorporated with Bifunctional Zwitterionic Polymer for Efficient Water Disinfection Applications

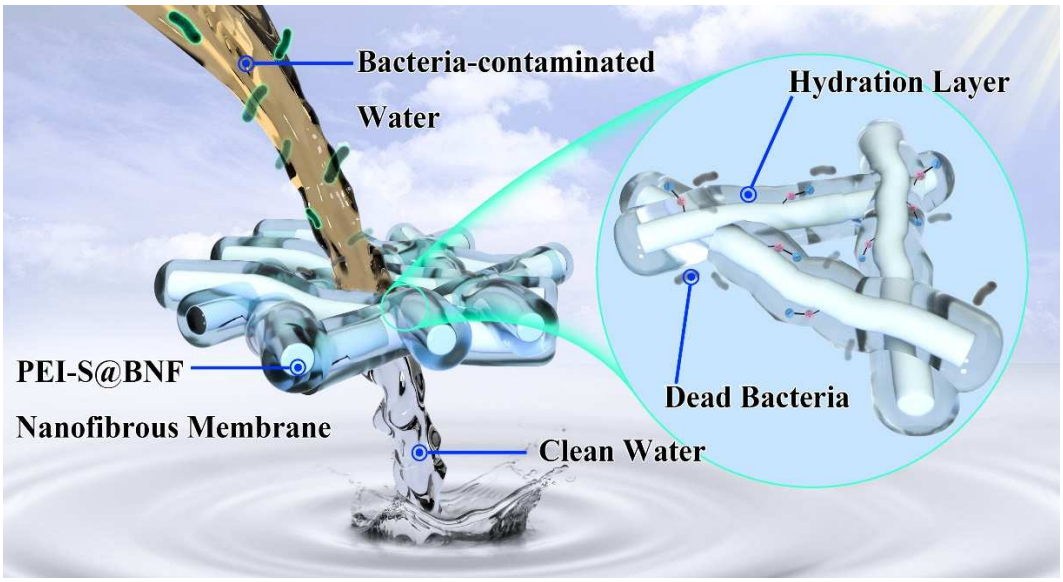

Abstract

An intrinsically hydrophilic nanofibrous membrane with chlorine rechargeable biocidal and antifouling functions was prepared by using a combination of chemically bonded N-halamine moieties and zwitterionic polymers (PEI-S). The promise for the designed nanofibrous membrane, named as PEI-S@BNF-2h, can exhibit integrated features of reduced bacterial adhesion, rechargeable biocidal activity, and easy release of killed bacteria by using mild hydrodynamic force. The representative functional performances of PEI-S@BNF-2h membrane include high active chlorine capacity (> 4000 ppm), large specific surface area, ease of chlorine rechargeability, long-term stability, and exceptional biocidal activity (99.9999% via contact killing). More importantly, the zwitterionic polymer moieties (PEI-S) brought robust antifouling properties to this biocidal membrane, therefore, reducing the biofouling-biofilm effect and prolonging the lifetime of the filtration membrane. These attributes enable the PEI-S@BNF-2h nanofibrous membrane to effectively disinfect the microbe-contaminated water in high fluxes (10000 L m^{-2} h^{-1}) and maintain itself clean for a long-term application.

Objectives

- Fabricate a biocidal and antifouling nanofibrous membrane (PEI-S@BNF) via an electrospinning technique.
- Characterize the physiochemical performances of the PEI-S@BNF, including thermal performance, mechanical property, and hydrophilicity.
- Investigate the active chlorine capacity and biocidal efficiency of the chlorinated PEI-S@BNF.

- Investigate resisting/ releasing mechanisms of the unchlorinated PEI-S@BNF using a model protein and evaluate the resisting/ releasing effect against bacteria.
- Evaluate the bacterial disinfection effect of the designed PEI-S@BNF under different permeate fluxes.

3.1 Introduction

Waterborne pathogenic contamination in natural and drinking water has been a global public health concern.[1-3] According to the World Health Organization (WHO) annual report in 2018, an estimated 2 billion people are drinking water from contaminated water sources, and 4.5 billion people are suffering from inadequate access to a qualified water sanitation system. [4] Due to the low disinfection efficiency towards the waterborne pathogens and the generation of toxic byproducts, conventional water disinfection methods, based on the addition of disinfectants directly and irreversibly to the water, may bring in the potential human health and environmental risks. [5-7] Alternatively, membrane technologies, such as ultrafiltration (UF), [8-10] reverse osmosis (RO), [6, 11] and nanofiltration (NF) [12, 13] have been applied to filter the contaminants based on the size-sieving effect. During the filtration process, the membrane surfaces are constantly in contact with the microorganism-contaminated feeding water, and the accumulated biofouling effect may result in a reduced permeate flux and a shortened shelf life of the filtration membranes.[14,15] Responding to this challenge, we previously reported a rechargeable biocidal N-halamine incorporated nanofibrous membrane (BNF), which exhibited a high disinfection efficiency (99.9999% via contact-killing) for the water treatment with a promising flowing flux (10000 $Lm^{-2}h^{-1}$). [16] However, even with such strong biocidal performance, the killed bacterial debris and any survival microorganisms could still foul on the membrane and block the active halamine sites, consequently hindering the biocidal activity and reducing the filtration fluxes. Therefore,

endowing the BNF membrane with a permanent antifouling function was considered as a potential solution to reduce the biofilm-biofouling effect on the biocidal materials.

The superhydrophilic zwitterions, carrying both cationic and anionic groups have been attractive as a new type of antifouling agent. [17,18] With such hydrophilicity, surfaces of zwitterion incorporated membranes could strongly interact with the surrounding water molecules, generating a dense hydration layer via either electrostatic interactions or hydrogen bonds, consequently, weakening the non-specific interaction with the biofoulants. [19] Many approaches have been reported to incorporate zwitterionic structures onto membranes, such as photo-, plasma-, thermal-induced graft polymerization, atom transfer radical polymerization (ATRP), reversible addition fragmentation chain transfer (RAFT), and initiated chemical vapor deposition (CVD). [20-25] However, these methods usually require a harsh reaction condition, leading to a decrease in the mechanical property of the obtained zwitterionic membranes, thereby limiting the application of them in a high flux water filtration system.

In this work, we designed and prepared a multifunctional nanofibrous membrane with both rechargeable biocidal and antifouling functions to disinfect the microbe-contaminated water and reduce the biofouling effect, therefore, prolonging the lifetime of such material as a filtration membrane. These functions were achieved by chemically crosslinking a sulfonated-polyethyleneimine (PEI-S), a zwitterionic polymer onto a poly(vinyl alcohol-co-ethylene)-g-N,N-diallylmelamine (BNF) nanofibrous membrane containing stable N-halamine precursors. The obtained membrane, named as PEI-S@BNF-2h, exhibited desired features of reduced bacterial adhesion, rechargeable biocidal activity, and easy release of the killed bacteria with application of mild hydrodynamic forces. The chlorinated PEI-S@BNF-2h nanofibrous membrane could serve

as a filter to effectively disinfect bacteria-contaminated water with high permeate fluxes, and the generated bacterial debris could be easily cleaned up, avoiding the formation of the biofilm.

3.2. Experimental Section

3.2.1 Materials

Polyethyleneimine (branched, Mw = 10,000) was purchased from Beantown Chemical, Inc. 1,3-propanesultone, glutaraldehyde solution (25 wt%), pierce^{TM} BCA protein assay reagent A and B, 2 wt% of osmium tetroxide (O_sO_4), hydrochloric acid, sodium hydroxide, sodium thiosulfate ($Na_2S_2O_3$), Phosphate-buffered saline (PBS), acetone, and dimethyl sulfoxide were purchased from Sigma-Aldrich (Louis, MO, USA). Luria-Bertani (LB) broth, LB agar, Tryptic soy broth (TSB), and Tryptic soy agar (TSA) were purchased from Thermo Fisher Scientific (Waltham, MA, USA). The Clorox bleach solution with a free chlorine content of 6.0 % was manufactured by Clorox Co., Ltd. (Oakland, CA, USA). Gram-negative *Escherichia coli O157: H7*, *Escherichia coli O157: H7-lux*, and Gram-positive *Listeria innocua* were produced by ATCC (Manassas, VA, USA)

3.2.2 Fabrication of PEI-S@BNF membrane

The production of the PVA-co-PE-g-DAM (BNF) nanofibrous membrane and the synthesis process of the zwitterionic polymer (PEI-S) were reported previously.[16, 26, 27] The BNF membranes were immersed in an aqueous solution containing 5 wt % of PEI-S. After 10 min, the BNF membranes were taken out and dried at ambient temperature for 1 hour. As-prepared BNF membranes loaded with PEI-S (BNF/PEI-S) were exposed to glutaraldehyde vapor for various durations inside a desiccator. After crosslinking, the nanofibrous membranes were washed by an

excess of water and acetone to remove any uncrosslinked PEI-S, and finally placed in a fume hood for 24 hours for dry.

3.2.3 Hydration ability of PEI-S@BNF membranes

The PEI-S@BNF membranes (5 mg) were soaked in 10 mL of DI-water overnight for equilibrium, and then, the excess surface water was removed using a filter paper. The hydrated membranes were immediately subjected to a Differential Scanning Calorimetry (DSC) test. The analysis was carried out in a standard program: (1) cool down the temperature to -60 □, (2) keep isothermal for 5 min, (3) heat the sample from -60 □ to room temperature at 2.5 □ min^{-1}. The transition enthalpy (ΔH) was measured by the DSC-60 analysis software. After the DSC test, the samples were dried in an oven at 100 □ overnight. The mass difference between the pro-DSC and post-drying gives the total water content (m_w). Data are expressed as the mean ± SD of five replicates.

3.2.4 Chlorination of PEI-S@BNF membranes

A chlorination solution with the active chlorine concentration of 200 ppm was prepared by diluting a Clorox bleach solution. The chlorination solutions with various pH were adjusted by applying hydrochloric acid and sodium hydroxide. In a typical chlorination process, the membranes were fully immersed in the chlorination solution with gentle shaking for a designed time. Subsequently, the chlorinated membranes were washed with an excess of DI-water to remove any free chlorine and then dried under room temperature. For a rechargeability test, after charged with chlorination solution for 1 hour, the active chlorine on membranes was quenched by an excess of sodium thiosulfate ($Na_2S_2O_3$) solution for 1 hour. The active chlorine content of each sample was quantified by an established iodometric titration method. [16, 20, 28] Active chlorine content (ppm) of the membranes could be calculated according to equation 3.1:

$$\frac{35.45\times(V_0-V_1)N\times500}{m_S} \quad \text{(Equation 3.1)}$$

Where V_0 and V_1 (L) are the volumes of the iodine solution consumed in titration without and with the chlorinated membrane, respectively. m_s is the dry weight (g) of the chlorinated membrane.

Data are expressed as the mean ± SD of three replicates.

3.2.5 Antibacterial assay against *E. coli* and *L. innocua*

Two typical etiological bacteria, Gram-negative *E. coli O157: H7* and Gram-positive *L. innocua*, were applied to conduct the biocidal experiments. 10 mL of LB broth and TSB were inoculated with a colony of *E. coli* and *L. innocua* and grown at 37□ for 18 hours, respectively. Subsequently, the bacteria were harvested by centrifugation at 5000 rpm for 10 min and washed three times by PBS buffer. The obtained bacteria were diluted with sterilized PBS buffer or standard nutrient broth solution (COD = 1000) to achieve the final concentration of 1×10^8 CFU mL^{-1}. The membrane samples in a size of 2 × 2 cm^2 were employed in the contact killing assay, which has been reported in the previous study. [16, 20] For the cyclic antibacterial test, the bacteria-contaminated membranes were recharged with the chlorination solution for 1 hour after each cyclic test.

3.2.6 Protein adsorption and releasing behaviors

Bovine Serum Albumins (BSA) protein was applied to evaluate the resisting and releasing functions of the unchlorinated membranes. In a typical kinetic protein adsorption experiment, 10 mg of unchlorinated BNF or unchlorinated PEI-S@BNF membranes were soaked in 10 mL of BSA solution with a concentration of 1 mg mL^{-1} (pH = 7.4) at room temperature for different time durations. For a static protein adsorption test, 10 mg of the unchlorinated membranes were immersed in 10 mL of BSA protein solution with various concentrations (pH = 7.4). And then, the

mixture was gently shaken in the room temperature until the system arrived at the equilibrium state. The concentration of residual BSA in the aqueous was quantified using an established BCA protein assay. [29, 30] The amount of BSA protein adsorbed by the unchlorinated membrane at time t, q_t (mg/g) was calculated according to equation 3.2:

$$q_t = \frac{(C_0 - C_t) \times V}{m} \qquad \text{(Equation 3.2)}$$

Where q_t is the adsorption capacity at a given time, V is the volume of protein solution, C_0 is the initial protein concentration, C_t is the protein concentration after adsorption for a given time, and m is the dry mass of the unchlorinated membranes.

For a protein releasing experiment, 100 μL of BSA protein solution with a concentration of 100 mg mL^{-1} were loaded onto the unchlorinated BNF and the unchlorinated PEI-S@BNF membranes (2 × 2 cm^2), and the samples were allowed to dry for 1 hour (BSA protein fixed on the fibers). Then, the unchlorinated membranes were incubated with 10 mL of PBS buffer with gentle shaking for various releasing times. At each time point, the concentration of BSA in the releasing solution was quantified using an established BCA method, and the acuminated release ratio of BSA was calculated based on equation 3.3:

$$y_t\ (\%) = \frac{C_t \times V}{10} \qquad \text{(Equation 3.3)}$$

where y_t (%) is cumulate release ratio, V (mL) is the volume of releasing solution, C_t (mg mL^{-1}) is the protein concentration after release for a given time.

3.3.7 Bacterial resisting and releasing behaviors

The bacterial resisting behavior of the unchlorinated membranes was evaluated by two testing methods: bacterial contact touch assay and bacterial incubation assay. In a typical bacterial contact

touch assay, 20 μL of *E. coli-lux* suspension with a high concentration of 10^8 CFU mL^{-1} was loaded to an agar plug (diameter = 15 mm; thickness = 1 cm), which could absorb the excess media and generate a layer of *E. coli-lux* on the top surface. [31] Subsequently, the bacteria infused agar plugs were contacted with the unchlorinated BNF and the unchlorinated PEI-S@BNF membranes for 20 s with 1 N force applied, respectively, and the contaminated membrane surfaces were quantitively analyzed using a widefield luminescence system. The bacterial incubation experiment and the bacterial releasing experiment were following the protocols in the literature. [20,24]

3.2.8 Water disinfection experiment

The microorganism-contaminated water was prepared by diluting the *E. coli* suspension to a final concentration of 8×10^6 CFU mL^{-1}. The nanofibrous membranes (the unchlorinated and the chlorinated BNF membranes as controls and the chlorinated PEI-S@BNF membranes as samples) with a diameter of 10 mm were sandwiched between two plastic tubes. The freshly prepared bacterial contaminated feedwater was pumped through the membrane by using a programmable syringe pump. The permeate fluxes were obtained by calculating the flow volume in 1 min from the valid flowing area of the membrane (S = 0.2 cm^2) (Equation 3.4). The amounts of live bacteria in the filtrated water were determined by using the colony-counting method. For monitoring the antifouling performances of the PEI-S@BNF, after the pumped with 5000 mL m^{-2} of bacteria-contaminated water, the filtration membranes were washed via pumping 20 mL of sterilized DI-water through the membrane with a flux of 10000 L m^{-2} h^{-1}.

$$J = \frac{V}{t \times A} \qquad \text{(Equation 3.4)}$$

where J (L m^{-2} h^{-1}) is the permeate flux, V (L) is the volume of liquid that penetrates the membrane, t (h) is the processing time, and A (m^2) is the effective filtration area.

3.2.9 SEM and widefield bioluminescence images

For the SEM imaging, bacteria were fixed in 2.5 wt% of glutaraldehyde solution for 4 hours at 4 □. Subsequently, the samples were rinsed with sequential ethanol/water mixtures with an increasing ethanol content of 25%, 50%, 75%, and 100%. Finally, the samples were placed on a sliver tape and coated with palladium before SEM analysis. [32]

For the widefield bioluminescence imaging, *E. coli O157: H7-lux*, containing a complete *lux* operon (*lux* CDABE; bioluminescence genes) was applied. The distribution of *E. coli-lux* on the sample membranes was characterized using a widefield bioluminescence imaging system equipped with an ICCD camera and a bandpass emission filter (558-583 nm). Moreover, the bioluminescence signals were represented using a pseudo-color signal intensity scale.

3.2.10 Biofilm adherence assay

BNF, PEI-S@BNF-2h, and chlorinated PEI-S@BNF-2h membranes were cut as a circle with a diameter of 15.6 mm, and placed in a sterilized 24-well plate. A volume of 0.1 mL of *E. coli* cultured overnight and 0.9 mL of the 1 × M9 medium supplemented with 0.4 % glucose and 0.4% tryptone were added to each well. The final concentration of the bacteria was about 1×10^8 CFU mL^{-1} with an optical density at 600 nm of 0.387. The 24-well plate was incubated in a dark condition at room temperature for 4 days. After that, the medium in the plate was discarded, and each well was gently rinsed with 1 mL of PBS buffer three times to remove the planktonic bacteria.[32] The biofilms growth on the membranes were stained with 0.1 % of crystal violet and washed with an excess of DI water, then solubilized in 2 mL of ethanol/acetone (2:8) mixture. The optical density of resuspended crystal violet was measured at 570 nm, and the relative biofilm formation was calculated based on equation 3.5:

$$Relative\ biofilm\ formed = \frac{Biofilm\ formation\ (\Delta OD_{570})}{Cell\ density\ for\ growth\ biofilm\ (OD_{600})} \quad \text{(Equation 3.5)}$$

Where ΔOD_{570} is the difference of the optical density at 570 nm between the membrane with biofilm and the BNF without biofilm. OD_{600} is 0.387.

Data are expressed as the mean ± SD of three replicates.

3.2.11 Characterization of PEI-S@BNF membrane

The FT-IR spectra were collected with a Nicolet 6700 spectrometer in the range of 500-4000 cm^{-1}. TGA and DSC curves were measured with a Shimadzu TGA-60 and DSC-60 with a heating rate of 5 □ min^{-1} and 2.5 □ min^{-1}, respectively. Surface hydrophilicity was assessed by measuring the static WCAs with a goniometer Kino SL 200B.

3.2.12 Statistical analysis and quantitative data analysis

Statistical analysis was performed using the SPSS Statistics software (version 24, IBM SPSS, Chicago, IL, USA) to evaluate the measurement sets of obtained data. All the experiments were performed in triplicates. A one- or two-way analysis of variance was used to determine the significant differences among the values of the selected measurements ($p < 0.05$).

3.3 Results and Discussion

3.3.1 Synthesis and characterization of PEI-S

As shown in Figure 3.1a, after the sulfonation of the PEI with 1,3-propanesulfonate, sulfonate groups were introduced on the PEI polymer chains, resulting in a zwitterionic polymer, named as PEI-S. As shown in Figure 3.1b, a new peak appearing at 1198 cm^{-1} in the FTIR spectrum of PEI-S could be attributed to the vibration of the sulfonate groups, confirming the existence of the zwitterionic structure, which could also be evidenced from the EDX spectrum of the PEI-S. The

characteristic peak of a surfer element with a photon energy of 2.3 keV could be detected (Figure 3.1c). Figure 3.1d exhibits the difference between the PEI and PEI-S in a thermal property. The PEI starts to lose weight at 300 □. However, the initial weight loss of the PEI-S is 250 □, attributing to the degradation of the incorporated sulfonate groups. These results proved the successful synthesis of the zwitterionic polymer, PEI-S.

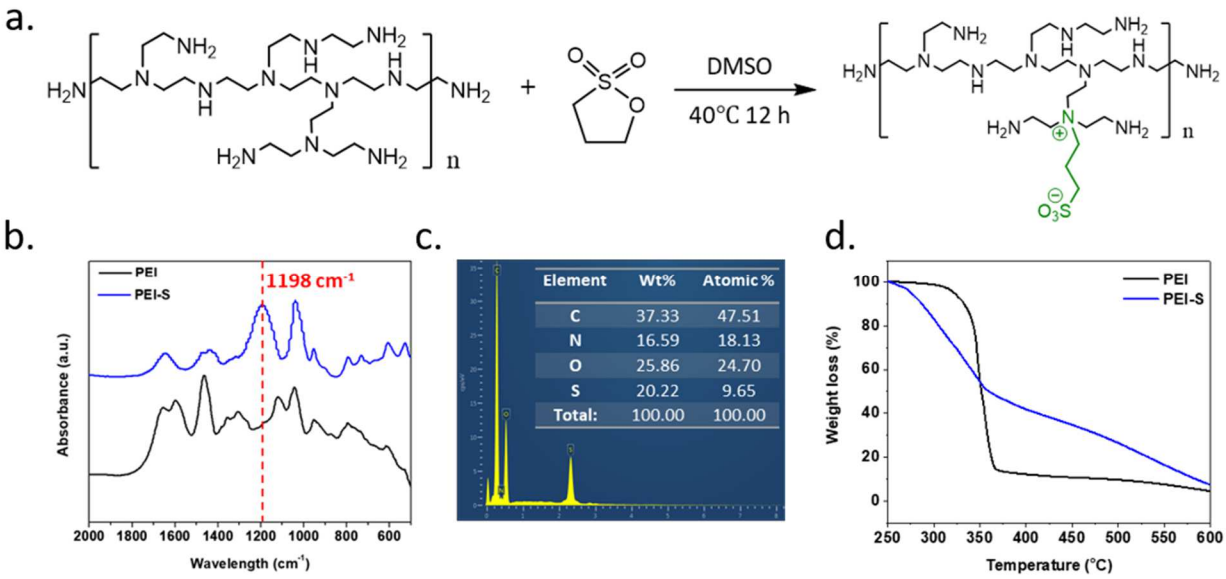

Figure 3.1. (a)Sulfonation reaction of the PEI. (b) FT-IR spectra and (d) TGA curves of PEI and PEI-S. (c) EDX spectrum and elemental compositions of the PEI-S.

3.3.2 Design and fabrication of PEI-S@BNF membranes

The manufacturing process of the renewable biocidal nanofibrous membrane (BNF) has been previously reported. [16] A superhydrophilic zwitterionic polymer (PEI-S) exhibiting promising antifouling function was prepared by sulfonating PEI side chains (Figure 3.1). [26, 27] Taking the advantages of both materials, we designed the PEI-S@BNF-2h nanofibrous membrane based on three criteria of structural features and performances: (1) the renewable biocidal N-halamine moieties and the zwitterionic moieties should be homogeneously and covalently bonded onto the

nanofibrous membrane matrix, (2) these two moieties should work independently and construct concerted microbial resisting, killing, and releasing functions to clean the water and reduce the biofouling effect, and (3) the membrane should retain porous structures and be able to continuously disinfect a large amount of microbes-contaminated water with high flowing fluxes.

To satisfy these requirements, we employed a crosslinker, glutaraldehyde (GA), which could diffuse into the system and react with both hydroxyl groups (on BNF) and amino groups (on BNF and PEI-S), generating ether bonds and C=N connections, respectively. At an optimized GA crosslinking time, the maximum amount of PEI-S layer could be covalently bonded onto the surfaces of the nanofibers in the BNF membrane with minimum consumption of amino and hydroxyl groups, therefore, providing stable and durable biocidal activity and antifouling performance of the PEI-S@BNF membrane. As shown in Figures 3.2a and 3.2b, the BNF membrane loaded with PEI-S (BNF/PEI-S) was sealed in a desiccator and exposed to GA vapor for different durations. With no GA crosslinking agent applied, the BNF/PEI-S exhibited a uniformed nanofibrous network with an average diameter of 618 nm (Figure 3.3a). After GA vapor treatment for 0.5, 1, 2, and 4h, the loaded PEI-S was crosslinked on the surface of the nanofibers and within the polymers, result in a zwitterionic coating. Increased crosslinking time would lead to more internal crosslinking of PEI-S and form a more fused coating layer between the fibers, but still maintaining the rigid 3D nanofibrous structure with an average diameter of 773, 855, 923, and 2593 nm, respectively (Figures 3.3b-3.3e). However, further prolonging the crosslink time (24 h) resulted in a loss of the nanofibrous morphology with reductions of specific surface area and porosity. Figure 3.2a also describes the rechargeable biocidal and antifouling performances of the PEI-S@BNF membrane. Once the microorganisms are approaching the surface, the zwitterionic polymer, PEI-S, makes them hard to attach to or be adsorbed on the surfaces of the membranes

via generating a robust hydration barrier, weakening the interactions between the membrane and microorganisms. Any bacteria touched on the surfaces of the membranes could be immediately killed by the active chlorine of the halamine structures. The resulting bacterial debris could be easily cleaned up by applying mild hydrodynamic force, and the consumed active chlorine could be effectively refreshed by a commercially available bleach solution. With a good combination of halamine and zwitterion moieties, PEI-S@BNF nanofibrous membrane provides an ideal filter media for the water purification system with prolonged service time and robust refreshable biocidal function.

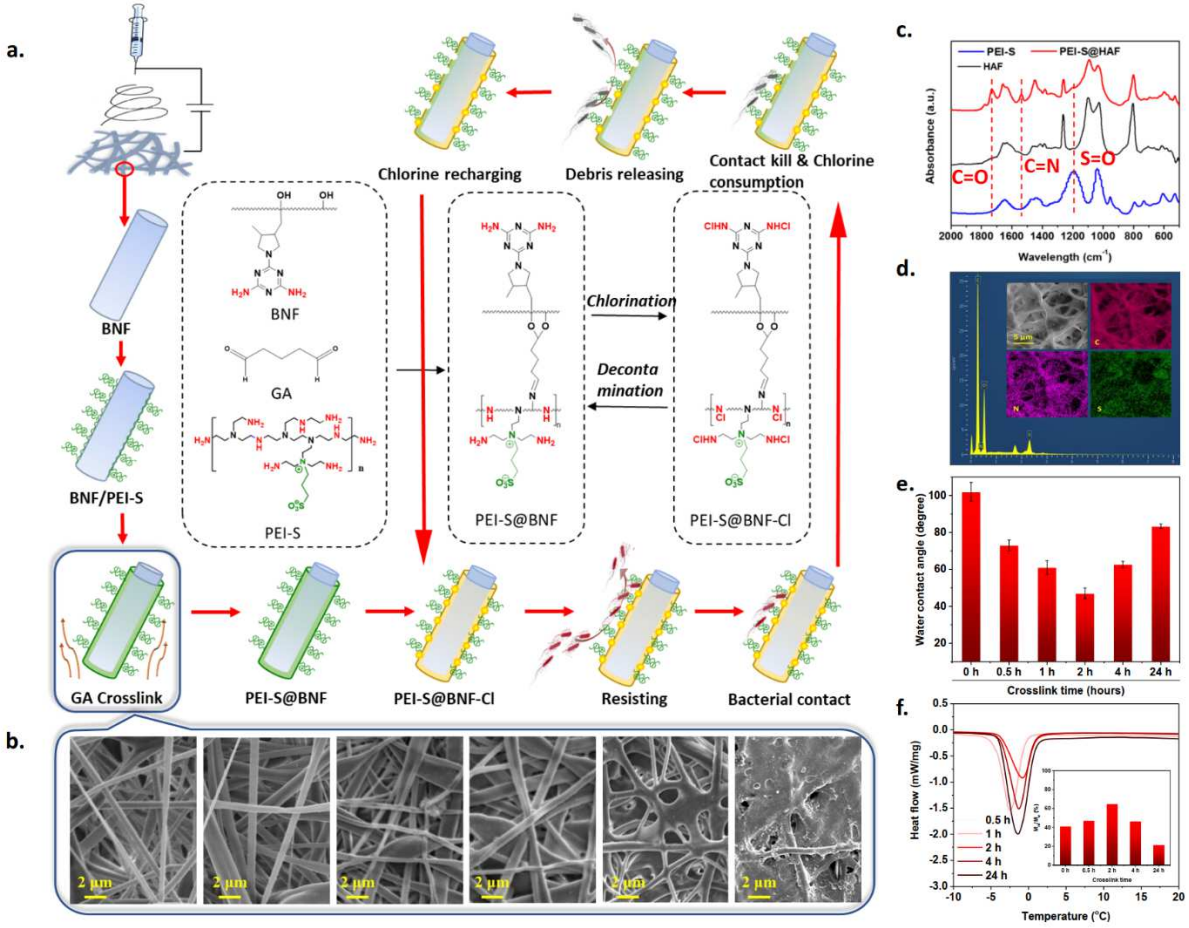

Figure 3.2. (a) Scheme of the manufacturing process, rechargeable biocidal, and antifouling performances of as-prepared PEI-S@BNF membrane. (b) SEM images, (e) water contact angle (WCA), (f) DSC spectra (insert of calculated non-freezable water ratio) of PEI-S@BNF membranes after 0h, 0.5h, 1h, 2h, 4h, and 24 h of GA crosslinking. (c) FT-IR spectra of PEI-S, BNF, and PEI-S@BNF-2h. (d) SEM-EDX results of PEI-S@BNF-2h membranes.

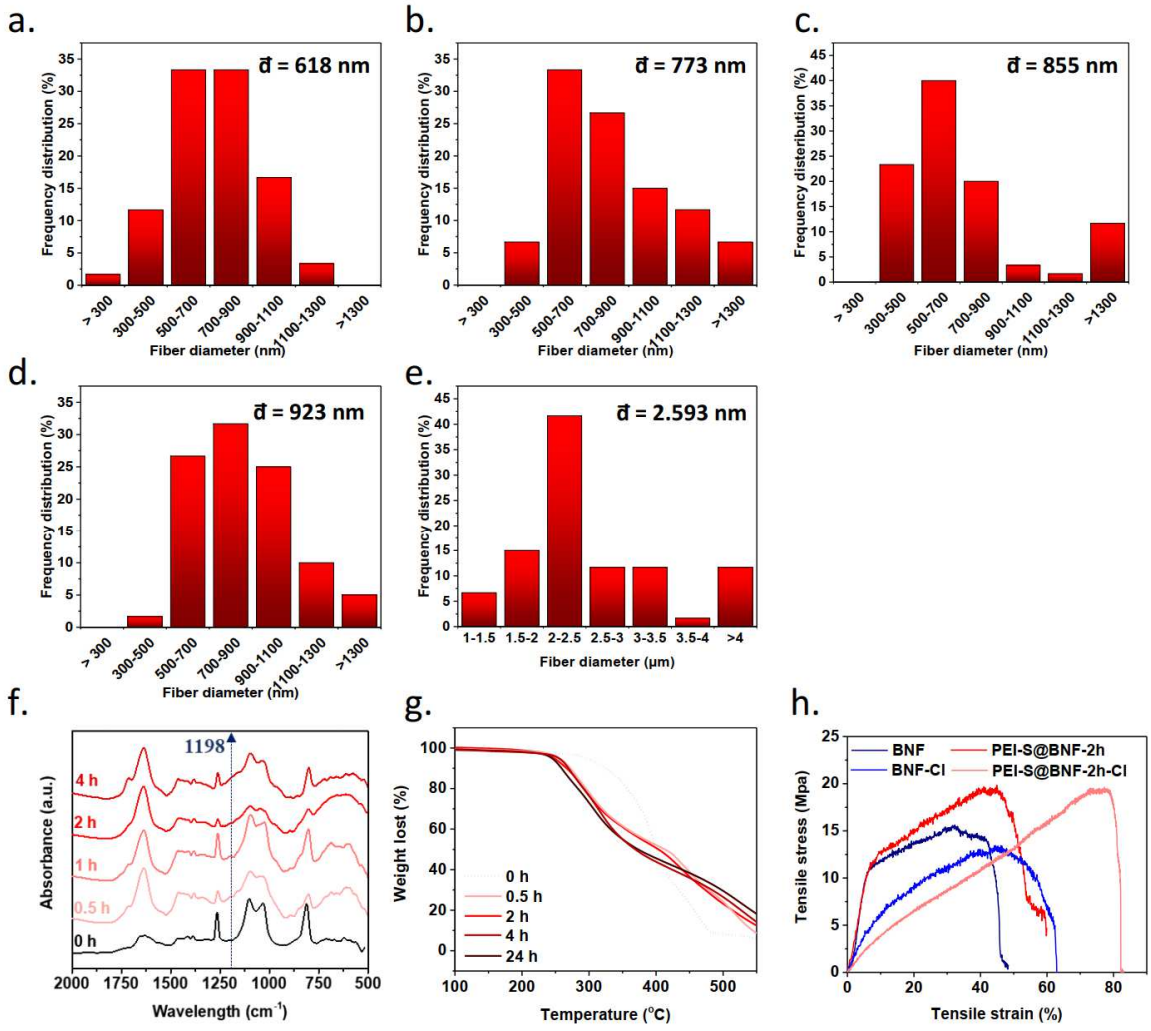

Figure 3.3. (a-e) Fiber diameter distributions of BNF, PEI-S@BNF-0.5 h, -1h, -2 h, -4 h, respectively. (f) FT-IR spectra and (g) TGA curves of the PEI-S@BNFs with a temperature range

of 100-550□. (h) Tensile stress-strain curves of the BNF, BNF-Cl, PEI-S@BNF-2h, and PEI-S@BNF-2h-Cl membranes.

3.3.3 Structural characterization and properties of PEI-S@BNF membranes

Fourier transform infrared (FT-IR) spectra (Figures 3.2c and 3.3f) provide evidence of the successful combination of zwitterionic polymer (PEI-S) and BNF. After exposure to GA vapor, the PEI-S was crosslinked, proven by the presence of the peaks at 1538 cm^{-1}, indicating the stretching vibration of imine groups (C=N).[33] The new peak around 1198 cm^{-1} came from stretching vibration of sulfonate groups appeared in the FT-IR spectra of both PEI-S polymer and PEI-S@BNF-xh membranes (with x hours GA crosslinking), confirming the existence of the zwitterionic structure, which could also be evidenced from scanning electron microscope energy dispersive X-ray spectroscopy (SEM-EDX). As shown in Figure 3.2d, about 5 wt% (2 At%) of the sulfur elements have been detected, and they were homogenously distributed along the entire nanofibrous membranes (inset of Figure 3.2d).

Hydrophilicity and hydration ability were evaluated as key features of the antifouling functions of the water filtration membranes. The hydrophilicity of the PEI-S@BNF membranes depends on the amounts of two structures, the incorporated zwitterionic structures and hydroxyl/amine groups existing on PVA-co-PE-g-DAM and PEI polymers. Increased zwitterionic structures could increase the hydrophilicity of the membranes, while crosslinking of hydroxyl and amine groups in the polymers by GA could reduce it. In addition, the over-crosslinked PEI-S@BNF will lose the porous structure and surface areas, which also lead to decreased hydrophilicity of the membranes. The overall effect could be observed from results of both static water contact angle (WCA) and DSC tests of the membranes undergoing through different crosslinking durations. As shown in

Figure 3.2e, the WCA exhibited significant GA crosslinking time dependence with the lowest WCA of 47° that was more than two times smaller than that of the pristine BNF membrane (102°). The WCA of the membranes was initially reduced as the crosslinking time was prolonged, an effect of increased PEI-S coating on surfaces of nanofibers. After the crosslinking reaction was moving into the PEI-S coating layer, specific surface areas of the membranes were reduced and less zwitterionic structures were exposed on surfaces, consequently hydrophobicity of the membranes was increased. The PEI-S@BNF membrane, containing zwitterionic structure, permanently carries both anionic and cationic moieties independent of the pH conditions. Owning to this character, it shows a strong hydration ability to bond non-freezable water, which benefits the suppression of the water evaporation. [34, 35] The quantification of the freezable water (m_f) could be estimated from the DSC spectra (Figure 3.2f). For example, the DSC spectrum of the PEI-S@BNF-2h shows an endothermic peak at -4□ with a total enthalpy (ΔH) of 344.53 mJ. Assuming the latent heat of fusion of water (ΔH_L) is 334.45 mJ mg^{-1},[30] the amount of freezable water (m_f) is 1.03 mg. The total water content (m_w) was obtained by measuring the weight difference before and after completely drying process. Therefore, the amount of non-freezable water was calculated based on equation 3.6:

$$m_{nf} = m_w - m_f = m_w - \frac{\Delta H}{\Delta H_L} \qquad \text{(Equation 3.6)}$$

The hydration ability of the membranes could be described as an abundance ratio of the non-freezable water (m_{nf}/m_w). [36, 37] After 2 hours of crosslinking, the PEI-S@BNF-2h membranes exhibited the most robust hydration ability, with nearly 65 wt % of non-freezable water being bonded (inset of Figure 3.2f). The promising hydration ability implies good microbial antifouling performances of the PEI-S@BNF-2h membranes. Additionally, such robust hydrophilicity

provides good contacts of the membrane surfaces with microbes, benefiting for the contact killing function of the active halamine structures.

Thermal stability is another important feature of water filtration materials. As shown in Figure 3.3g, PEI-S@BNF-xh membranes exhibit typical two weight-loss stages with the temperature increase: (1) the initial weight loss ranging from 250 to 300 □, attributing to the degradation of the sulfonate groups, and (2) the second stages, 300-500 □, corresponding to the degradation of the polymer mainchain. Overall, the membranes exhibited good thermal stability without any weight loss below 250 □. Figure 3.3h demonstrated the mechanical performances of the membranes before and after chlorination. The BNF and the PEI-S@BNF-2h exhibited similar young's modulus, with yielding stress of > 10 Mpa and a strain < 5 %. While the GA crosslinked PEI-S@BNF-2h membrane showed improvements over the BNF membrane in breaking stress and strain due to the stronger interaction among the polymer chains. After chlorination, both BNF-Cl and PEI-S@BNF-Cl exhibited a significant increase in breaking strain, which could be ascribed to the loss of hydrogen bonding between molecules. The PEI-S@BNF membranes with great thermal stability and mechanical performance exhibited a great potential to serve as a filter membrane for water treatment applications.

3.3.4 Rechargeable chlorination of PEI-S@BNF membranes

N-Halamine precursors containing one or more nitrogen-hydrogen (N-H) covalent bonds of imide, amide, or amine groups could become biocidal after halogenation. [38] For PEI-S@BNF membranes, both PEI and BNF contain halamine precursors, responding to the promising biocidal properties of the membrane after chlorination. The active chlorine contents of the PEI-S@BNF membranes were influenced by two parameters: amounts of N-H bond from the crosslinked PEI-S and consumption of the N-H during the crosslinking reaction. Therefore, we investigated the

chlorination profiles of the PEI-S@BNF membranes with different crosslinking times. To test the chlorination capability, we prepared a chlorination solution with active chlorine of 200 ppm by diluting a commercial bleach solution, and the active chlorine contents of the chlorinated membranes were determined via an iodometric titration method. Figure 3.4a demonstrates the active chlorine contents of the membranes as a function of chlorination time. With the increase of chlorination time, the curves exhibited two characteristic regions: a rapid growth at the first 1 hour and then a saturation plateau. The active chlorine contents of PEI-S@BNF-0h (BNF), -0.5h, -2h, and -24h were 3916, 3399, 4472, and 1857 ppm after 1-hour chlorination, respectively. The decrease in the active chlorine content of the PEI-S@BNF-24 h could be attributed to the loss of the halamine precursors (N-H bonds) during the long time crosslinking by GA.

The chlorination of halamine precursors occurs by the reactions between amine groups (R_1NH_2/ $R_1NH_3^+$; R_1R_2NH /$R_1R_2NH_2^+$) and hypochlorous moieties (HOCl/ ClO^-), which are affected by pH values of the chlorination solutions.[16] Figure 3.4b demonstrates the active chlorine contents of relevant membranes with various pH conditions. The chlorination process exhibited maximum efficiency around a neutral pH of 7 for all the membranes. Under the low pH conditions, amine groups on DAM and PEI could be protonated, turning to $R_1NH_3^+$ and $R_1R_2NH_2^+$, which could not be chlorinated and convert to N-halamine structures (R_1NH-Cl, R_1R_2N-Cl). At the alkaline condition, hypochlorite (ClO^-) with weaker chlorination ability becomes the major moieties in the bleach solution, leading to a significant decrease of the active chlorine content of the membranes. This neutral pH treatment condition is also beneficial for practical applications of the PEI-S@BNF membrane in the water filtration systems.

Durability for long time use is another practical concern for biocidal water filtration membranes. After chlorination, the membranes were fully dried and placed in a dark condition under a constant

temperature of 20 □ and a constant moisture content of 30 %. As shown in Figure 3.4c, the active chlorine contents of the PEI-S@BNF -0.5h, -2h, and 24h showed a significant decrease in the first three days, which could be mainly attributed to dehalogenation reaction of the unstable N-halamine structure from PEI moieties (existence of α-hydrogen).[38] For further storage, all the membranes demonstrated a similar decreased dissociation rate of the active chlorine. Because, in this period, the residual active chlorine mainly came from the chlorinated amine groups of the DAM structure. Without the existence of the α-hydrogen, DAM structures exhibited an expected better active chlorine stability, which ensures the biocidal activity of the chlorinated PEI-S@BNF membranes even after long time storage. Moreover, the PEI-S@BNF membranes demonstrated a promising rechargeability of the functional N-halamine structure. As shown in Figure 3.4d, for each cycle, the PEI-S@BNF-2h, as an example, was first chlorinated for 1 h at an optimized chlorination solution and then was fully quenched with an excess amount of sodium thiosulfate solution. After repeating 7 times of charging-quenching processes, more than 80 % of the original charging capacity still retained, which could be attributed to the robust covalent bonding between N-halamine moieties and polymer backbones. The PEI-S@BNF-2h membranes, with the highest active chlorine capacity, the robust rechargeability, and the strongest hydration ability, were selected as an example for the following experiments.

3.3.5 Contact killing against bacteria

The biocidal activities of the membranes were evaluated against two typical pathological bacteria, Gram-negative *Escherichia coli O157: H7* and Gram-positive *Listeria innocua*. The bacterial proliferation was assessed by agar plate counting. An appropriate diluted LB broth solution was used to simulate chemical oxygen demand (COD) encountered in the water system. For the contact-killing assay, control membranes (unchlorinated PEI-S@BNF-2h membrane) and

chlorinated PEI-S@BNF-2h membranes with a size of 2 × 2 cm^2 were loaded with 10 μL of bacterial suspension (10^8 colony-forming unit per mL ($CFUmL^{-1}$)) in water (COD = 0 mg L^{-1}) or diluted broth solution containing COD of 1000 mg L^{-1}. As shown in Figures 3.4e and 3.4f, the control membranes did not provide any noticeable reduction of both *E. coli* and *L. innocua* even after 30 minutes of contact. In contrast, the chlorinated PEI-S@BNF-2h membranes exhibited rapid and effective contact-killing performance. In the case of COD = 0 mg L^{-1}, the membranes achieved more than 6 log CFU reduction (> 99.9999%) of both *E. coli* and *L. innocua* after 10 minutes of contact. At a high COD condition, about 6 log and 4 log CFU reduction of *E. coli* and *L. innocua* were achieved after 10 minutes of contact between the chlorinated PEI-S@BNF membranes and the microbes, respectively. The slight decrease of biocidal activity could be attributed to the additional active chlorine consumption by the introduced reducing substances in the bacterial suspension. Additionally, the good stability and rechargeability of the N-halamine structures are also responsible for the promising long-term usable and renewable biocidal performances of the chlorinated PEI-S@BNF-2h membranes against bacteria for the water disinfection applications. As shown in Figure 3.4g, after 7 days of storage (in a dark condition under a temperature of 20 □ and a moisture content of 30 %), even though 50 % of the active chlorine content was lost with a residual active chlorine content of 2000 ppm (Figure 3.4c). The membranes still maintained great biocidal performances with more than 5 log CFU reduction of the bacteria. As shown in Figure 3.4h, the results of five cyclic antimicrobial tests revealed the biocidal activity of the chlorinated PEI-S@BNF-2h was nearly constant with more than 5 log CFU reduction of both *E. coli* and *L. innocua*, which is consistent with the results of rechargeability test of the active chlorine content (Figure 3.4d). These results highlighted the good long-term stability, the robust reusability, and the strong biocidal activity of the PEI-S@BNF-2h membranes.

The biocidal function of the chlorinated PEI-S@BNF-2h membranes could result in complete inactivation of bacteria by destroying cell structures, which was demonstrated by the morphological changes of the bacteria after contacting with unchlorinated or the chlorinated PEI-S@BNF-2h membranes. As shown in Figures 3.4i and 3.4k, both *E. coli* and *L. innocua* cells contacting with unchlorinated membranes remained cell structures intact with smooth surfaces. In contrast, cellular deformation and surface collapse were found on both *E. coli* and *L. innocua* cells after exposure to the chlorinated membranes for 10 min (Figures 3.4j and 3.4l). These results revealed that the chlorinated PEI-S@BNF-2h membranes shared a similar biocidal mechanism with chlorine disinfectants commercially applied in the water infiltration area, destroying bacterial cell structures with more effective biocidal activity and reusability.[16,24]

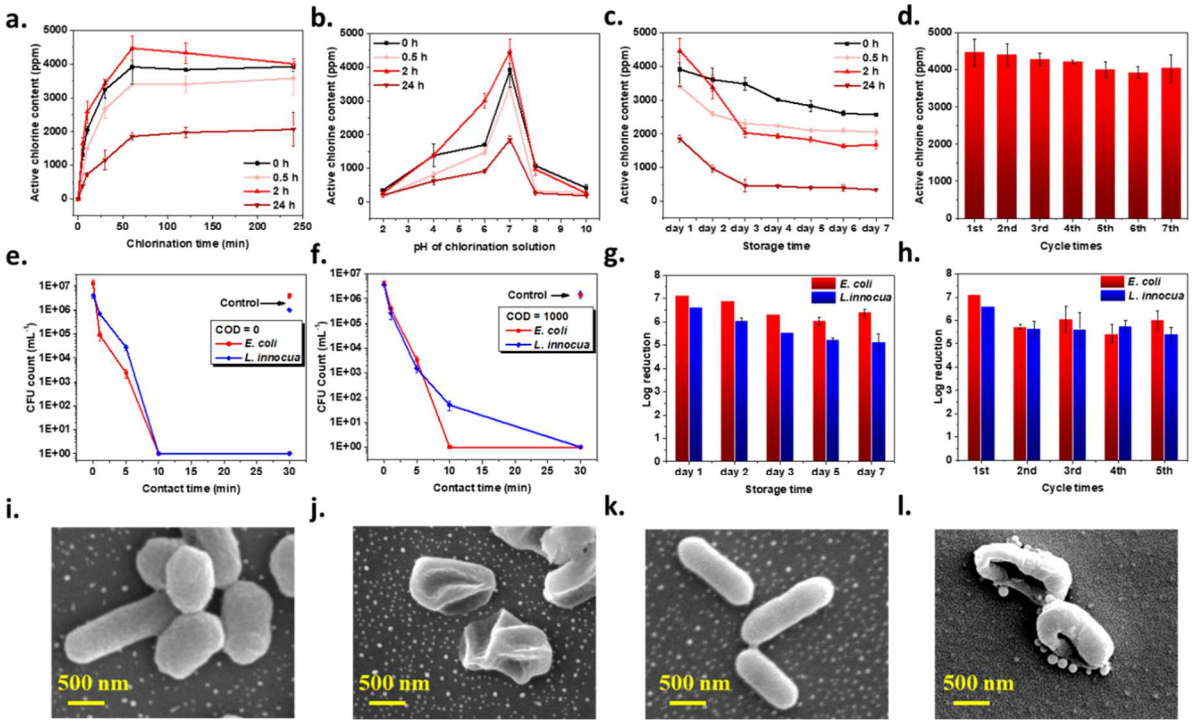

Figure 3.4. Active chlorine contents of PEI-S@BNF-xh as a function of (a) chlorination time, (b) pH of chlorination solutions, and (c) storage time. (d) Active chlorine contents of PEI-S@BNF-2h

membranes with 7 chlorine charging-quenching cycle tests. Time-dependent biocidal activities of the control membrane and the chlorinated PEI-S@BNF-2h membranes against *E. coli* and *L. innocua* with a COD condition of (e) 0 and (f) 1000 mg L^{-1}, respectively. Biocidal activity of chlorinated PEI-S@BNF-2h versus (g) storage time and (h) chlorine charging-quenching cycles (COD = 0 mg L^{-1}). SEM images of (i, j) *E. coli* and (k, l) *L. innocua* after exposing to (i, k) the control and (j, l) the chlorinated PEI-S@BNF-2h membrane, respectively.

3.3.6 Resisting function of PEI-S@BNF membranes

The N-halamine incorporated PEI-S@BNF membranes demonstrated the robust biocidal effects, which could significantly reduce the waterborne pathogens induced illnesses. However, the destroyed bacterial cell debris could still stay on the surfaces of the membranes, resulting in the formation of the biofilm, which then can hinder the biocidal effect and reduce the flowing fluxes. The introduced zwitterionic polymer (PEI-S) on the surfaces of the fibers in the membranes should bring expected resistance against biofoulants adhesion. Bovine Serum Albumins (BSA) was chosen as a model protein to assess the microbial resisting properties of the membranes. [24, 39, 40] Figure 3.5a depicts the varied amounts of absorbed BSA protein under different adsorption times on the control (unchlorinated BNF) and the sample (unchlorinated PEI-S@BNF-2h) membranes with an initial BSA concentration of 1 mg mL^{-1}. A total of 734 mg g^{-1} of BSA was captured by the control membrane after 720 min of adsorption. However, the sample membrane, containing PEI-S moieties, demonstrated a total of 430 mg g^{-1} of captured BSA, a 40 % of reduction compared to the control sample. In addition, the kinetics of the BSA adsorption can be described as a pseudo-first-order process, demonstrated in Figures 3.6a-3.6c. The predicted equilibrium BSA uptake over the unchlorinated PEI-S@BNF membrane (383.8 mg g^{-1}) was lower than that over the control membrane (628.9 mg g^{-1}), matching well with the experimental results.

The isothermal protein adsorption capacities of the control (unchlorinated BNF) and the sample (unchlorinated PEI-S@BNF-2h) membranes were investigated with various initial protein concentrations. As shown in Figure 3.5b, at constant room temperature, the saturated BSA adsorption capacity of the sample membrane was 800 mg g^{-1}, which only accounted for 60 % of the control membrane. These isothermal adsorption profiles were analyzed by both the Langmuir (Equation 3.7) and Freundlich isotherm linear models (Equation 3.8):

$$\frac{1}{C_{AS}} = \frac{1}{K_a C_s}\left(\frac{1}{C_e}\right) + \frac{1}{C_s} \qquad \text{(Equation 3.7)}$$

$$ln^{C_{AS}} = ln^{K_F} + n\, ln^{C_e} \qquad \text{(Equation 3.8)}$$

Where C_{AS} is the amount of adsorbed BSA per each gram of membrane, C_S is the maximum protein adsorption capacity, C_e is the equilibrium concentration of the protein, K_a and K_F are the Langmuir constant and Freundlich constant, respectively.

As shown in Figures 3.6d-3.6f, the isothermal adsorption behaviors of both the control and the sample groups fitted better with the monolayer Langmuir model ($R^2_{L,\ BNF} = 0.91$ and $R^2_{L,\ PEI\text{-}S@BNF} = 0.92$). With the presence of zwitterionic polymer, the sample membrane exhibited lower K_a and C_s values, which could be attributed to the generation of the electro-induced hydration layer, thereby reducing the affinity with the BSA protein and the overall adsorption capacity.

To evaluate the microbial resisting ability of the PEI-S@BNF membrane, we designed a touch-assay and incubate-assay to mimic the bacterial transfer process under dry and wet conditions, respectively. Following the touch-assay, *E. coli O157: H7-lux* (containing a complete *lux* operon *lux* CDABE; bioluminescence genes) coated agar plugs were "touched" with the unchlorinated membranes for 20 seconds. Widefield bioluminescence images were employed to determine the spatial distribution of *E. coli-lux* and intensities of bio-illumination signal (performed as Region

of Interest number with a total sample area of 2 × 2 cm^2) were measured to establish the magnitude of bacterial contamination. As shown in Figure 3.5c, the intensities of the bio-illumination signals of the unchlorinated PEI-S@BNF-2h and the unchlorinated BNF exhibit little difference with the ROI of 2.35 × 10^5 and 3.35 × 10^5 [p/s]/[μW/cm^2], respectively. For such bacteria touch assay, nearly no free water was involved, which significantly limited the generation of the hydration layer. Therefore, with the existence of the zwitterionic polymer moieties, the unchlorinated PEI-S@BNF, however, did not show the expected advantage over resisting the microbial adhesion. In the incubate-assay, the unchlorinated membranes were incubated in steady bacterial suspensions for 24 h, and then rinsed with fresh PBS buffer to remove planktonic bacteria. As shown in Figure 3.5d, the bio-illumination signal intensity of the control membrane (ROI_{BNF} = 2.98 × 10^6 [p/s]/[μW/cm^2]) was 3 times stronger than that of the unchlorinated PEI-S@BNF-2h membranes ($ROI_{PEI\text{-}S@BNF\text{-}2h}$ = 0.91 × 10^6 [p/s]/[μW/cm^2]). Individual bacterial distribution was described by the SEM images (Figures 3.5e-3.5h). After 24 h bacterial incubation, more *E. coli* bacteria could be found on the surface of the control membrane, and some of them aggregated together, which is an early warning of biofilm formation (Figure 3.5f). In contrast, the added zwitterion moieties reduced the amount of adhered bacteria on the PEI-S@BNF-2h membrane. These findings are well in agreement with the quantitative results of widefield bioluminescence images. As expected, when the zwitterionic polymer (PEI-S) was incorporated with the BNF membrane, it could effectively reduce the bacterial adhesion in the wet contamination conditions and hinder the formation of the biofilm via weakening the protein-membrane interaction.

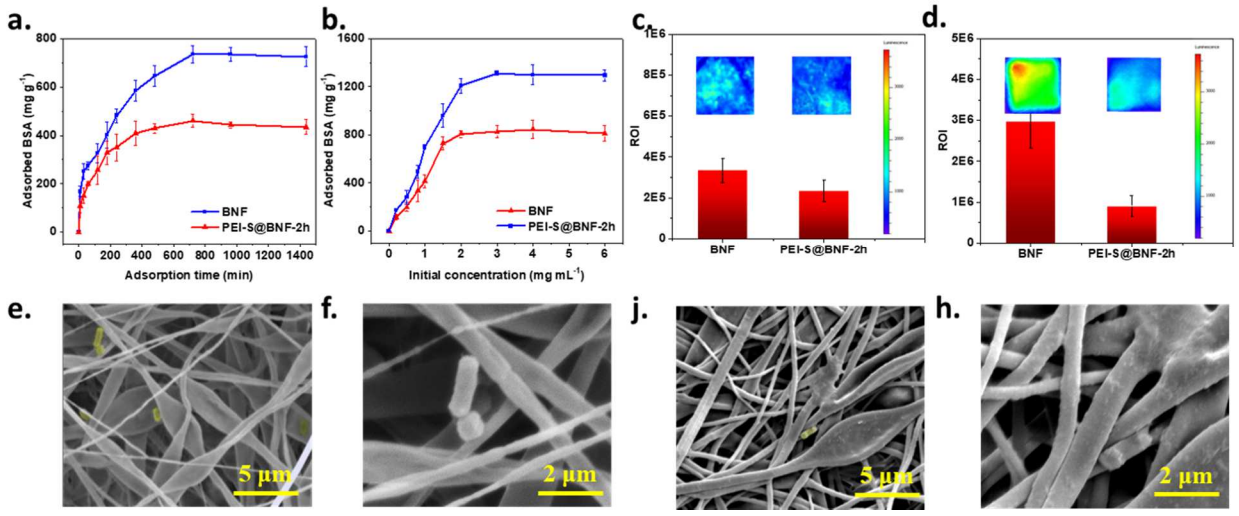

Figure 3.5. (a) Kinetic and (b) isotherm BSA adsorption profiles of the unchlorinated BNF and the unchlorinated PEI-S@BNF-2h membrane at room temperature. Widefield bioluminescence images of the unchlorinated BNF and the unchlorinated PEI-S@BNF-2h tested by (c) touch-assay and (d) incubate assay, respectively. SEM images of (e, f) the unchlorinated BNF and (j, h) the unchlorinated PEI-S@BNF membranes after incubating with *E. coli* suspension for 24 h.

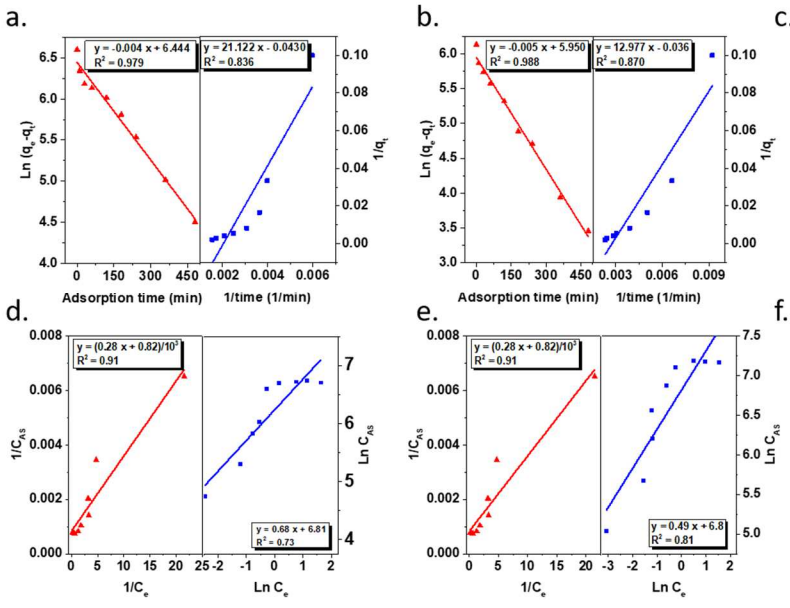

c.

		BNF	PEI-S@BNF-2h
Pseudo 1st order	q_e	628.9	383.8
	$K_1\times10^{-3}$	9.2	11.5
	R^2	0.979	0.988
Pseudo 2nd order	q_e	-2.3	-27.7
	$K_2\times10^{-3}$	8.8	10
	R^2	0.836	0.87

f.

		BNF	PEI-S@BNF-2h
Langmuir model	C_s	1226.1	869.6
	K_a	2.9	1.7
	R^2	0.91	0.92
Fruendlich model	K_f	906.9	453.9
	n	0.5	0.7
	R^2	0.81	0.73

Figure 3.6. The linear fittings of isothermal adsorption kinetics of BSA protein by pseudo 1st order and Pseudo 2nd order kinetic models on (a) BNF and (b) PEI-S@BNF-2h. The linear fittings of BSA adsorption isotherms by Langmuir model and Freundlich model on (d) BNF and (e) PEI-S@BNF-2h. Tables of (c) adsorption kinetic parameters and (f) adsorption isotherm parameters.

3.3.7 Releasing function of PEI-S@BNF membranes

The PEI-S@BNF membranes also possess microorganisms releasing functions, which were studied in this work. BSA protein was employed as a model biofoulant in the study of the releasing mechanism of biomolecules on the membranes. The unchlorinated control (BNF) and the unchlorinated sample (PEI-S@BNF-2h) membranes were loaded with the same amount of the BSA protein, and then incubated in PBS buffers for different releasing times. A proposed scheme of the loaded protein distribution (without releasing) on the nanofibrous membrane is displayed as Figure 3.7a. There are mainly three positions of the proteins: on the top membrane surface (area □), near the membrane surface (area □), and inside the nanofibrous network (area □), corresponding to three stages (stage □-□) of whole-lifetime protein releasing profile (Figure 3.7b), respectively. At the initial 3 min releasing time (stage I), both the control and the sample membranes exhibited a burst release with more than 80 % of the protein released into the external medium. These proteins may mainly aggregate on the outside surface of the membranes (area i). Therefore, the weak interaction between proteins and fibers caused rapid and large amounts of protein release in a short time. To future investigate the releasing behavior, these data were fitted into the Ritger-Peppas model, as shown in equation 3.9: [41, 42]

$$\frac{M_t}{M_\infty} = kt^n \qquad \text{Equation (3.9)}$$

Where M_t is the cumulative amount of the protein released at time t. M_∞ is the total amount released protein. K is the kinetic constant, and n is the diffusion exponent. In the cylindrical case, when n < 0.45, the release mechanism is typical Fickian diffusion.

As shown in Figure 3.8a, the first stage followed a typical Fickian diffusion with mild influence from the membranes ($n_{1,\ BNF} = 0.40 \approx n_{2,\ PEI\text{-}S@BNF\text{-}2h} = 0.42 < 0.45$); therefore, we ignored the stage I and adjusted the starting point as $t_0 = 3$ min. (Figures 3.7c and 3.8b). At Stage □, the releasing rate of the sample membrane is $k_{2,\ PEI\text{-}S@BNF\text{-}2h} = 0.56\ min^{-1}$, higher than that of the control membrane ($k_{2,\ BNF} = 0.43\ min^{-1}$). With the presence of superhydrophilic zwitterionic polymer (PEI-S), the stronger interaction between the PEI-S and surrounding water molecules allows the formation of a hydration layer, leading to a faster release of the protein located on area ii. At Stage □, a longer diffusion time is required for the proteins to transfer from the inside membrane to the external medium. Therefore, the protein releasing rates at stage □ showed a significant decrease with $k_{3,\ BNF} = 0.06\ min^{-1}$, and $k_{3,\ PEI\text{-}S@BNF\text{-}2h} = 0.09\ min^{-1}$.

The bacterial releasing performances of the unchlorinated BNF and unchlorinated PEI-S@BNF-2h membranes were investigated by applying *E. coli* and *E. coli-lux*. Figure 3.7d depicts the bacterial releasing curves of the unchlorinated membrane as a function of releasing time, which could be divided into two stages. Both the unchlorinated BNF and the unchlorinated PEI-S@BNF-2h showed a similar releasing performance, with about 3 log CFU of *E. coli* released from the membranes to the releasing buffer at the beginning 5 min, corresponding to the Stage I in Figure 3.7a. At the second bacterial releasing stage, the unchlorinated PEI-S@BNF-2h exhibited a stronger releasing performance with 6 log CFU of coated *E. coli* released after 30 min of incubation with the PBS solution. However, without the existence of zwitterionic polymer, the unchlorinated BNF membranes required 60 min to release the same amount of the loaded *E. coli*. Widefield

bioluminescence microscope and SEM imaging were applied to visualize the release of *E. coli-lux* and *E. coli* from the unchlorinated membranes, respectively. After 30 min release, the unchlorinated BNF membrane only achieved a 4-fold decrease in bio-illumination signal compared with that before release. ($ROI_{BNF} = 0.64 \times 10^6$; $ROI_{before\ release} = 2.29 \times 10^6$ [p/s]/[μW/cm^2]). In contrast, the unchlorinated PEI-S@BNF-2h showed a 56-fold decrease with $ROI_{PEI\text{-}S@BNF\text{-}2h} = 0.0429 \times 10^6$ [p/s]/[μW/cm^2], indicating that most of the *E. coli-lux* have been released to the PBS solution. Figures 3.7f i) and ii) exhibit the distributions of the coated *E. coli* on the unchlorinated membranes. Before release, similar to the proposed protein distribution (Figure 3.7a, area i), abundance and stacking of bacteria aggregated on the membrane surface. After 15 min release, as shown in Figures 3.7f iii)-vi), the aggregated bacteria were washed off, and only a small amount of bacteria were scattered on the unchlorinated BNF membranes. With the existence of the zwitterionic polymer, even fewer bacteria could be found on the unchlorinated PEI-S@BNF-2h membrane surface compared with the BNF one. These findings are consistent with the results of the widefield bioluminescence images and agar plate CFU counts, confirming the good releasing behavior of the PEI-S@BNF-2h membranes.

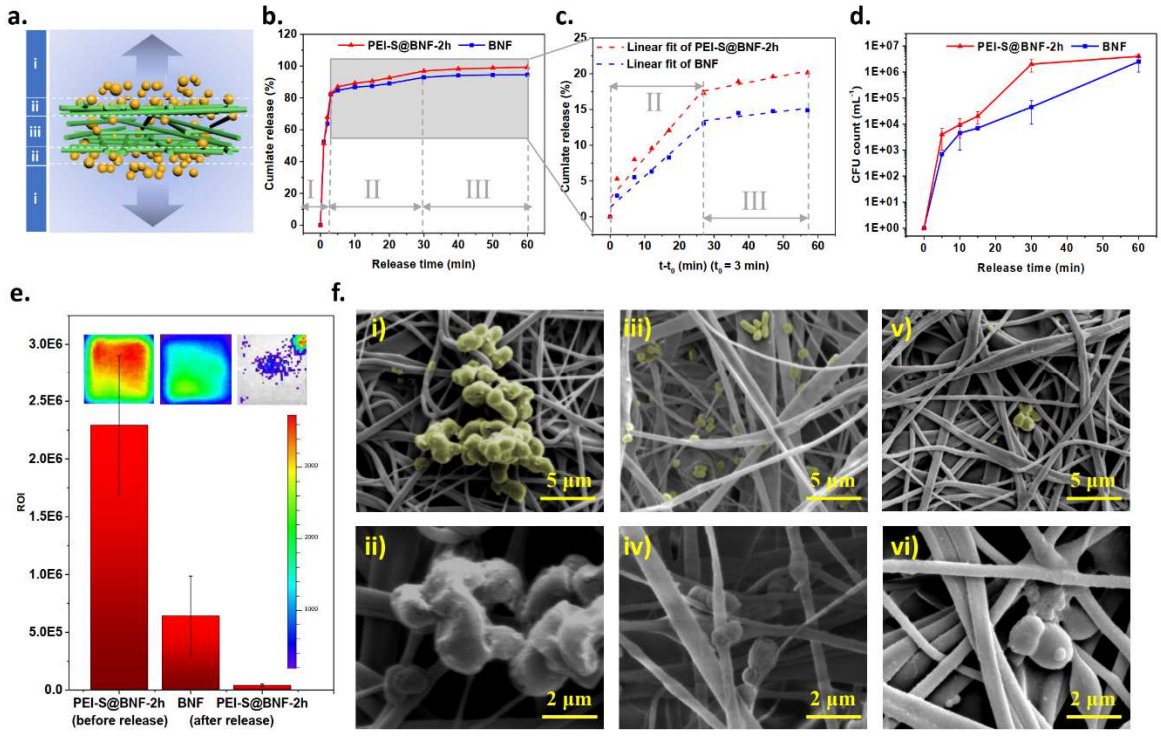

Figure 3.7. (a) Schematic illustration of the loaded BSA distribution on the membrane divided into three areas. Cumulative BSA releasing rates of the unchlorinated BNF and the unchlorinated PEI-S@BNF-2h with (b) t_0 = 0 min and (c) t_0 = 3 min, respectively. (d) Time-dependent microbial releasing performance of the unchlorinated BNF and the unchlorinated PEI-S@BNF-2h assessed by a plate counting method. (e) Widefield bioluminescence images and (f) SEM images of the unchlorinated PEI-S@BNF-2h (i, ii) before and (v, vi) after 30 min of release, and the unchlorinated BNF (iii, iv) after 30 min of release.

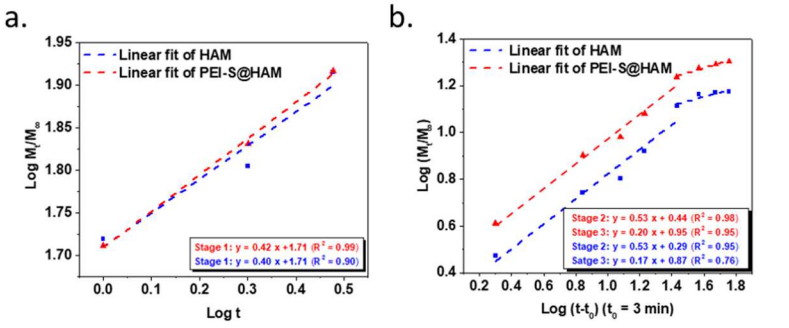

c.

n value	Stage I	Stage II	Stage III
BNF	0.4	0.53	0.17
PEI-S@BNF-2h	0.42	0.53	0.2

Figure 3.8. The BSA protein release profiles at (a) stage I and (b) stage □ and □ fitting by the Ritger-Peppas model. (c) Table of n values.

3.3.8 Disinfection of *E. coli* contaminated water

The water disinfection test by direct filtration was performed on the membranes, as shown in the inset of Figure 3.9a. The chlorinated PEI-S@BNF-2h membranes were fixed between two sterilized plastic tubes, and a fluid (bacterial suspension or sterilized water) was pumped through the membrane using a programed syringe pump. With the bacterial suspensions flow through the membranes, the bacteria were intercepted and killed in touch with the chlorinated PEI-S@BNF-2h membranes. Furthermore, the contaminated membranes were washed by pumping sterilized water to remove adhered live/dead bacteria, therefore, avoiding the formation of the biofilm. As shown in Figure 3.9a, when the filtration fluxes were less than 6000 L m^{-2} h^{-1}, only about 1 log of bacteria were trapped inside the unchlorinated BNF membranes. In sharp contrast, the chlorinated PEI-S@BNF-2h membrane achieved 6 log CFU reduction of the *E. coli* even with a high flux of 10000 L m^{-2} h^{-1}. To test the durability of the biocidal activity of membranes, the bacteria-contaminated water (8×10^6 CFU mL^{-1}) was continuously injected through the filtration module with a constant flux of 10000 L m^{-2} h^{-1}. As shown in Figure 3.9b, the chlorinated PEI-S@BNF-2h effectively killed 6 log CFU of the *E, coli* within the test filtration amount of 7143 L m^{-2}. With a further increase of filtration amount of the liquid, more survival bacteria in the filtered water could be detected as a cumulative consumption of the active chlorine. Considering the active chlorine of the PEI-S@BNF-2h membrane could be easily recharged by chlorination in a diluted chlorine bleach solution, such a high biocidal efficiency provides a guarantee for water disinfection. However, with solely the biocidal function available, the membranes may suffer from the declines

of the disinfection efficiency and flowing fluxes due to the biofouling effect after long-term and repeated usage.

The addition of zwitterionic polymer moieties, PEI-S, enables the membrane with promising antifouling performance and prolong the lifetime of services. Such a function can be demonstrated in an easy clean-water backwashing process without involving harsh cleaning conditions reported in the literature.[43, 44] After disinfecting 1000 mL of concentrated bacteria-contaminated water (8×10^6 CFU mL^{-1}), the filter membranes were washed with 20 mL of the sterilized water in the opposite direction. The cleaning effects were evaluated by the SEM images. As shown in Figure 3.9c, the chlorinated BNF membrane, with solely biocidal function, destroyed the bacterial cellular structure; however, the generated bacterial debris aggregated together and trapped inside the nanofibrous network. In contrast, nearly no bacterial debris could be observed on the chlorinated PEI-S@BNF-2h membrane, which indicated the good antifouling function of the introduced zwitterionic polymer (PEI-S) (Figure 3.9d).

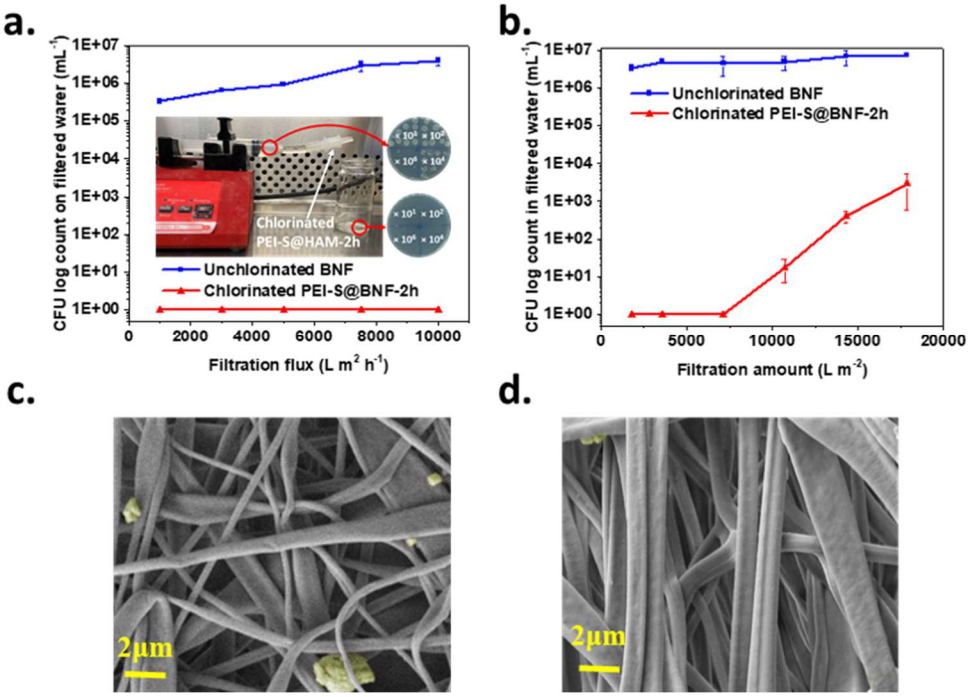

Figure 3.9. CFU log count of *E. coli* in filtered water as a function of (a) filtration fluxes and (b) filtration amounts. SEM images of (c) the chlorinated BNF and (d) the chlorinated PEI-S@BNF-2h after disinfected 1000 mL of bacteria-contaminated water.

3.3.9 Biocidal, antifouling, and antibiofilm performances of the PEI-S@BNF membranes

As shown in Figure 3.10, the BNF, the PEI-S@BNF, and the PEI-S@BNF-Cl were shaped and fixed onto a glass chip, and then incubated it with an *E. coli-lux* solution with a concentration of 10^8 CFU mL^{-1} for 1 hour. Subsequently, the planktonic bacteria were rinsed away using an excess amount of sterilized DI water. The distributions of the bacteria are displayed in step 4. The PEI-S@BNF-Cl containing active chlorine killed the bacteria with no bio-illumination signal detected. With a zwitterionic polymer, PEI-S, the PEI-S@BNF showed weaker bio-illumination signal intensity compared with the BNF square frame.

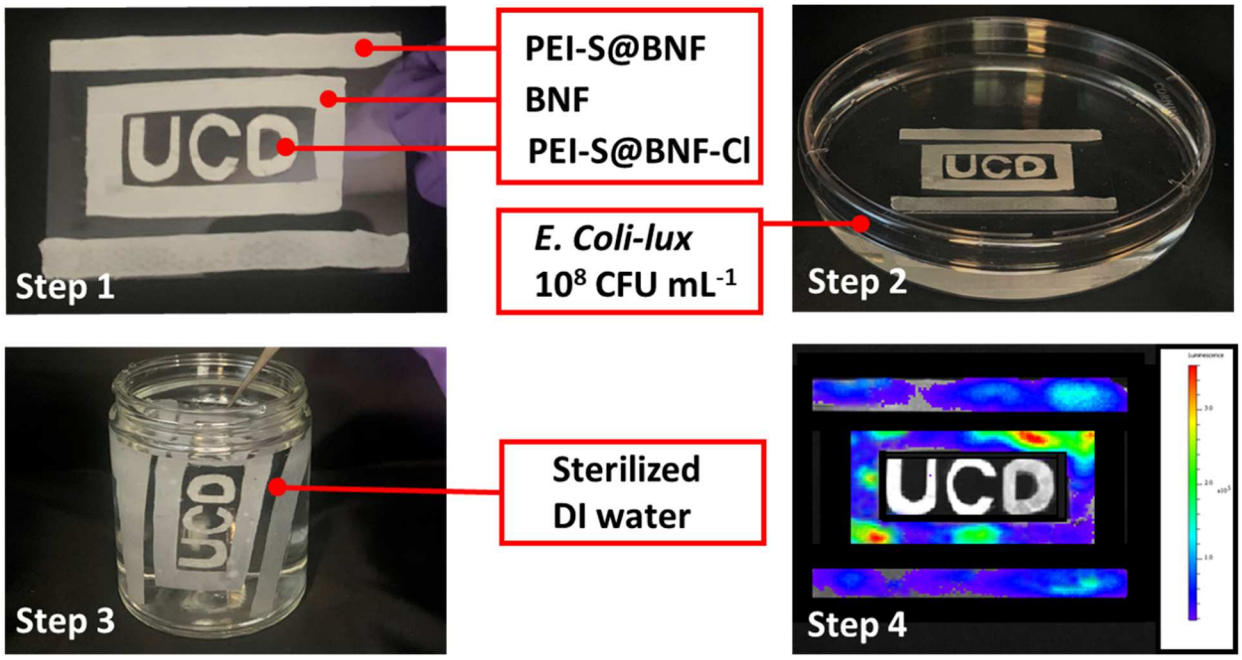

Figure 3.10. Illustration of showing the experimental process (step 1-3) and the result of the *E. coli-lux* distribution (step 4).

Antibiofilm function of the PEI-S@BNF-2h membrane was further evaluated by using a colorimetric stain test. Biofilm adherence assay is described in the supplementary discussion. In brief, the membranes were exposed to *E. coli* culture for four days, and the formed biofilms on the membranes were stained by using 0.1% crystal violet solution. Optical densities of the samples were measured at 570 nm using a UV-vis spectrophotometer, revealing the extents of formed biofilms on the membranes. As shown in Figure 3.11, the combination of antimicrobial and antifouling function on the PEI-S@BNF-Cl membrane demonstrated desirable antibiofilm formation performance, with 84% reduction of relative biofilm formation compared with that of the BNF membrane. Solely introduction of the zwitterionic polymer could also reduce about 50% of it. The results further support the superhydrophilic function of the zwitterionic structures and

the combined functions of resisting, biocidal, and releasing of microorganisms of the PEI-S@BNF-Cl membranes, as well as a desired antibiofilm effect on the materials.

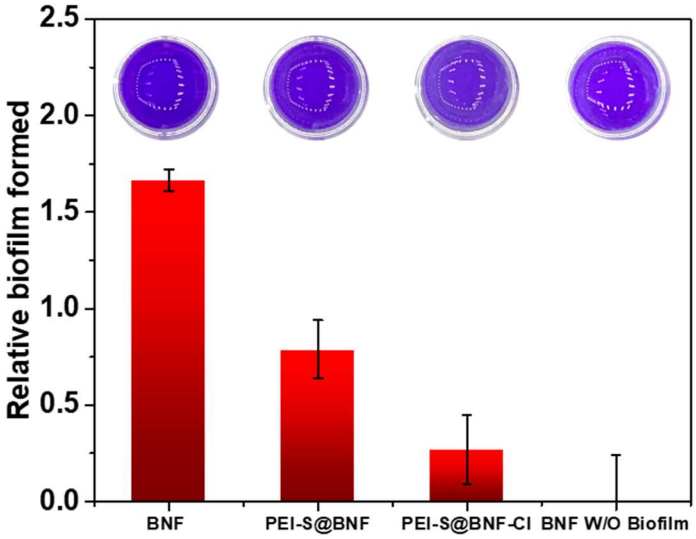

Figure 3.11. Crystal violet biofilm assay for *E. coli* and representative images of the well containing the resuspended crystal violet as a measure of the extent of biofilm formation.

3.4 Conclusions

A multifunctional nanofibrous membrane was successfully prepared by combining a zwitterionic polymer (PEI-S) with a halamine grafted PVA-co-PE nanofibrous membrane (BNF) to disinfect the microbe-contaminated water and limit the biofouling effect. The obtained PEI-S@BNF-2h membrane, with high active chlorine content, large specific surface area, ease of chlorine rechargeability, and long-term stability exhibited a promising biocidal activity, achieving 6 and 4 log CFU reduction of *E. coli* and *L. innocua*, respectively, in a short contact time of 10 min even at a high COD condition. More importantly, the zwitterionic polymer moieties (PEI-S) brought robust antifouling properties to this biocidal membrane, therefore, reducing the formation of biofilm and prolonging the lifetime of the filtration membrane. These attributes enable the PEI-

S@BNF-2h to effectively disinfect the microbe-contaminated water in high fluxes and maintain itself clean for a long-term application.

3.5 References

1. Zeng, X.; McCarthy, D. T.; Deletic, A.; Zhang, X., Silver/reduced graphene oxide hydrogel as novel bactericidal filter for point□of□use water disinfection. *Advanced Functional Materials* **2015,** *25* (27), 4344-4351.
2. Mekonnen, M. M.; Hoekstra, A. Y., Four billion people facing severe water scarcity. *Science Advances* **2016,** *2* (2), e1500323.
3. Vilela, D.; Stanton, M. M.; Parmar, J.; Sánchez, S., Microbots decorated with silver nanoparticles kill bacteria in aqueous media. *ACS Applied Materials & Interfaces* **2017,** *9* (27), 22093-22100.
4. WHO global water, sanitation and hygiene annual report 2018, https://apps.who.int/iris/bitstream/handle/10665/327118/WHO-CED-PHE-WSH-19.147-eng.pdf?ua=1, accessed: August 2020.
5. Alonso, A.; Muñoz□Berbel, X.; Vigués, N.; Rodríguez□Rodríguez, R.; Macanás, J.; Muñoz, M.; Mas, J.; Muraviev, D. N., Superparamagnetic Ag@ Co□nanocomposites on granulated cation exchange polymeric matrices with enhanced antibacterial activity for the environmentally safe purification of water. *Advanced Functional Materials* **2013,** *23* (19), 2450-2458.
6. Wen, J.; Tan, X.; Hu, Y.; Guo, Q.; Hong, X., Filtration and electrochemical disinfection performance of PAN/PANI/AgNWs-CC composite nanofiber membrane. *Environmental Science & Technology* **2017,** *51* (11), 6395-6403.
7. Smith, E. M.; Plewa, M. J.; Lindell, C. L.; Richardson, S. D.; Mitch, W. A., Comparison of byproduct formation in waters treated with chlorine and iodine: relevance to point-of-use treatment. *Environmental Science & Technology* **2010,** *44* (22), 8446-8452.

8. Zhang, X.; Zhang, T.; Ng, J.; Sun, D. D., High□performance multifunctional TiO2 nanowire ultrafiltration membrane with a hierarchical layer structure for water treatment. *Advanced Functional Materials* **2009,** *19* (23), 3731-3736.
9. Shao, S.; Liang, H.; Qu, F.; Li, K.; Chang, H.; Yu, H.; Li, G., Combined influence by humic acid (HA) and powdered activated carbon (PAC) particles on ultrafiltration membrane fouling. *Journal of Membrane Science* **2016,** *500*, 99-105.
10. Shao, P.; Yao, R.; Li, G.; Zhang, M.; Yuan, S.; Wang, X.; Zhu, Y.; Zhang, X.; Zhang, L.; Feng, X., Molecular□Sieving membrane by partitioning the channels in ultrafiltration membrane by in situ polymerization. *Angewandte Chemie International Edition* **2020,** *59* (11), 4401-4405.
11. Wang, F.; Zheng, T.; Xiong, R.; Wang, P.; Ma, J., CDs@ ZIF-8 modified thin film polyamide nanocomposite membrane for simultaneous enhancement of chlorine-resistance and disinfection byproducts removal in drinking water. *ACS Applied Materials & Interfaces* **2019,** *11* (36), 33033-33042.
12. Wang, Z.; Wang, Z.; Lin, S.; Jin, H.; Gao, S.; Zhu, Y.; Jin, J., Nanoparticle-templated nanofiltration membranes for ultrahigh performance desalination. *Nature Communications* **2018,** *9* (1), 1-9.
13. Han, Y.; Xu, Z.; Gao, C., Ultrathin graphene nanofiltration membrane for water purification. *Advanced Functional Materials* **2013,** *23* (29), 3693-3700.
14. Ding, Y.; Ma, B.; Liu, H.; Qu, J., Effects of protein properties on ultrafiltration membrane fouling performance in water treatment. *Journal of Environmental Sciences* **2019,** *77*, 273-281.
15. Herzberg, M.; Elimelech, M., Biofouling of reverse osmosis membranes: role of biofilm-enhanced osmotic pressure. *Journal of Membrane Science* **2007,** *295* (1-2), 11-20.

16. Si, Y.; Li, J.; Zhao, C.; Deng, Y.; Ma, Y.; Wang, D.; Sun, G., Biocidal and rechargeable N-halamine nanofibrous membranes for highly efficient water disinfection. *ACS Biomaterials Science & Engineering* **2017,** *3* (5), 854-862.
17. Zhu, Y.; Wang, J.; Zhang, F.; Gao, S.; Wang, A.; Fang, W.; Jin, J., Zwitterionic nanohydrogel grafted PVDF membranes with comprehensive antifouling property and superior cycle stability for oil□in□water emulsion separation. *Advanced Functional Materials* **2018,** *28* (40), 1804121.
18. Jiang, S.; Cao, Z., Ultralow□fouling, functionalizable, and hydrolyzable zwitterionic materials and their derivatives for biological applications. *Advanced Materials* **2010,** *22* (9), 920-932.
19. Hung, H. C.; Jain, P.; Zhang, P.; Sun, F.; Sinclair, A.; Bai, T.; Li, B.; Wu, K.; Tsao, C.; Liu, E. J., A coating□free nonfouling polymeric elastomer. *Advanced Materials* **2017,** *29* (31), 1700617.
20. Ma, Y.; Li, J.; Si, Y.; Huang, K.; Nitin, N.; Sun, G., Rechargeable antibacterial N-halamine films with antifouling function for food packaging applications. *ACS Applied Materials & Interfaces* **2019,** *11* (19), 17814-17822.
21. Venault, A.; Wei, T.-C.; Shih, H.-L.; Yeh, C.-C.; Chinnathambi, A.; Alharbi, S. A.; Carretier, S.; Aimar, P.; Lai, J.-Y.; Chang, Y., Antifouling pseudo-zwitterionic poly (vinylidene fluoride) membranes with efficient mixed-charge surface grafting via glow dielectric barrier discharge plasma-induced copolymerization. *Journal of Membrane Science* **2016,** *516*, 13-25.
22. Li, M.-Z.; Li, J.-H.; Shao, X.-S.; Miao, J.; Wang, J.-B.; Zhang, Q.-Q.; Xu, X.-P., Grafting zwitterionic brush on the surface of PVDF membrane using physisorbed free radical grafting technique. *Journal of Membrane Science* **2012,** *405*, 141-148.

23. Li, N.; Li, T.; Qiao, X.-Y.; Li, R.; Yao, Y.; Gong, Y.-K., Universal strategy for efficient fabrication of blood compatible surfaces via polydopamine-assisted surface-initiated activators regenerated by electron transfer atom-transfer radical polymerization of zwitterions. *ACS Applied Materials & Interfaces* **2020,** *12* (10), 12337-12344.
24. Ma, Y.; Zhang, Z.; Nitin, N.; Sun, G., Integration of photo-induced biocidal and hydrophilic antifouling functions on nanofibrous membranes with demonstrated reduction of biofilm formation. *Journal of Colloid and Interface Science* **2020,** *578*, 779-787.
25. Amadei, C. A.; Yang, R.; Chiesa, M.; Gleason, K. K.; Santos, S., Revealing amphiphilic nanodomains of anti-biofouling polymer coatings. *ACS Applied Materials & Interfaces* **2014,** *6* (7), 4705-4712.
26. Chen, S.; Xie, Y.; Xiao, T.; Zhao, W.; Li, J.; Zhao, C., Tannic acid-inspiration and post-crosslinking of zwitterionic polymer as a universal approach towards antifouling surface. *Chemical Engineering Journal* **2018,** *337*, 122-132.
27. Yao, L.; He, C.; Chen, S.; Zhao, W.; Xie, Y.; Sun, S.; Nie, S.; Zhao, C., Codeposition of polydopamine and zwitterionic polymer on membrane surface with enhanced stability and antibiofouling property. *Langmuir* **2018,** *35* (5), 1430-1439.
28. Si, Y.; Cossu, A.; Nitin, N.; Ma, Y.; Zhao, C.; Chiou, B. s.; Cao, T.; Wang, D.; Sun, G., Mechanically robust and transparent N□halamine grafted PVA□co□PE films with renewable antimicrobial activity. *Macromolecular Bioscience* **2017,** *17* (3), 1600304.
29. Zhao, C.; Si, Y.; Pan, B.; Taha, A. Y.; Pan, T.; Sun, G., Design and fabrication of a highly sensitive and naked-eye distinguishable colorimetric biosensor for chloramphenicol detection by using ELISA on nanofibrous membranes. *Talanta* **2020**, 121054.

30. Bainor, A.; Chang, L.; McQuade, T. J.; Webb, B.; Gestwicki, J. E., Bicinchoninic acid (BCA) assay in low volume. *Analytical Biochemistry* **2011,** *410* (2), 310-312.

31. Imani, S. M.; Maclachlan, R.; Rachwalski, K.; Chan, Y.; Lee, B.; McInnes, M.; Grandfield, K.; Brown, E. D.; Didar, T. F.; Soleymani, L., Flexible hierarchical wraps repel drug-resistant gram-negative and positive bacteria. *ACS Nano* **2019,** *14* (1), 454-465.

32. Huang, K.; Dou, F.; Nitin, N., Biobased sanitizer delivery system for improved sanitation of bacterial and fungal biofilms. *ACS Applied Materials & Interfaces* **2019,** *11* (19), 17204-17214.

33. You, Y.; Sun, X.; Cui, Q.; Wang, B.; Ma, J., The retention and drainage behavior of cross-linked gelatin with glutaraldehyde in a papermaking system. *BioResources* **2016,** *11* (3), 6162-6173.

34. Peng, X.; Liu, H.; Yin, Q.; Wu, J.; Chen, P.; Zhang, G.; Liu, G.; Wu, C.; Xie, Y., A zwitterionic gel electrolyte for efficient solid-state supercapacitors. *Nature Communications* **2016,** *7* (1), 1-8.

35. Shahkaramipour, N.; Tran, T. N.; Ramanan, S.; Lin, H., Membranes with surface-enhanced antifouling properties for water purification. *Membranes* **2017,** *7* (1), 13.

36. Yudianti, R.; Karina, M.; Sakamoto, M.; Azuma, J.-i., DSC analysis on water state of salvia hydrogels. *Macromolecular Research* **2009,** *17* (12), 1015-1020.

37. Hatakeyma, T.; Kasuga, H.; Tanaka, M.; Hatakeyama, H., Cold crystallization of poly (ethylene glycol)–water systems. *Thermochimica Acta* **2007,** *465* (1-2), 59-66.

38. Hui, F.; Debiemme-Chouvy, C., Antimicrobial N-halamine polymers and coatings: a review of their synthesis, characterization, and applications. *Biomacromolecules* **2013,** *14* (3), 585-60.

39. Zhi, Z.; Su, Y.; Xi, Y.; Tian, L.; Xu, M.; Wang, Q.; Padidan, S.; Li, P.; Huang, W., Dual-functional polyethylene glycol-b-polyhexanide surface coating with in vitro and in vivo

antimicrobial and antifouling activities. *ACS Applied Materials & Interfaces* **2017,** *9* (12), 10383-10397.

40. Chen, H.; Zhang, M.; Yang, J.; Zhao, C.; Hu, R.; Chen, Q.; Chang, Y.; Zheng, J., Synthesis and characterization of antifouling poly (N-acryloylaminoethoxyethanol) with ultralow protein adsorption and cell attachment. *Langmuir* **2014,** *30* (34), 10398-10409.
41. Wu, J.; Zhang, Z.; Zhou, W.; Liang, X.; Zhou, G.; Han, C. C.; Xu, S.; Liu, Y., Mechanism of a long-term controlled drug release system based on simple blended electrospun fibers. *Journal of Controlled Release* **2020,** *320*, 337-346.
42. Srikar, R.; Yarin, A.; Megaridis, C.; Bazilevsky, A.; Kelley, E., Desorption-limited mechanism of release from polymer nanofibers. *Langmuir* **2008,** *24* (3), 965-974.
43. Lim, A.; Bai, R., Membrane fouling and cleaning in microfiltration of activated sludge wastewater. *Journal of Membrane Science* **2003,** *216* (1-2), 279-290.
44. Mi, B.; Elimelech, M., Organic fouling of forward osmosis membranes: fouling reversibility and cleaning without chemical reagents. *Journal of Membrane Science* **2010,** *348* (1-2), 337-345.

Chapter 4. Integration of Photo-induced Biocidal and Hydrophilic Antifouling Functions on Nanofibrous Membranes with Demonstrated Reduction of Biofilm Formation

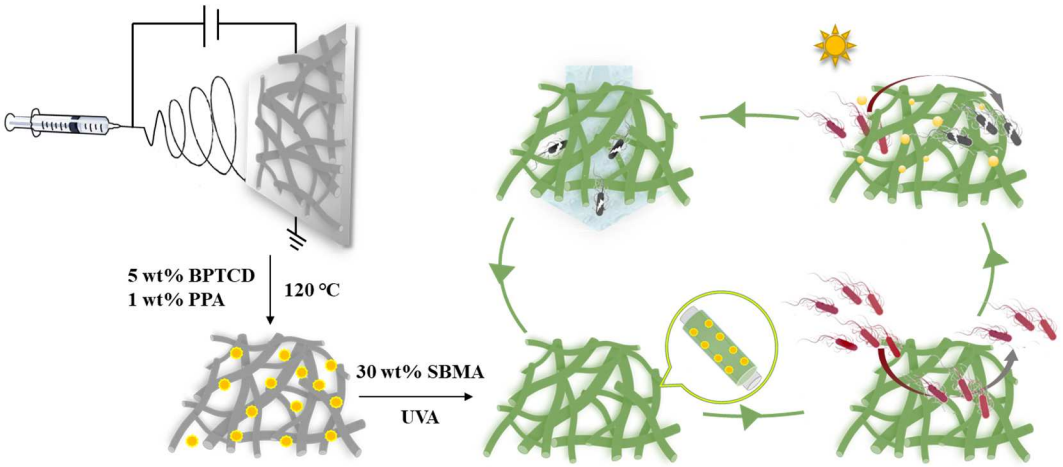

Abstract

Survival and pathogenic microbial adhesions on surfaces of materials followed by the formation of biofilms with robust resistance to antibiotics constitute the forefront of disease transmissions. Conventional strategies responding to this challenge are rather limited due to the biofouling effect of microorganisms or the irreversible consumption of antimicrobial agents embedded into the materials. Herein, we report an approach of combining photo-induced rechargeable biocidal properties with microbial resisting and releasing zwitterionic hydrophilic functions on surfaces of materials to improve antifouling performances. Poly(vinyl alcohol-co-ethylene) (EVOH) nanofibrous membranes (NFMs) were chemically incorporated with both 3,3′,4,4′-benzophenonetetracarboxylic dianhydride (BPTCD), a photoactive chemical, and [2-(methacryloyloxy)ethyl]dimethyl-(3-sulfopropyl)ammonium hydroxide (SBMA), a zwitterionic monomer. Both functional agents work independently and construct concerted microbial resisting, killing, and releasing functions to reduce biofilm formation and microbial contamination. The resulted SBMA@EVOH NFMs exhibited integrated features of large ROS production capacity, ease of photoactive rechargeability and controllability, long-term stability, high biocidal efficacy (> 99.9999% via contact killing), and promising antifouling performance, which enable the SBMA@EVOH NFMs to serve as a biocidal material for food safety and medical applications.

Objectives

- Fabricate a photo-induced biocidal and antifouling nanofibrous membrane (SBMA@EVOH).
- Characterize the physiochemical performances of the obtained SBMA@EVOH, including thermal performance, mechanical property, and hydrophilicity.

- Evaluate the ROS generation and antimicrobial performance of the designed nanofibrous membrane under different lighting conditions.
- Evaluate the resisting/ releasing effect of the designed SBMA@EVOH against bacteria.

4.1 Introduction

Foodborne disease outbreaks have been frequent public concerns,[1,2] highlighted by a World Health Organization (WHO) news in 2019. 23 million people suffer from foodborne illnesses, and an estimated 4700 deaths each year in Europe.[3] Surface contaminations of food packages and food processing devices contribute to microbial transfer, cross-contamination, and spread of diseases.[4,5] A common strategy responding to this challenge has been directly applying antimicrobials, such as chitosan, peptides, essential oils, and silver nanoparticles, onto the highly risky surfaces to reduce pathogen populations.[6-10] However, the application of antimicrobial agents has limited effect on reducing bacterial adhesion and preventing the formation of biofilms.[11,12] Once the biofilm is formed, its removal is very difficult to be achieved due to complex exopolysaccharides matrix structure of the biofilm, which could physically hinder the mass transfer of the antimicrobial agents, consequently weaken the antimicrobial effect.[11,13]

An ideal strategy for prevention of the biofilm formation has been proposed and implemented in our previous study by integrating both chlorine rechargeable biocidal properties and hydrophilic antifouling functions together on surfaces of materials.[14] The rechargeable biocidal function ensures the speed, efficiency, and reusability of the function in a long-term application;[15,16] and antifouling function may include microbial resisting and releasing abilities to non-specific biomass adhesion.[17, 18] N-halamine, as a rechargeable biocidal moiety, has been proven effective in providing satisfying killing performance against various pathogens.[19-21] However, the use of chlorine bleach solution as a recharging agent for the materials significantly limits their

applications due to corrosive and hazardous effects of chlorine.[22] Photoactive chemicals can produce reactive oxygen species (ROS) including hydroxyl radicals, hydrogen peroxide, and singlet oxygen under light irradiation and have exhibited light-rechargeable and stable biocidal efficiency against a broad spectrum of pathogens, which could be a good alternative to the halamines.[22,23] Benzophenone derivatives could effectively produce ROS under daylight and UVA irradiations, in this regard, would be a promising candidate to serve as a biocidal agent for the food contact surface and medical applications.[23-26] Polyethylene glycol (PEG) and oligoethylene glycol (OEG) have been wildly reported as hydrophilic antifouling reagents.[27-29] However, the chemical stability of these compounds is insufficient as they tend to be auto-oxidized, especially under photo irradiation, forming aldehydes and ethers in the presence of oxygen.[30,31] Zwitterionic structures are advantages since they are chemically stable and can generate a dense electrostatically induced hydration layer, therefore, offering the surface with good antifouling performance.[14,32] Thus, zwitterion chemicals are considered as a promising candidate to constructing an antifouling surface for food and medical applications. [33, 34]

Herein, we report the development of nanofibrous membranes (NFMs) possessing both photo-induced rechargeable biocidal and antifouling functions to prove the concept. Poly (vinyl alcohol-co-ethylene) nanofibrous membranes (PVA-co-PE NFMs or EVOH NFMs) were chemically modified by incorporating both 3,3′,4,4′-benzophenonetetracarboxylic dianhydride (BPTCD), a photoactive chemical, and [2-(methacryloyloxy)ethyl]dimethyl-(3-sulfopropyl)ammonium hydroxide (SBMA), a zwitterionic monomer. The obtained nanofibrous membranes, named as SBMA@EVOH NFMs, exhibited integrated features of (i) reduced non-specific adsorption of microorganisms due to the low affinity between SBMA@EVOH and protein (Langmuir constant K_a = 0.36 mL/mg), (ii) rechargeable and storable biocidal activity to microorganisms due to the

existence of photoactive benzophenone group, and (iii) effective releasing of the attached and killed microorganisms to reduce the biofouling due to the superhydrophilicity of the grafted SBMA moieties.

4.2 Experimental Sections

4.2.1 Materials

PVA-co-PE (ethylene content of 27 mol%), 3,3′,4,4′-benzophenonetetracarboxylic dianhydride (BPTCD), polyphosphoric acid (PPA), [2-(methacryloyloxy)ethyl]dimethyl-(3-sulfopropyl)ammonium hydroxide (SBMA), pierce^{TM} BCA protein assay reagent A and B, SYBR green dye (SG dye), 2 wt% of osmium tetroxide (O_sO_4), tetrahydrofuran (THF), isopropanol, ethanol, and acetone were purchased from Sigma-Aldrich (Louis, MO, USA) and used without further purification. Glutaraldehyde solution (30 wt%), *p*-Nitrosodimethylaniline (*p*-NDA), Luria-Bertani (LB) broth, LB agar were purchased from Thermo Fisher Scientific (Waltham, MA, USA). Phosphate-buffered saline (PBS) was obtained from USB Co. Ltd.

4.2.2 Fabrication of SBMA@EVOH NFM

The process of manufacturing PVA-co-PE (EVOH) nanofibrous membrane via electrospinning has been reported in a previous study, [35] and the final obtained EVOH membranes were dried in a vacuum oven overnight at 50 □ to remove the residual solvent. Solutions containing 5 wt% of BPTCD and 1 wt% of PPA were prepared in THF at 50 □, and then, the EVOH NFM was immersed into the as-prepared solution with a bath ratio of 1: 50. After 5 min, the EVOH NFM was taken out and dried in the air. Then, the EVOH NFM was cured at 120 □ for 30 min. The resulted BPTCD EVOH NFMs were washed with hot THF for three times to remove any unreacted BPTCD. SBMA@EVOH NFMs were obtained via a photo-induced free radical graft

polymerization reaction on the BPTCD EVOH NFMs, which were immersed in a 30 wt% of SBMA aqueous solution for 1 h. After drying under vacuum, the obtained NFMs were exposed to a UVA (365 nm) for 10 min per each side. After washed with acetone for three times, the SBMA@EVOH NFMs were obtained.

4.2.3 Measurement of ROS

A UVA irradiation device (Specrolinker XL-1000, Spectronics Corporation) was employed in this experiment. The output power was 3.0 mW cm^{-2} at a distance of 12 cm from a light source of five 8W lamps. Hydroxyl radical (OH·), as a typical reactive oxygen species (ROS), was measured. The amount of yielded OH· was quantified by color bleaching of *p*-NDA, which was a selective scavenger to quench the OH·. In a typical experiment, 5 mg of NFMs were soaked into 10 mL of *p*-NDA solution with a concentration of 50 μmol L^{-1}, and the mixture was exposed under the UVA irradiation or dark condition for a certain time. The residual *p*-NDA in the solution was quantified by a UV-vis spectroscopy with the absorbance at λ_{max} = 440 nm. The amounts of hydroxyl radicals generated by the materials under UVA (365nm) were calculated based on equation 4.1:

$$OH \cdot (\mu g\ g^{-1}) = 34 \times 10^{6} \times \frac{\Delta C \times V}{m} \qquad \text{Equation (4.1)}$$

Where ΔC is the concentration difference of *p*-NDA solution (mol L^{-1}) before and after UVA irradiation, V is the volume of *p*-NDA solution (L), and m is the mass of NFMs (g).

4.2.4 Antimicrobial assays against *E. coli*

A typical Gram-negative bacterium, *E. coli* O157: H17 culture with a concentration of 3×10^{8} CFU mL^{-1} (assessed by plate counting assay) was applied for the following experiments. The contact killing assay basically is the same as a previous report. [14,19] Membrane samples in a size

of 2×2 cm^2 were exposed to either UVA light or dark conditions for different time durations. For the cyclic antimicrobial assays, after each test, the samples were treated with sonicated for 30 min, and then immersed in excess of quenching solution (methanol: water = 1 : 30; pH = 10) to quench the residual ROS. As-cleaned NFMs were good for the next cycle test. [36]

4.2.5 Protein adsorption study

Protein adsorption was evaluated with BSA protein (isoelectric point = 4.7). For kinetic protein adsorption experiment, 10 mg of EVOH, uncharged BPTCD EVOH, and uncharged SBMA@EVOH NFMs were soaked in 10 mL of BSA solution (2 mg/mL in PBS buffer; pH = 7.4) for different duration times, respectively. At each time point, the concentrations of residual BSA solution were quantified with an established BCA protein assay.[37] The amount of adsorbed protein by NMF at time t, q_t (mg/g) was calculated by equation 4.2:

$$q_t = \frac{(C_0 - C_t) \times V}{m} \qquad \text{Equation (4.2)}$$

where q_t is the adsorption capacity at a given time, V is the volume of protein solution, C_0 is the initial protein concentration, C_t is the protein concentration after adsorption for a given time, and m is the dry mass of the used NFMs.

In a typical static protein adsorption experiment, 10 mg of uncharged relevant NFMs were immersed in a BSA solution with various concentrations, and then the mixed solution was shaken at room temperature until the system arrived at equilibrium state. Subsequently, the NFMs were taken out, and a BCA protein assay was applied to quantify the residual BSA solution based on the equation 4.2.

4.2.6 Bacterial resisting and releasing behaviors

The bacterial resisting and releasing experiments were following protocols established in the literature.[14] The membranes were first fully quenched with an excess of the quenching solution (methanol: water = 1:30; pH =10), and the whole processes were conducted under the dark condition to exclude the potential influence of light.

4.2.7 Fluorescence microscopy and SEM imaging

For the fluorescence microscope imaging, 10 μL of SG dye with a concentration of 5 μg mL^{-1} was spotted on control NFMs (uncharged BPTCD EVOH) and sample NFMs (uncharged SBMA@EVOH), respectively. After staining for 15 min, the NFMs were gently rinsed and examined by applying a widefield fluorescence system (IVIS 100 Series), which equipped with an ICCD camera and a fluorescein isothiocyanate filter (ex 490 nm/em 525 nm). The distribution of *E. coli* O157: H7 contaminated on NFMs can be described by the intensity of the fluorescence signal.

For the SEM imaging, bacteria attached NFMs specimens were fixed with 4 wt% of glutaraldehyde for 4 hours, then rinsed with 5 mL of DI water and incubated overnight at 4 □. Free bacteria specimens were harvested by vortexing the bacteria contaminated SBMA@EVOH NFMs with 1 mL of DI water, which were exposed or unexposed to the light condition. Then the same fixing process was conducted for bacteria attached NFMs specimens.

4.2.8 Characterization of NFM

FT-IR spectra were obtained with a Nicolet 6700 spectrometer in the range of 500-2000 cm^{-1}. TGA measurements were performed with a Shimadzu TGA-60 system with a heating rate of 5 □ min^{-1}. Water infiltration times (10 μL of a water droplet) were recorded using a goniometer Kino SL200B. FE-SEM images and EDX scanning electron microscopy were examined by a Philips FEI XL30.

4.2.9 Statistical analysis and quantitative data analysis

Statistical analysis was performed using the SPSS Statistics software (version 24, IBM SPSS, Chicago, IL, USA) to evaluate the measurement sets of obtained data. All the experiments were performed in triplicates. A one- or two-way analysis of variance was used to determine the significant differences among the values of the selected measurements ($p < 0.05$).

4.3 Results and Discussion

4.3.1 Design and preparation of SBMA@EVOH NFMs

The SBMA@EVOH NFMs were designed based on four criteria: (1) the nanofibrous membrane matrix can provide excess reaction sides, (2) the biocidal activity of the membrane should be rechargeable and controllable, (3) the membrane must be able to effectively resist the biomass adsorption and easily release attached ones with mild hydrodynamic force applied, and (4) these functions work independently and construct concerted microbial resisting, killing, and releasing functions to reduce the microbial contamination. The first requirement was satisfied by using an electrospun PVA-co-PE (EVOH)nanofibrous membrane, which provided numerous hydroxyl groups with an extremally high specific surface area. To satisfy other requirements, a benzophenone derivative, BPTCD, and a zwitterion, SBMA were chemically bonded to the EVOH matrix via an esterification reaction and a free radical graft polymerization reaction, respectively.

Figure 4.1a shows the synthesis, biocidal, and antifouling function pathways. BPTCD, as a photosensitizer containing acid anhydride, can form ester bond with the hydroxyl groups of the PVA-co-PE with the presence of polyphosphoric acid. The bonded benzophenone derivatives could also serve as a photo-initiator to initiate a free radical graft polymerization reaction of SBMA on PVA-co-PE under UVA (365 nm) irradiation.[25,38] Benzophenone derivative molecules at

excited triplet state (^{3}BPTCD*) could abstract hydrogen atoms from tertiary C-H bonds on the EVOH polymer, generating polymeric free radicals. Then these polymeric radicals further initiated a radical graft polymerization reaction of SBMA monomer onto the polymer chain, and the final products of SBMA@EVOH NFMs were obtained (Figures 4.2a and 4.2b). Figure 4.1a also demonstrates the biocidal and antifouling effects of the SBMA@EVOH NFMs against microorganisms. When bacteria are approaching the SBMA@EVOH NFMs, the grafted SBMA moieties weaken interactions between microorganisms and nanofibrous membrane matrix, making them difficult to adhere onto and adsorb into the SBMA@EVOH NFMs. Any bacteria intercepted by the nanofibrous network could be immediately killed by the ROS (Reactive Oxygen Species) generated from the BPTCD structure. Furthermore, the killed bacteria debris could be easily removed from the NFMs due to the superhydrophilicity of the SBMA. Figures 4.1b-4.1d exhibited the architecture changes of the nanofibrous membranes. The representative SEM image of the EVOH NFMs revealed randomly oriented 3D network structure with an average fiber diameter of 522 nm. After reacting with BPTCD, the membrane retained the microporous and nanofibrous structure with the average fiber diameter increased to 735 nm. After UVA induced free radical graft polymerization, the membrane morphology was unchanged as well, and the average fiber diameter changed to 663 nm. (Figures 4.2c-4.2e)

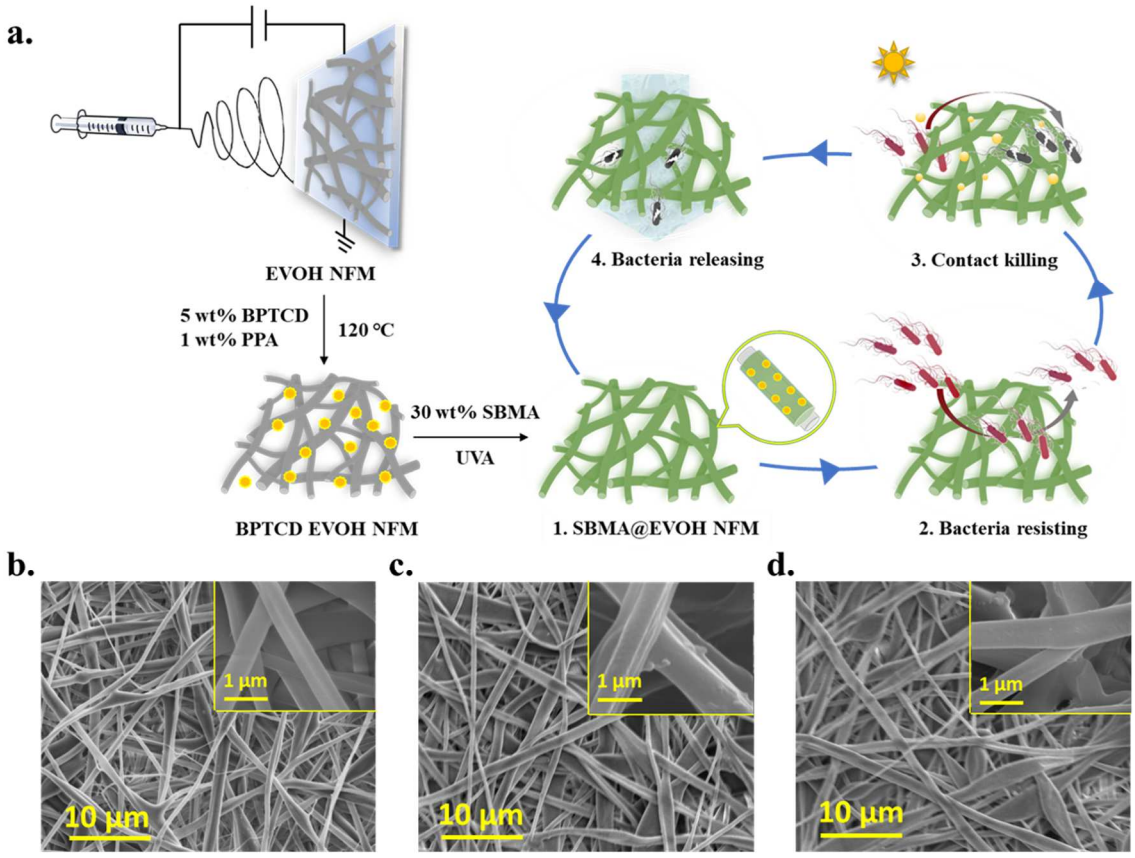

Figure 4.1. (a) Scheme of the manufacturing process, antimicrobial, and antifouling functions of as-prepared SBMA@EVOH NFMs. SEM images of (b) EVOH, (c) BPTCD EVOH, and (d) SBMA@EVOH membranes.

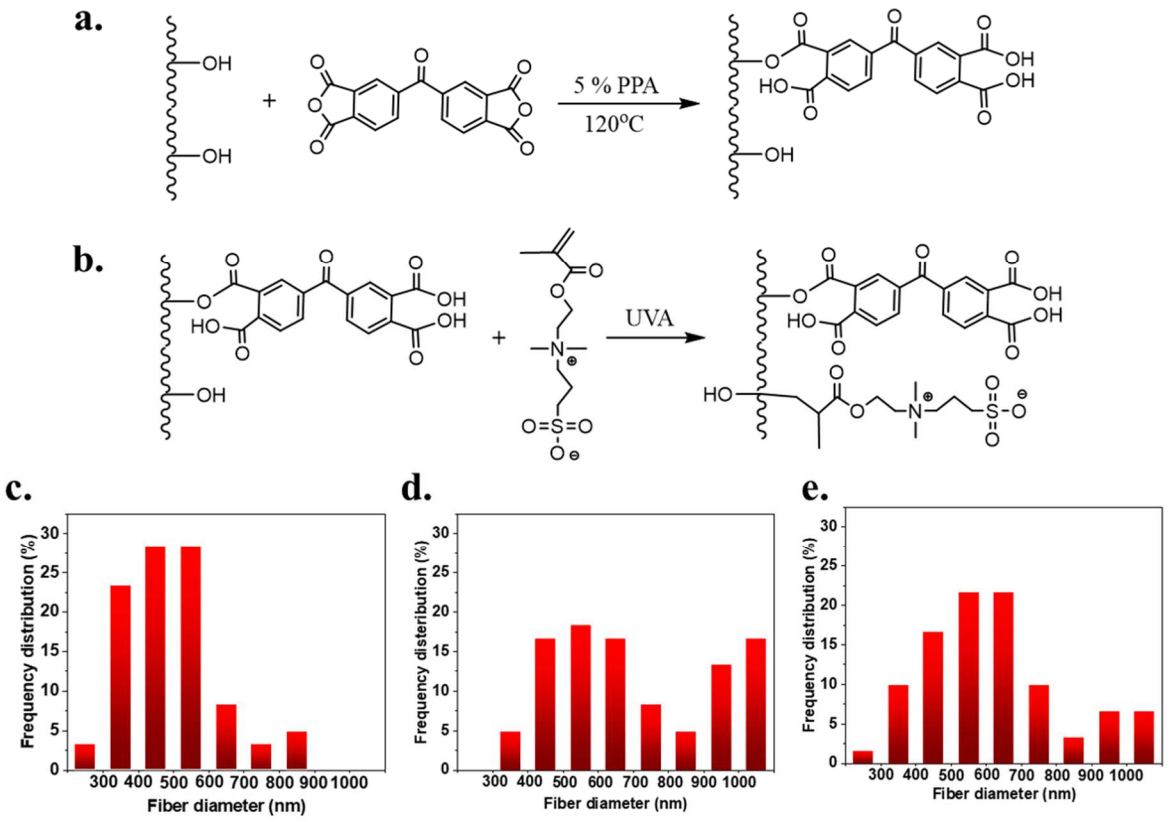

Figure 4.2. (a) Esterification reaction of EVOH NFMs with BPTCD. (b) Self-initiated graft polymerization reactions of BPTCD EVOH with SBMA. (c-e) Fiber diameter distribution of EVOH, BPTCD EVOH, and SBMA@EVOH NFMs, respectively.

4.3.2 Structure characterization and properties of SBMA@EVOH NFMs

Characterizations of the SBMA@EVOH NFMs were conducted using different testing processes. Figure 4.3a shows optical images of the membrane before and after 10-minute UVA irradiation. The presence of benzophenone groups and SBMA on the membranes was confirmed by using FT-IR. As shown in Figure 4.3b, a peak at 1735 cm^{-1} in both BPTCD EVOH and SBMA@EVOH is assigned to the stretching vibration of the ester bonds (C=O) formed between BPTCD and EVOH.[39] And the new peaks at 1184 cm^{-1} and 1305 cm^{-1} come from the vibration of sulfonate groups only existed in the spectrum of SBMA@EVOH, confirming the successful chemical

grafting of the SBMA on the nanofibrous membrane.[40-42] Scanning electron microscope-energy dispersive X-ray spectroscopy (SEM-EDX) results could serve as additional evidence of the successful incorporation of the functional groups (Figures 4.3c and 4.3d). As shown in elemental abundance spectra, about 3.8 % of the sulfur element could be detected, and the existence of nitrogen element could be observed as well. Furthermore, the sulfur elemental mapping of the SBMA@EVOH presented the homogenous distribution of SBMA on the membrane. Figure 4.3e exhibits the hydrophilicity of the different NFMs. The pristine EVOH with numerous hydroxyl groups on the polymer chain took 50 s to demonstrate water infiltration with an initial contact angle of 43^{o}. After treated with BPTCD, the membrane became more hydrophilic with the infiltration time shortened to 30 s due to the addition of carboxylic acid groups from hydrolyzed BPTCD.[39] The hydrophilicity of the SBMA@EVOH NFM was further increased with a 2 s infiltration time due to the grafted superhydrophilic zwitterionic groups. The thermal stabilities of the relevant NFMs were evaluated by conducting thermogravimetric analysis (TGA), and the results are shown in Figure 4.3f. There were two distinct weight-loss phases: the initial weight-loss phase (200-350 □) occurred due to the degradation of grafted BPTCD and SBMA, and the second weight-loss phase (350-550 □) corresponded for the degradation of the polymer mainchain. Overall, the SBMA@EVOH exhibited promising thermal stability without any weight loss below 200 □.

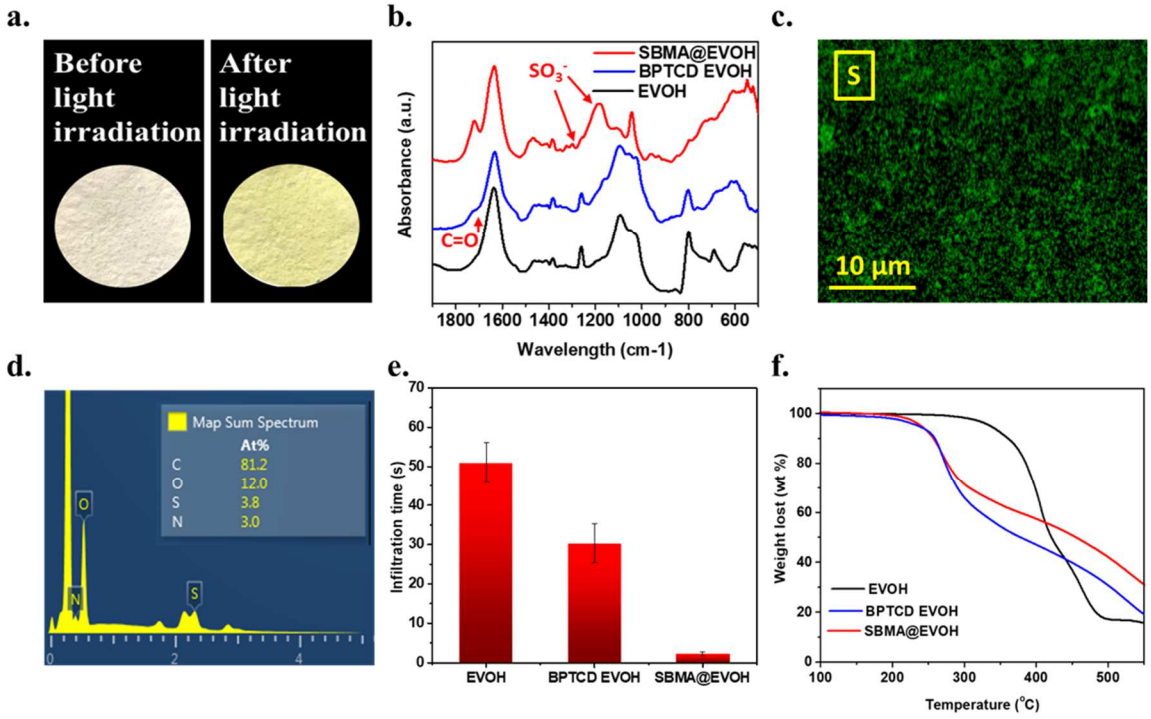

Figure 4.3. (a) Optical images of SBMA@EVOH before and after light irradiation (diameter = 2.5 cm). (b) FT-IR spectra, (c,d) SEM-EDX results of SBMA@EVOH NFMs. (e) Water permeation results, and (f) TGA plots of EVOH, BPTCD EVOH, and SBMA@EVOH NFMs, respectively.

4.3.3 Photoactivity of SBMA@EVOH NFMs

Benzophenone derivatives possess robust photoactivity and could generate numerous ROS species, and the reaction mechanism has already been discussed in previous studies.[22] As shown in Figures 4.2b, 4.4a, and 4.4b, the benzophenone structure of BPTCD was initially photoexcited to graft SBMA monomer onto the membrane, and residual unreacted benzophenone groups could further undergo the photo-excitation again on the membranes and generated a quinone radical (BPTCD-H·) by extracting a hydrogen atom from vicinal locations. Under aerobic conditions, BPTCD-H· could react with oxygen molecules and simultaneously generate active ROS. However, in an

anaerobic environment, the structure of BPTCD-H· could be rearranged and proceed to a second hydrogen extraction, forming a metastable structure (LAT-BPTCD) with photoactivity stored.[22,34] Once LAT-BPTCD exposed to oxygen molecules, it will produce ROS even under dark conditions.

The photoactivities of the EVOH, BPTCD EVOH, and SBMA@EVOH NFMs were examined by quantifying amounts of OH· generated by the membranes under 365nm (UVA) irradiation or dark conditions. Figure 4.4c depicts the generation of OH· as a function of UVA irradiation time. The photo-induced productions of OH radicals by both BPTCD EVOH and SBMA@EVOH NFMs were fast and sustainable, following a zero-order kinetic process with reaction rates k = 20.22 and 14.87 μg g^{-1} min^{-1}, respectively. Additionally, the production of OH· could be well controlled by adjusting the lighting condition. The relevant NFMs were subjected to repeated irradiation tests of 20-min UVA exposure and another 20 min under dark fatigue cycles. As shown in Figure 4.4d, the generation of OH· was mainly observed during the UVA irradiation with no significant decrease in the photoactivity even after four cycles. Moreover, the generation of OH· could be easily paused by switching to a dark condition. The photoactivity difference between BPTCD EVOH and SBMA@EVOH NFMs could be attributed to the absolute mass reduction of BPTCD moieties in a unit gram of NFM after the addition of grafted SBMA. The benzophenone (BP) structure may have the ability to store the photo-activity by forming a transient structure (LAT-BPTCD). To evaluate the storage-production of the ROS capacity of the BP structure, we first charged the relevant NFMs under UVA irradiation for 2 hours and then measured the amount of OH· generated by the membrane under the dark condition. As shown in Figure 4.4e, at first 2 hours, the light charged BPTCD EVOH and SBMA@EVOH NFMs showed similar OH· production rates of 8.63 and 7.77 μg g^{-1} min^{-1}, respectively. After that, the BPTCD EVOH continued to generate OH· in this rate for another 3 hours with a total of 1980 μg g^{-1} OH· yielded. However, the SBMA@

EVOH NFMs, due to reduced BPTCD moieties per unit mass of the NFM after initiation of the graft polymerization, exhibited a saturation region after the first 2 hours with OH· releasing amount of 1200 μg g^{-1}. Moreover, a light charging and dark releasing cyclic test of these membranes was conducted as displayed in Figure 4.4f. The samples were first charged with UVA irradiation for 2 hours, and productions of OH· were tested by an excess amount of *p*-NDA solution for 5 hours under dark. Repeated productions of OH· were observed for both BPTCD EVOH and SBMA@EVOH NFMs for five cyclic tests, and about 70 % of the original charging capacity still retained. The slight decrease could be attributed to the accumulative loss of the benzophenone groups in the LAT status and consumption of unrenewable tertiary C-H bonds from PVA-co-PE, which served as a major hydrogen donor to trigger the ROS generation. [22]

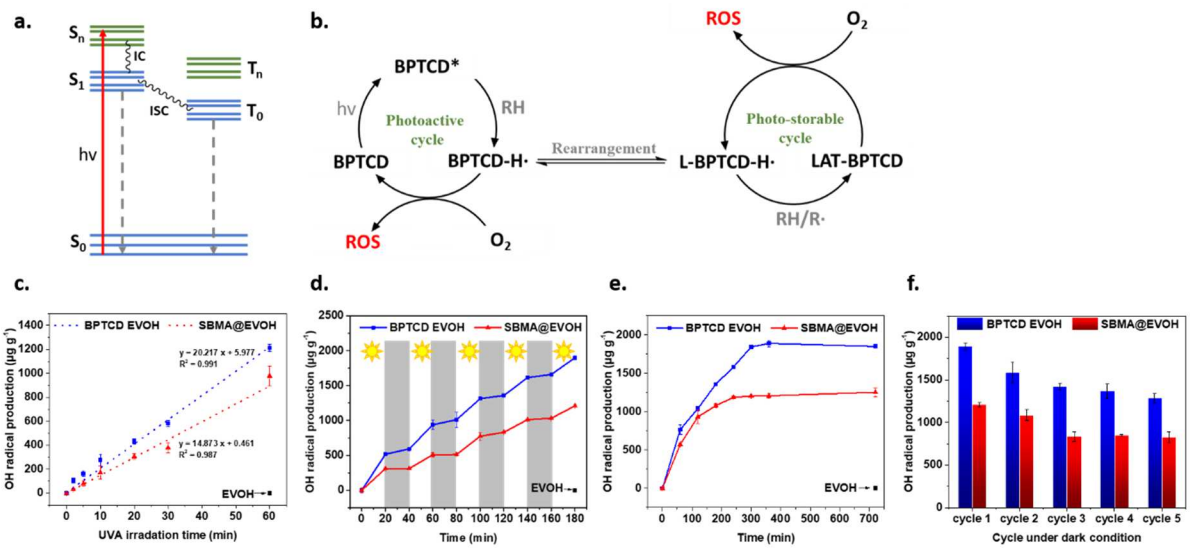

Figure 4.4. (a) Jablonski diagrams representing the photoexcitation process of BPTCD. (b) Mechanism of the photoactive and photo-storage cycles. Quantification of OH radical production of EVOH, BPTCD EVOH, and SBMA@EVOH NFMs under (c) continuously UVA irradiation, (d) alternating UVA exposure and dark condition (irradiation in white and dark in grey), and (e)

Under dark condition after 2-hour of UVA irradiation. (f) Rechargeable capability of BPTCD EVOH and SBMA@EVOH NFMs (Five cycles of repeated UVA exposure and dark quenching).

4.3.4 Contact-Killing against *E. coli*

The antibacterial activity of SBMA@EVOH NFMs was evaluated against *E. coli* O157: H7 bacterium, a typical etiological pathogenic bacterium. Figure 4.5a depicts the time-dependent antimicrobial profiles of the BPTCD EVOH and SBMA@EVOH NFMs under UVA irradiation condition. The control sample (pristine EVOH NFM) showed significant bacteria growth even after 1 hour of UVA irradiation. However, both BPTCD EVOH and SBMA@EVOH NFMs exhibited promising killing efficiency, achieving 6 logs reduction of *E. coli* within 1-hour UVA irradiation. Moreover, both BPTCD EVOH and SBMA@EVOH NFMs could store biocidal activity obtained under UVA irradiation and kill the bacteria under dark condition due to the specific chemical structure of benzophenone group (LAT-BPTCD). As shown in Figure 4.5c, after 2 hours of UVA irradiation, the photo charged BPTCD EVOH and SBMA@EVOH exhibited 6 log CFU (Colony-Forming Unit) reduction of *E. coli* after 2 hours of contact without light exposure. In addition, the rechargeability feature was demonstrated by the renewable biocidal functions of the SBMA@EVOH NFMs against the microorganism. As shown in Figures 4.5b and 4.5d, both BPTCD EVOH and SBMA@EVOH NFMs could provide 5 log CFU reduction of the bacterium for five repeated tests, no matter with or without light exposure, consistent with the results of productions of $OH\cdot$ by the membranes (Figures 4.4d and 4.4f). These results revealed good ROS productivity of the benzophenone groups and highlighted the robust refreshable biocidal character of the SBMA@EVOH NFM.

The photo generated ROS can completely inactivate the bacteria by destroying the cell structures, which can be demonstrated by the morphological change of bacteria in contact with the BPTCD

EVOH and SBMA@EVOH NFMs under 1-hour UVA exposure. As shown in Figures 4.5f-4.5h, *E. coli* cells on the EVOH NFM remained intact cell structure with smooth surfaces. In sharp contrast, cell structure deformation and the surface collapse of *E. coli* on surfaces of both BPTCD EVOH and SBMA@EVOH NFMs under the UVA irradiation could be clearly observed. These results revealed the robust biocidal activity of the BPTCD containing NFMs.

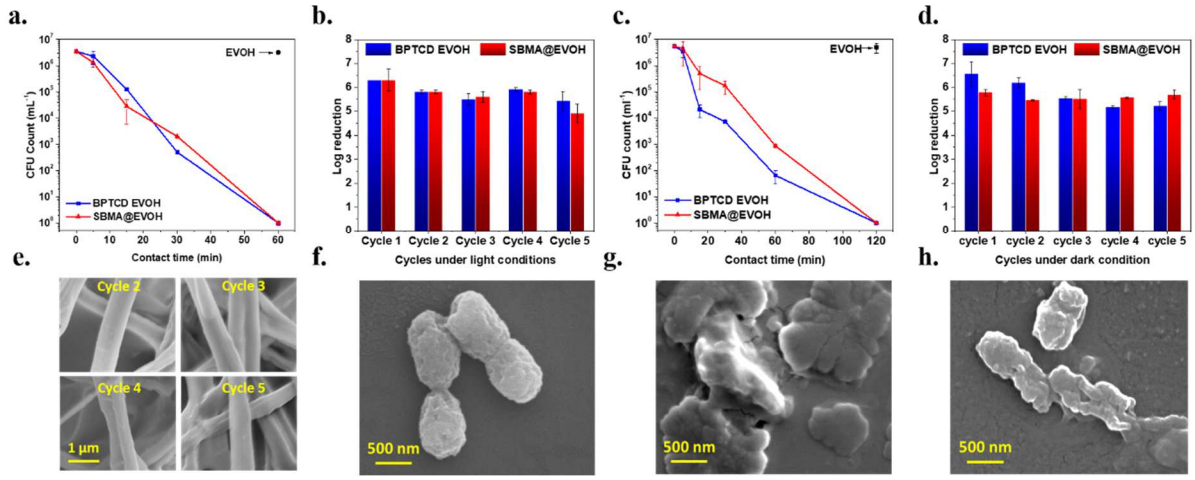

Figure 4.5. Antimicrobial activity against *E. coli* of relevant NFMs under (a) UVA irradiation and (c) dark condition after 2-hours UVA irradiation. Five cycles of antimicrobial tests of BPTCD EVOH and SBMA@EVOH NFMs under (b) UVA irradiation (1h contact time) and UVA (2h) charged NFMs under (d) dark condition (2h contact time). Field emission scanning electron microscopy (FE-SEM) images of (e) SBMA@EVOH NFMs after antimicrobial test, *E. coli* after exposure to (f) EVOH, (g) BPTCD EVOH, and (h) SBMA@EVOH NFMs under UVA condition for 1 hour.

4.3.5 Microbial resisting functions of SBMA@EVOH NFMs

The membranes containing benzophenone structures in the polymers demonstrated powerful biocidal effects. However, the destroyed bacteria cell debris is still on the surfaces of the materials

and could still result in the formation of biofilms, which then can increase chemical oxygen demand (COD) content in the system, leading to biofouling on the membranes.[43] The grafted zwitterion groups should bring expected resistance to adhesion of cell debris and microorganisms. To investigate whether the SBMA@EVOH NFMs possess such functions, a representative protein, Bovine Serum Albumins (BSA), was employed as a model probe to evaluate the microbial resisting behaviors of the membranes.[44,45] A comparative adsorption kinetic study was conducted for the membranes under a neutral pH condition at room temperature. As shown in Figure 4.6a, 633, 637 and 373 mg g^{-1} of BSA (initial concentration of BSA = 2 mg/mL) were captured by EVOH, BPTCD EVOH, and SBMA@EVOH NFMs after 480 min of soaking, respectively, indicating that the SBMA moieties significantly reduced protein adsorption on the nanofibrous membrane. Additionally, the kinetics of adsorption can be well described as a pseudo-second-order process (Figure 4.7).

The adsorption capacities of EVOH, BPTCD EVOH, and SBMA@EVOH towards BSA protein were further investigated with different initial BSA concentrations (C_e) at a constant temperature (PBS buffer as a solvent with pH = 7.4). As shown in Figure 4.6b, the adsorption capacities of three types of NFMs steadily increased with the C_A ranging from 0.2 to 6 mg mL^{-1}. The BSA protein adsorption capacities of the SBMA@EVOH NFMs were significantly lower than the other NFMs, less than half of the others in the entire tested initial BSA concentration range. To uncover the adsorption mechanism of these NFMs, the experimental adsorption data were fitted into two classical isotherms models, Langmuir (Equation.4.3) and Freundlich (Equation.4.4), respectively.

$$q_e = \frac{K_a q_{max} C_e}{1 + K_a C_e} \qquad \text{Equation (4.3)}$$

$$q_e = k_F C_e^n \qquad \text{Equation (4.4)}$$

Where q_e is the BSA adsorption amount at different initial concentrations, q_{max} is the maximum adsorption capacity. C_e is the equilibrium concentration, K_a and K_F are the Langmuir and Freundlich constant, respectively.

The relevant fitting curves are shown in Figure 4.8. Langmuir model exhibited higher regressors ($R^2 \geq 0.972$) than that derived from the Freundlich model ($R^2 \leq 0.957$) for all three NFMs, suggesting that the adsorption behaviors refer to the monolayer Langmuir isotherm. At pH=7.4, both BSA protein (isoelectric point = 4.7) and BPTCD EVOH. Therefore, BPTCD EVOH NFMs exhibited poor affinity to the BSA compared with EVOH NFMs due to the charge repulsion interaction, which explains its reduced Langmuir constant (K_a). However, the electro-repulsion effect cannot reduce the total adsorption site at equilibrium state (q_{max} BPTCD EVOH $\approx$ q_{max} EVOH). SBMA, with unique charge distribution, can weaken the interaction between BSA and NFMs by building up a dense hydration layer serving as a barrier. This fact was supported by the further decreased K_a (0.36) and q_{max} (678.21 mg/g of NFM) values of SBMA@EVOH compared with the other NFMs. Overall, SBMA@EVOH NFMs exhibited the lowest affinity and lowest total adsorption sites to BSA protein due to both the electro-repulsion interaction and the robust hydration effect, revealing the good bacteria resisting performance of the materials.

To further demonstrate the bacteria resisting performance of the membranes, the uncharged NFMs (the photoactivity was fully quenched by an excess of methanol/ water solution) were incubated in *E. coli* suspensions (1×10^8 CFU) for 24-hour, and then gently rinsed with fresh PBS buffer to remove the planktonic bacteria. Widefield fluorescence images of the NFMs were obtained to determine the spatial distribution of the *E. coli* cells on the NFMs. As shown in Figure 4.6c, the SBMA@EVOH exhibited lower fluorescence signal intensity with Region of Interest (ROI) of 1.52×10^{10} [p/s] / [μW/cm²], around 35 % fluorescence signal reduction compared with that of the

BPTCD EVOH (ROI = 2.35 × 10^{10} [p/s] / [μW/cm²]). Individual bacterial distribution was described by the results of SEM images (Figure 4.6d). Obviously, more bacteria cells could be observed on the surface of the BPTCD EVOH NFMs compared with that on the surfaces of the SBMA@EVOH NFMs. This significant difference in bacteria population between these two NFMs indicates that the presence of SBMA moieties could effectively reduce the bacterial adhesion and hinder the biofilm formation via weakening the protein-NFM interaction.

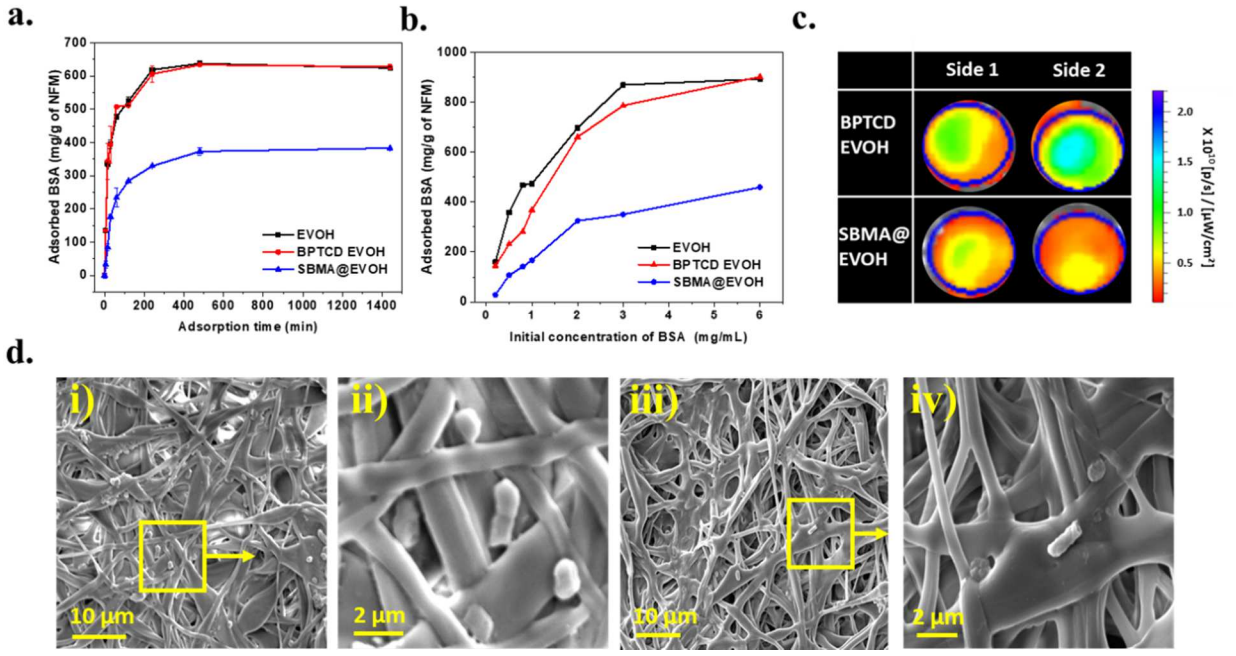

Figure 4.6. Changes of BSA protein adsorption capacities of relevant NFMs as a function of (a) adsorption time, and (b) initial BSA concentration at room temperature, respectively. (c) SG-stained fluorescence widefield microscopy images and (d) FE-SEM images uncharged BPTCD EVOH (i and ii), and uncharged SBMA@EVOH (v and vi) NFMs after incubating with *E. coli* suspension under dark condition.

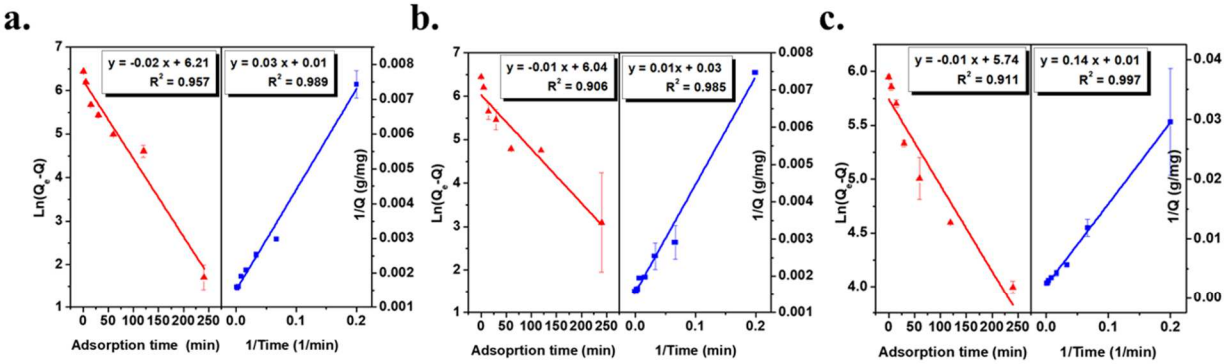

d.

	Pseudo 2nd order			Pseudo 1st order		
	Q_e (mg/g)	K_2 (g/mg min)	R^2	Q_e (mg/g)	K_1 (g/mg min)	R^2
EVOH	100	0.0033	0.989	497.70	0.02	0.957
BPTCD EVOH	33.33	0.090	0.985	419.89	0.01	0.906
SBMA@EVOH	100	0.00071	0.997	311.06	0.01	0.911

Figure 4.7. The linear fitting of isothermal adsorption kinetics of BSA protein by pseudo-1st-order and Pseudo-2nd-order kinetic models on (a) EVOH, (b) BPTCD EVOH, and (c) SBMA@EVOH NFMs (C_0 = 2 mg/mL). (d) Table of adsorption kinetic parameters.

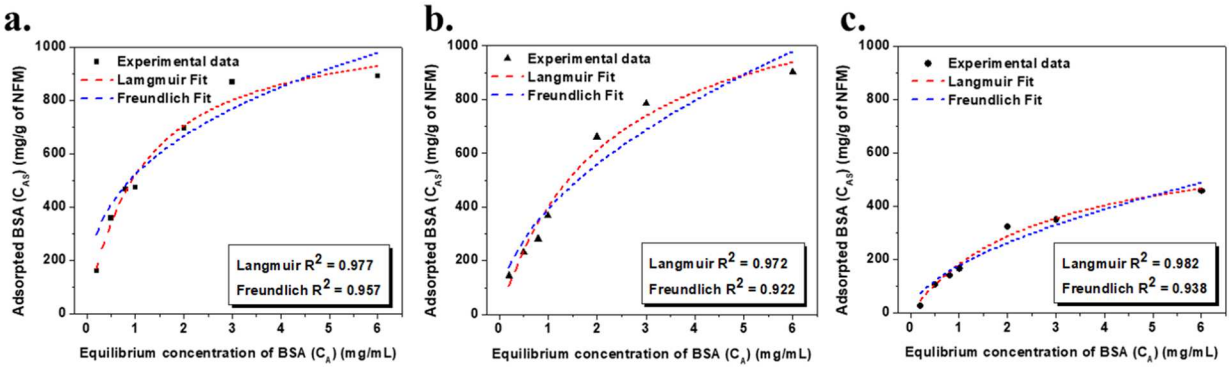

d.

	Freundlich isotherm			Langmuir isotherm		
	n	K_f	R^2	Ka	Cs(mg/g)	R^2
EVOH	0.35	523.18	0.957	0.9	1098.98	0.977
BPTCD EVOH	0.51	391.9	0.922	0.46	1281.31	0.972
SBMA@EVOH	0.56	177.46	0.938	0.36	678.21	0.982

Figure 4.8. The nonlinear fitting of BSA adsorption isotherms by Langmuir model and Freundlich model on (a) EVOH, (b) BPTCD EVOH, and (c) SBMA@EVOH NFMs, respectively. (d) Table of adsorption isotherm parameters.

4.3.6 Microbial releasing functions of SBMA@EVOH NFMs

The SBMA@EVOH NFMs also possess bacteria releasing functions, which was investigated by the following procedure. 10 μL of 10^8 CFU mL^{-1} *E. coli* suspensions were loaded on the uncharged membranes (without light exposure). After soaking in PBS buffer for certain times, the released bacteria from the membrane samples were assessed by using the plate counting method. Figure 4.9a shows the bacterial-releasing behaviors of the relevant uncharged membranes as a function of incubation time. Both BPTCD EVOH and EVOH NFMs exhibited limited bacterial-releasing capacity, about 3 log CFU of attached *E. coli* after 2-hour soaking in the PBS solution. In contrast, the SBMA@EVOH NFM could release almost 6 log CFU of adhered bacteria. Interestingly, at the initial 15 minutes, all the membranes exhibited similar releasing behavior with 3 log CFU of bacteria released. These bacteria might come from the out layer of the membrane surface. After that, only the superhydrophilic SBMA@EVOH NFMs could further release additional 3 log CFU of bacteria till 60 min, evidence of reduced interactions between the biomolecules and surfaces of the materials. To gain a straightforward view of the bacterial-releasing function of the SBMA@EVOH NFMs, we investigated the bacterial distributions and populations on the NFMs before/after the 2 hours of releasing process by using both widefield microscope and SEM. As shown in Figure 4.9b, after 2 hours of release, the SBMA@EVOH showed the weakest fluorescence signal with ROI number reduced from 5.91×10^{10} to 1.36×10^{10} [p/s] / [μW/cm²], indicating that most of coated *E. coli* were released from the NFM. In contrast, the BPTCD EVOH NFM released less coated bacteria with ROI = 2.56×10^{10} [p/s] / [μW/cm²]. The SEM test was also

performed to identify the differences in bacterial-releasing behaviors among the NFMs. As shown in Figure 4.9c, after a 120-min release test, numerous bacteria still aggregated together and tightly trapped in the nanofibrous network structure of the BPTCD EVOH NFM. Comparatively, the SBMA@EVOH NFMs exhibited promising releasing behavior with little of bacteria left on the membrane. The significant difference between the uncharged BPTCD EVOH and uncharged SBMA@EVOH NFMs proved the success of this rechargeable biocidal and antifouling functional NFM.

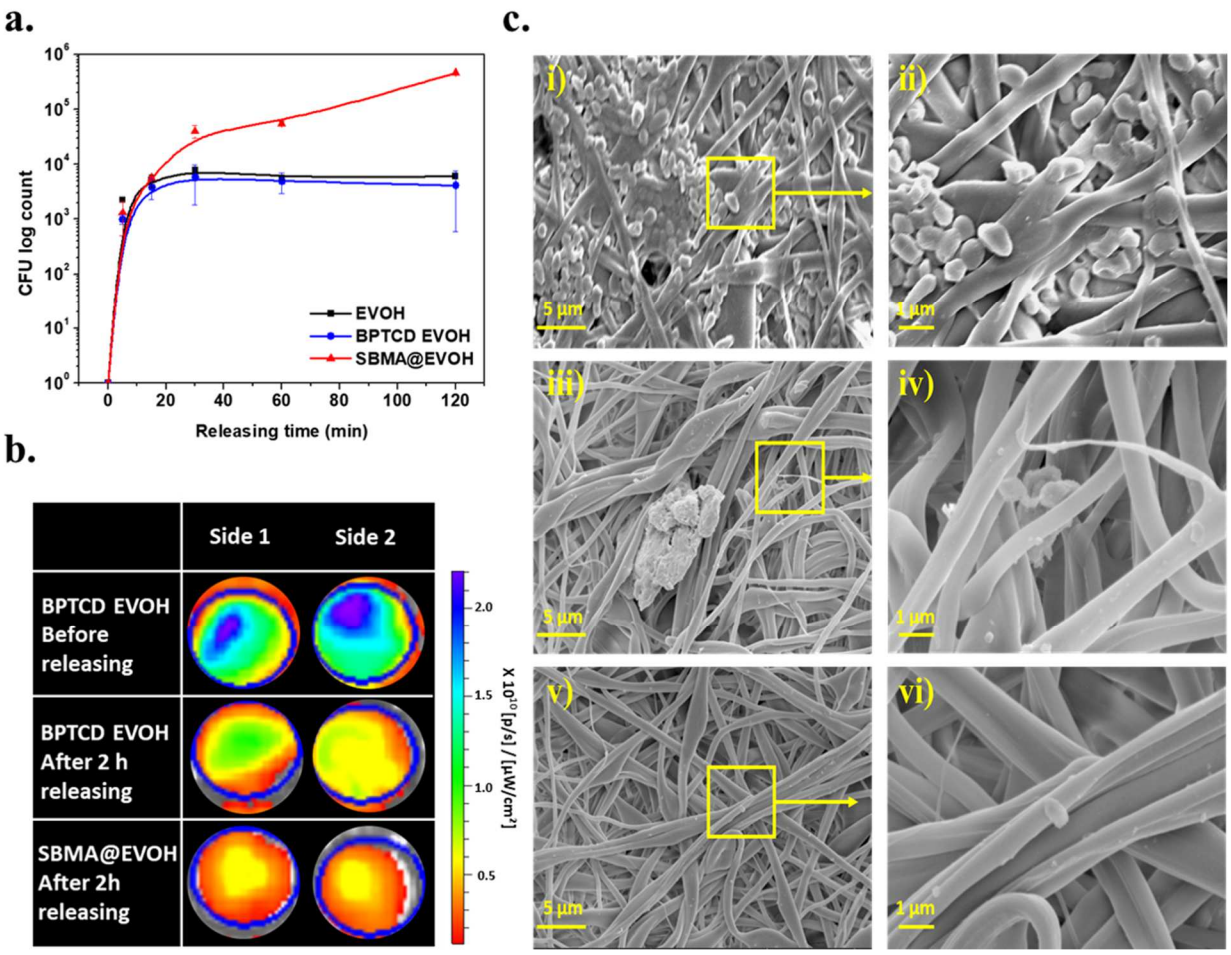

Figure 4.9. (a) Releasing behavior of uncharged EVOH, BPTCD EVOH, and SBMA@EVOH NFMs against *E. coli* under dark condition via the plate-counting method. (b) SG-stained

fluorescence widefield microscopy images and (c) FE-SEM images of BPTCD EVOH before (i and ii) and after (iii and iv) 2-hour *E. coli* releasing, and SBMA@EVOH NFMs after (v and vi) 2-hour *E. coli* releasing under dark condition.

4.4 Conclusions

We demonstrated the fabrication of a photo-induced rechargeable biocidal and antifouling materials by incorporating both photosensitizers (BPTCD) and zwitterions (SBMA) onto PVA-co-PE nanofibrous membranes. The obtained multifunctional NFMs exhibited a controllable biocidal activity via continuous generation of ROS, or storing the photoactivity under light condition, then readily releasing ROS under the dark condition. Additionally, the grafted SBMA moieties brought robust antifouling properties to the biocidal NFMs, therefore, reducing the bacterial adhesion and making the attached bacteria easier to be released. The combination of biocidal and antifouling functions could significantly inhibit microbial contamination and prevent the biofilm formation, which is suitable for applications in food contact surfaces and medical areas.

4.5 References

1. Lu, B.; Lu, F.; Ran, L.; Yu, K.; Xiao, Y.; Li, Z.; Dai, F.; Wu, D.; Lan, G., Imidazole-molecule-capped chitosan–gold nanocomposites with enhanced antimicrobial activity for treating biofilm-related infections. *Journal of Colloid and Interface Science* **2018,** *531*, 269-281.
2. Duncan, T. V., Applications of nanotechnology in food packaging and food safety: barrier materials, antimicrobials and sensors. *Journal of Colloid and Interface Science* **2011,** *363* (1), 1-24.
3. Available at: http://www.euro.who.int/en/media-centre/sections/press-releases/2019/23-million-people-falling-ill-from-unsafe-food-each-year-in-europe-is-just-the-tip-of-the-iceberg, accessed: December 2020.
4. Yi, J.; Huang, K.; Young, G. M.; Nitin, N., Quantitative analysis and influences of contact dynamics on bacterial cross-contamination from contaminated fresh produce. *Journal of Food Engineering* **2020,** *270*, 109771.
5. Imani, S. M.; Maclachlan, R.; Rachwalski, K.; Chan, Y.; Lee, B.; McInnes, M.; Grandfield, K.; Brown, E. D.; Didar, T. F.; Soleymani, L., Flexible hierarchical wraps repel drug-resistant gram-negative and positive bacteria. *ACS Nano* **2020,** *14*, 454-465.
6. Konwar, A.; Kalita, S.; Kotoky, J.; Chowdhury, D., Chitosan–iron oxide coated graphene oxide nanocomposite hydrogel: a robust and soft antimicrobial biofilm. *ACS Applied Materials & Interfaces* **2016,** *8* (32), 20625-20634.
7. Judzewitsch, P. R.; Nguyen, T. K.; Shanmugam, S.; Wong, E. H.; Boyer, C., Towards sequence-controlled antimicrobial polymers: effect of polymer block order on antimicrobial activity. *Angewandte Chemie International Edition* **2018,** *57* (17), 4559-4564.

8. Huang, C.; Hu, C.; Sun, G.; Ji, B.; Yan, K., Antimicrobial finish of cotton fabrics treated by sophorolipids combined with 1, 2, 3, 4-butanetetracarboxyic acid. *Cellulose* **2020,** 1-14.
9. Li, M.-C.; Wu, Q.; Song, K.; Cheng, H.; Suzuki, S.; Lei, T., Chitin nanofibers as reinforcing and antimicrobial agents in carboxymethyl cellulose films: Influence of partial deacetylation. *ACS Sustainable Chemistry & Engineering* **2016,** *4* (8), 4385-4395.
10. GhavamiNejad, A.; Park, C. H.; Kim, C. S., In situ synthesis of antimicrobial silver nanoparticles within antifouling zwitterionic hydrogels by catecholic redox chemistry for wound healing application. *Biomacromolecules* **2016,** *17* (3), 1213-1223.
11. Cossu, A.; Si, Y.; Sun, G.; Nitin, N., Antibiofilm effect of poly (vinyl alcohol-co-ethylene) halamine film against *Listeria innocua* and *Escherichia coli O157: H7. Applied and Environmental Microbiology* **2017,** *83* (19), e00975-17.
12. Cao, Z.; Mi, L.; Mendiola, J.; Ella-Menye, J. R.; Zhang, L.; Xue, H.; Jiang, S., Reversibly switching the function of a surface between attacking and defending against bacteria. *Angewandte Chemie International Edition* **2012,** *51* (11), 2602-2605.
13. Liu, Y.; Shi, L.; Su, L.; van der Mei, H. C.; Jutte, P. C.; Ren, Y.; Busscher, H. J., Nanotechnology-based antimicrobials and delivery systems for biofilm-infection control. *Chemical Society Reviews* **2019,** *48* (2), 428-446.
14. Ma, Y.; Li, J.; Si, Y.; Huang, K.; Nitin, N.; Sun, G., Rechargeable antibacterial N-halamine films with antifouling function for food packaging applications. *ACS Applied Materials & Interfaces* **2019,** *11* (19), 17814-17822.
15. Zeng, Q.; Zhu, Y.; Yu, B.; Sun, Y.; Ding, X.; Xu, C.; Wu, Y.-W.; Tang, Z.; Xu, F.-J., Antimicrobial and antifouling polymeric agents for surface functionalization of medical implants. *Biomacromolecules* **2018,** *19* (7), 2805-2811.

16. Si, Y.; Cossu, A.; Nitin, N.; Ma, Y.; Zhao, C.; Chiou, B. s.; Cao, T.; Wang, D.; Sun, G., Mechanically robust and transparent N-halamine grafted PVA-co-PE films with renewable antimicrobial Activity. *Macromolecular Bioscience* **2017,** *17* (3), 1600304.
17. Cao, Z.; Mi, L.; Mendiola, J.; Ella-Menye, J. R.; Zhang, L.; Xue, H.; Jiang, S., Reversibly switching the function of a surface between attacking and defending against bacteria. *Angewandte Chemie International Edition* **2012,** *51* (11), 2602-2605.
18. Zhao, X.; Su, Y.; Li, Y.; Zhang, R.; Zhao, J.; Jiang, Z., Engineering amphiphilic membrane surfaces based on PEO and PDMS segments for improved antifouling performances. *Journal of Membrane Science* 2014, 450, 111-123.
19. Si, Y.; Li, J.; Zhao, C.; Deng, Y.; Ma, Y.; Wang, D.; Sun, G., Biocidal and rechargeable N-halamine nanofibrous membranes for highly efficient water disinfection. *ACS Biomaterials Science & Engineering* **2017,** *3* (5), 854-862.
20. Wang, Y.; Wen, J.; Ren, X.; Sun, Y., Reactions of phenolic compounds with monomeric N-halamines and mesoporous material-supported N-halamines. *Journal of Hazardous Materials* **2019,** *366*, 651-658.
21. Bai, R.; Zhang, Q.; Li, L.; Li, P.; Wang, Y.-J.; Simalou, O.; Zhang, Y.; Gao, G.; Dong, A., N-halamine-containing electrospun fibers kill bacteria via a contact/release co-determined antibacterial pathway. *ACS Applied Materials & Interfaces* **2016,** *8* (46), 31530-31540.
22. Si, Y.; Zhang, Z.; Wu, W.; Fu, Q.; Huang, K.; Nitin, N.; Ding, B.; Sun, G., Daylight-driven rechargeable antibacterial and antiviral nanofibrous membranes for bioprotective applications. *Science Advances* **2018,** *4* (3), eaar5931.

23. Zhang, Z.; Si, Y.; Sun, G., Photoactivities of vitamin K derivatives and potential applications as daylight-activated antimicrobial agents. *ACS Sustainable Chemistry & Engineering* **2019,** *7* (22), 18493-18504.

24. Thapa, B.; Munk, B. H.; Burrows, C. J.; Schlegel, H. B., Computational study of the radical mediated mechanism of the formation of C8, C5, and C4 guanine: lysine adducts in the presence of the benzophenone photosensitizer. *Chemical Research in Toxicology* **2016,** *29* (9), 1396-1409.

25. Dewanji, A.; Krach, P. E.; Rueping, M., The dual role of benzophenone in visible-light/nickel photoredox - catalyzed C− H arylations: Hydrogen - atom transfer and energy transfer. *Angewandte Chemie International Edition* **2019,** *58* (11), 3566-3570.

26. Gao, J.; White, E. M.; Liu, Q.; Locklin, J., Evidence for the phospholipid sponge effect as the biocidal mechanism in surface-bound polyquaternary ammonium coatings with variable cross-linking density. *ACS Applied Materials & Interfaces* **2017,** *9* (8), 7745-7751.

27. Xing, C.-M.; Meng, F.-N.; Quan, M.; Ding, K.; Dang, Y.; Gong, Y.-K., Quantitative fabrication, performance optimization and comparison of PEG and zwitterionic polymer antifouling coatings. *Acta Biomaterialia* **2017,** *59*, 129-138.

28. Li, Z.; Yang, X.; Liu, H.; Yang, X.; Shan, Y.; Xu, X.; Shang, S.; Song, Z., Dual-functional antimicrobial coating based on a quaternary ammonium salt from rosin acid with in vitro and in vivo antimicrobial and antifouling properties. *Chemical Engineering Journal* **2019,** *374*, 564-575.

29. Kim, S.; Gim, T.; Kang, S. M., Versatile, tannic acid-mediated surface PEGylation for marine antifouling applications. *ACS Applied Materials & Interfaces* **2015,** *7* (12), 6412-6416.

30. Hucknall, A.; Rangarajan, S.; Chilkoti, A., In pursuit of zero: polymer brushes that resist the adsorption of proteins. *Advanced Materials* **2009,** *21* (23), 2441-2446.
31. Giroto, J. A.; Teixeira, A. C. S. C.; Nascimento, C. A. O.; Guardani, R., Degradation of poly(ethylene glycol) in aqueous solution by photo-fenton and H2O2/UV processes. *Industrial & Engineering Chemistry Research* **2010,** *49* (7), 3200-3206.
32. Shao, Q.; Jiang, S., Molecular understanding and design of zwitterionic materials. *Advanced Materials* **2015,** *27* (1), 15-26.
33. Chang, C. C.; Kolewe, K. W.; Li, Y.; Kosif, I.; Freeman, B. D.; Carter, K. R.; Schiffman, J. D.; Emrick, T., Underwater superoleophobic surfaces prepared from polymer zwitterion/dopamine composite coatings. *Advanced Materials Interfaces* **2016,** *3* (6), 1500521.
34. Zhang, P.; Jain, P.; Tsao, C.; Yuan, Z.; Li, W.; Li, B.; Wu, K.; Hung, H. C.; Lin, X.; Jiang, S., Polypeptides with high zwitterion density for safe and effective therapeutics. *Angewandte Chemie* **2018,** *130* (26), 7869-7873.
35. El-Moghazy, A. Y.; Zhao, C.; Istamboulie, G.; Amaly, N.; Si, Y.; Noguer, T.; Sun, G., Ultrasensitive label-free electrochemical immunosensor based on PVA-co-PE nanofibrous membrane for the detection of chloramphenicol residues in milk. *Biosensors and Bioelectronics* **2018,** *117*, 838-844.
36. Oelgemöller, M.; Mattay, J.; Görner, H., Direct photooxidation and xanthene-sensitized oxidation of naphthols: quantum yields and mechanism. *The Journal of Physical Chemistry A* **2011,** *115* (3), 280-285.
37. Kobayashi, S.; Wakui, M.; Iwata, Y.; Tanaka, M., Poly (ω-methoxyalkyl acrylate) s: nonthrombogenic polymer family with tunable protein adsorption. *Biomacromolecules* **2017,** *18* (12), 4214-4223.

38. Wang, G.; Hill, N. S.; Zhu, D.; Xiao, P.; Coote, M. L.; Stenzel, M. H., Efficient photoinitiating system based on diaminoanthraquinone for 3D printing of polymer/carbon nanotube nanocomposites under visible light. *ACS Applied Polymer Materials* **2019,** *1* (5), 1129-1135.
39. Yi, S.; Zou, Y.; Sun, S.; Dai, F.; Si, Y.; Sun, G., Rechargeable photoactive silk-derived nanofibrous membranes for degradation of reactive red 195. *ACS Sustainable Chemistry & Engineering* **2018,** *7* (1), 986-993.
40. Ye, G.; Lee, J.; Perreault, F. o.; Elimelech, M., Controlled architecture of dual-functional block copolymer brushes on thin-film composite membranes for integrated "defending" and "attacking" strategies against biofouling. *ACS Applied Materials & Interfaces* **2015,** *7* (41), 23069-23079.
41. Liu, C.; Lee, J.; Ma, J.; Elimelech, M., Antifouling thin-film composite membranes by controlled architecture of zwitterionic polymer brush layer. *Environmental Science & Technology* **2017,** *51* (4), 2161-2169.
42. Li, G.; Liu, B.; Bai, L.; Shi, Z.; Tang, X.; Wang, J.; Liang, H.; Zhang, Y.; Van der Bruggen, B., Improving the performance of loose nanofiltration membranes by poly-dopamine/zwitterionic polymer coating with hydroxyl radical activation. *Separation and Purification Technology* **2020,** *238*, 116412.
43. Li, X.; Liu, X.; Wu, S.; Rasool, A.; Zuo, J.; Li, C.; Liu, G., Microbial diversity and community distribution in different functional zones of continuous aerobic–anaerobic coupled process for sludge in situ reduction. *Chemical Engineering Journal* **2014,** *257*, 74-81.
44. Zhi, Z.; Su, Y.; Xi, Y.; Tian, L.; Xu, M.; Wang, Q.; Padidan, S.; Li, P.; Huang, W., Dual-functional polyethylene glycol-b-polyhexanide surface coating with in vitro and in vivo

antimicrobial and antifouling activities. *ACS Applied Materials & Interfaces* **2017,** *9* (12), 10383-10397.

45. Chen, H.; Zhang, M.; Yang, J.; Zhao, C.; Hu, R.; Chen, Q.; Chang, Y.; Zheng, J., Synthesis and characterization of antifouling poly (N-acryloylaminoethoxyethanol) with ultralow protein adsorption and cell attachment. *Langmuir* **2014,** *30* (34), 10398-10409.

Chapter 5. Durable and Chlorine Rechargeable Biocidal Composite Material for Improved Food Safety

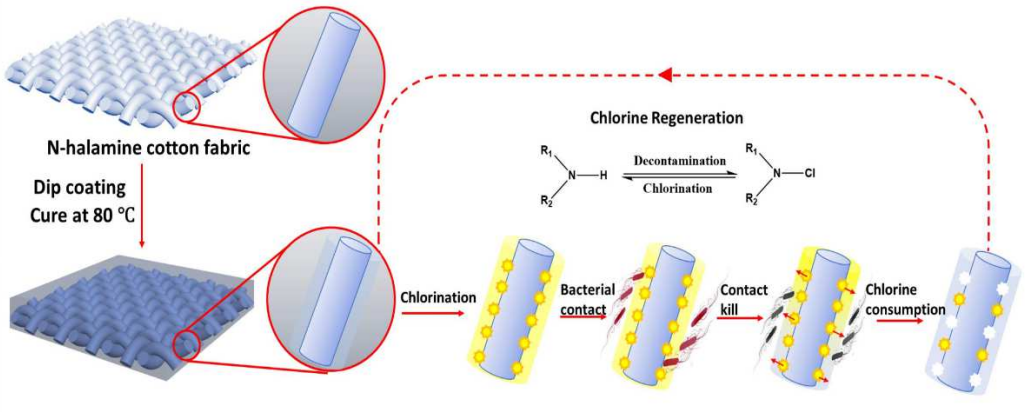

Abstract

Food spoilage and foodborne diseases are caused by pathogenic microbial contaminations, which occur at multi-stages of the food supply chain. The development of materials with chlorine refreshable biocidal functions, which could be integrated with many current food processing procedures, are necessary for food contact surfaces, such as convey belts and food packages. Taking the advantages of biocidal and serviceability of a previously developed durable and regenerable biocidal antimicrobial cellulose fabric (DMH-g-Cotton fabric), we demonstrated a scalable strategy for fabrication of a chlorine rechargeable antimicrobial composite material consisting of the DMH-g-Cotton, serving as a reinforcement component and a reservoir of active chlorine, and an amine-halamine polymer ((2,4-diamino-6-diallylamino-1,3,5-triazine) grafted poly(vinyl alcohol-co-ethylene, PVA-co-PE-g-DAM) as a coating component. The as-prepared halamine composite fabric (HCF) exhibited the integrated properties of a high content of active chlorine, ease of rechargeability, rapid biocidal efficacy even at high chemical oxygen demand (COD) condition, reduced cross-contamination risk, and desired mechanical properties. The halamine cellulose fabric played an important role to serve as a reinforcement material and active chlorine reservoir for the composite. Additionally, the incorporation of HCFs as a biocidal food pad resulted in the prolonged shelf life of prepackaged strawberries.

Objectives

- Fabricate a fabric-based halamine composite material (HCF) via an industrial scalable dip-coating method.
- Characterize the physiochemical performances of the obtained HCF, including thermal performance, mechanical property, and hydrophilicity.
- Evaluate the active chlorine content and antimicrobial performance of the designed HCF.

- Investigate the reduced cross-contamination and food preservation effects when the designed HCF is applied as a food contact pad.

5.1 Introduction

Food spoilage accounts for a huge loss of foods produced annually, and the real lost economic value is difficult to be estimated.[1-4] It is generally considered that nearly 30 % of the manufacturing food products are spoiled before being consumed because of microbial contamination.[1,2,5] Microbial contamination is not only a food quality issue but also a food safety concern. The frequent outbreaks of foodborne diseases are a major burden to public health. [6-8] A United States Center for Disease Control and Prevention (CDC) report estimated that each year about 48 million of sickness, 128000 hospitalizations, and 3000 deaths are related to the foodborne diseases in the United States. [9, 10] A current strategy to reduce food contamination during the processing is the direct application of diluted chlorine bleach to prewash the foods and sanitize food-contact devices. [11, 12] However, microbial contamination can occur at multiple stages of the food supply chain. [9, 13, 14] The prewashed foods and the sanitized surfaces of the devices will soon be contaminated during the transportation and the sales periods, increasing the cross-contamination risk and accelerating the spoilage of the foods. [15, 16] Thus, it is necessary to develop an antimicrobial food-contact surface to limit the bacterial transfer and reduce the microbial contaminations. [17-19]

Two major characteristics are required for desirable antimicrobial food-contact materials, i.e., (1) durable and refreshable biocidal activity, and (2) desired mechanical serviceability. With a combination of a high active chlorine content, robust biocidal activity, intrinsically rechargeability, flexibility, and pliability, the N-halamine fabrics have exhibited great potentials in the fabrication of antimicrobial food-contact materials. [20, 21] As an example, dimethylol-5,5-dimethylhydantoin (DMDMH) treated cotton fabrics, DMH-g-Cotton containing imide and amide halamine structures,

were initially developed (Figure 5.1a).[22] Mixing of an amine halamine precursor 2,2,5,5□ tetramethylimidazolidin□4□one (TMIO) with DMDMH resulted in a system containing a combination of amine-, amide-, and imide-halamine structures with long-term chlorine stability, durable and rapid killing activity provided by the varied halamine structures. [23-25] Thus, an amine-halamine polymeric coating on the DMH-g-Cotton could be an alternative approach for the development of durable and refreshable biocidal composite materials from the DMH-g-Cotton. The coating layer of the halamine polymer could improve the mechanical properties and reduce moisture absorption of the composite.[26] Moreover, the high contents of active chlorine from the inner side of the halamine cotton substance could serve as a reservoir of active chlorine to a stable but could be consumed amine halamine structure on the surfaces. [24, 27]

An amine-halamine (2,4-diamino-6-diallylamino-1,3,5-triazine) poly(vinyl alcohol-co-ethylene) (PVA-co-PE-g-DAM) was produced in a reactive extrusion method with a high grafting ratio of 4 wt% (Figure 5.1b). [7, 8, 28] In this work, we demonstrated a scalable process in the fabrication of a rechargeable antimicrobial composite material by coating PVA-co-PE-g-DAM polymer onto the DMH-g-Cotton fabrics, serving as reinforcement substances. The new halamine composite fabric materials (HCF) could show a desired combination of high active chlorine content and proper mechanical properties required for food processing materials. The integrated properties of large chlorination capacity, ease of rechargeability, rapid biocidal efficacy even at high chemical oxygen demand (COD) conditions, and reduced cross-contamination risk were demonstrated on the HCF materials. Additionally, the incorporation of HCFs as a biocidal food pad was demonstrated to achieve a prolonged shelf life of prepackaged strawberries.

5.2 Experimental Section

5.2.1 Materials

Poly(vinyl alcohol-co-ethylene)-g-2,4-diamino-6-diallylamino-1,3,5-triazine (PVA-co-PE-g-DAM) was synthesized by a free radical graft polymerization reaction.[7] Cotton fabrics grafted with 1,3-dimethlylol-5,5-dimethylhydantoin (DMH-g-Cotton) were prepared as previously reported.[22] Sterile maximum recovery diluent (MRD), 0.1 M iodine standard solution, hydrochloric acid, sodium hydroxide, sodium thiosulfate, and isopropanol were purchased from Sigma-Aldrich and used without purification. Luria-Bertani (LB) broth, LB agar, Tryptic soy broth (TSB), and Tryptic soy agar (TSA) were purchased from Thermo Fisher Scientific. The bleach solution with an active chlorine concentration of 6.0 % was produced by Clorox Co., Ltd. Baby spinaches and the strawberries were purchased from Trader Joe's.

5.2.2 Fabrication of HCF

The PVA-co-PE-g-DAM coated DMH-g-Cotton composite (HCF) was fabricated using a simple "coating and drying" process. [29] Different concentrations of PVA-co-PE-g-DAM polymer were dissolved into a mixture of isopropanol and water (7: 3) with continuous stirring at 80 □, and then the washed DMH-g-cotton fabrics were soaked in the prepared polymer solutions for 30 min, allowing the full diffusion of the polymer solution. Subsequently, such polymer coated DMH-g-cotton fabrics were cured at 80 □ for 5 min to obtain the final products, HCFs.

5.2.3 Chlorination of HCF

A chlorination solution was prepared by diluting a Clorox bleach solution to a final active chlorine concentration of 1 wt%. The active chlorine contents of the chlorinated HCF were measured by an established iodometric titration method and were calculated according to Equation (4.1). The experimental processes followed the protocols previously reported. [7, 8, 29]

$$\text{Active chlorine content (ppm)} = \frac{35.45 \times (V_0 - V_S) N \times 500}{m_s} \qquad \text{(Equation 4.1)}$$

Where V_0 and V_s (L) are the volumes of the iodine solution consumed in titration with and without chlorinated HCFs, respectively. m_s (g) is the dry weight of the chlorinated HCFs.

Data are expressed as the mean ± SD of three replicates.

5.2.4 Incubation of bacterial cultures

Two typical pathogenic bacteria, Gram-negative *E. Coli O157: H7* and Gram-positive *L. innocua,* were applied in the antimicrobial experiments. A colony of *E. coli* was incubated in 10 mL of LB broth at 37 for 18 h with gentle shaking. Similarly, *L. innocua* was incubated under the same condition but changed the LB broth to TSB. The final concentrations of *E. coli* and *L. innocua* were 10^8 CFU/mL and applied for the following experiments.

5.2.5 Antimicrobial assays against *E. coli* and *L. innocua*

In a typical experiment, 10 spots of 10 μL (total of 100 μL) of the bacterial (*E. coli* or *L. innocua*) suspension in sterile PBS or diluted nutrition broth solution (COD = 1000) were placed on the surfaces of unchlorinated (control group) or chlorinated HCFs, in a size of 4 × 4 cm^2, and then the inoculated fabric was placed in a plastic petri-dish for various times. At each time point, presence of the inoculated bacterial strain was detected by transferring the HCFs to a 2oz Whirl-Pak bag containing 30 mL of sterile maximum recovery diluent (MRD) and sodium thiosulfate (1wt%), then the sample was hand massaged vigorously for 1 minute and allowed to stand for 1 min. At each time point, the samples were serially diluted and duplicate spread□plated on TSA agar plates for quantification of bacterial number. Bacterial counts were performed after the incubation period to enumerate the bacteria (*E. coli* or *L. innocua*) remaining on the fabrics. The results were reported in colony-forming units (CFU/mL). Data are expressed as the mean ± SD of three replicates.

5.2.6 SEM images

The bacterial suspensions with a concentration of 1×10^8 CFU/mL were loaded onto the surfaces of unchlorinated and chlorinated HCFs for 10 minutes of contact. Subsequently, the bacteria were harvested by vortexing the contaminated HCFs with 1 mL of sterilized PBS buffer containing 2.5 wt % of glutaraldehyde. Such bacteria suspensions were incubated overnight at 4□. Then the bacterial samples were dehydrated by sequential ethanol/water mixtures with increasing ethanol contents of 25, 50, 75, and 100 %. Finally, 10 μL of bacteria suspension was spotted on a glass chip and coated with golden before SEM analysis.

5.2.7 Stimulated leaf-to-leaf cross-contamination

Baby spinach leaves with a diameter of 2.5 cm were firstly prewashed by the sterilized DI-water and then incubated with 10 mL of *E. coli* suspensions (10^7 CFU/ mL) for 2 hours. After incubation, the contaminated leaves were gently rinsed twice with 5 mL of PBS buffer for removing the planktonic *E. coli* and let them dry in the air. To control the same moisture contents of the leaf surfaces, more importantly, to stimulate bacterial transfer in a wet condition, which is a common condition in the practical fresh produce manufacturing process, these contaminated dry leaves were loaded with 100 μL of water droplets and conducted the following experiment immediately. As shown in Figure 5.7a, the obtained contaminated leaf (leaf A) with $2.14 \pm 1.73 \times 10^4$ CFU/cm^2 (accessed by plate counting assay) adaxially contacted with the relevant fabrics (2.5 × 2.5 cm), and then the contaminated side of these fabrics further attach with a non-contaminated leaf (leaf B). During the contact process, a standard weight was placed on the non-contaminated side of the fabrics for 1 min to provide a 1 N of additional contact force.[30] The population of the bacteria transferred to the relevant fabrics (after contact with the leaf A) and the leaf Bs were accessed by a plate counting method. The bacteria transfer efficiency (BTE) was calculated as Equation (4.2)-(4.4).[31]

$$BTE_1 = [N_{fabric} / N_{leaf\ A}] \times 100\% \quad \text{(Equation 4.2)}$$

$$BTE_2 = [N_{Leaf\ B} / N_{fabric}] \times 100\% \quad \text{(Equation 4.3)}$$

$$BTE_{overall} = BTE_1 \times BTE_2 = [N_{Leaf\ B} / N_{leaf\ A}] \times 100\% \quad \text{(Equation 4.4)}$$

Where N_{fabric} and $N_{Leaf\ B}$ are the number of living bacteria on the contaminated side of the fabric and leaf B, respectively, and $N_{leaf\ A} = 1.07 \pm 0.86 \times 10^4$ CFU/cm^2 (assume the distribution of the bacteria on two sides of leaf A is uniform).

5.2.8 Characterization of physicochemical properties

SEM images were examined by a Thermo Fisher Quattro S. FT-IR spectrum were obtained with a Nicolet 5700 spectrometer at the range of 500 – 2000 cm^{-1}. The tensile stress-strain curves and the abrasion resistance of the materials were tested using an INSTRON 5565 testing system and a TABER 5150 abraser, respectively. The air permeability of the fabrics was measured according to ASTM D 737 test standard by using a Frazier FAP-HP air permeability tester**.** The wettability of the fabrics was established by a wicking test, according to the AATCC TM 197.

5.2.9 Statistical analysis and quantitative data analysis

Statistical analysis was performed using the SPSS Statistics software (version 24, IBM SPSS, Chicago, IL, USA) to evaluate the measurement sets of obtained data. All the experiments were performed in triplicates. A one- or two-way analysis of variance was used to determine the significant differences among the values of the selected measurements ($p < 0.05$).

5.3 Results and Discussion

5.3.1 Design and preparation of HCF

An ideal antibacterial packaging material should provide durable and rechargeable biocidal functions, good mechanical performance, flexibility, and resistance to repeated sanitization during operations. A composite structure of using exiting PVA-co-PE-g-DAM and DMH-g-Cotton can provide these desired functions. Active chlorine on these three halamine structures could transfer in a thermodynamically spontaneous process according to the literature.[27] Therefore, the DAM, as an amine halamine precursor, could deliver the active chlorine from the chlorinated DMH to the surface, once the active chlorine on the surface consumed by the microorganisms via a contact killing pathway (Figure 5.2a). Additionally, the DAM itself, could also be chlorinated and subsequently replenished as well during exposure to chlorine solutions. A combination of the woven structure of DMH-g-Cotton and coating of PVA-co-PE-g-DAM could bring in controllable wettability and mechanical properties of the composite materials.

Figure 5.2a depicts the fabrication and the biocidal function pathways of the HCFs. PVA-co-PE-g-DAM were dissolved in a mixture of water/ isopropanol (3: 7) with various concentrations of 0, 1, 2.5, 5, and 7.5 wt %. Then the solutions were coated onto the DMH-g-Cotton fabric via an easy "coating and drying" process. [29] The obtained composite materials coated with x wt% of the PVA-co-PE-g-DAM were denoted as halamine composite fabric-x (HCF-x). The chlorination reaction of the HCF-x could occur at amine, amide, and imide structures located in the polymeric coating layer and cotton substance, due to potential active chlorine transfers among all halamine groups in a unique composite system, converting to bactericidal N-Cl structures.[27] When the pathogens contact the chlorinated HCF, the active chlorine of the amine-halamine located on the outside surface could be firstly consumed via a direct contact killing pathway, converting to precursor amine (N-H) structures. Then the active chlorines could transfer from the internally chlorinated hydantoin to such amine structures, ensuring the durable high biocidal activity of the HCF surface.

If all the active chlorines were exhausted, the biocidal activity of the HCF material could be easily regenerated by soaking in a sodium hypochlorite solution. Figure 5.3 demonstrates a large HCF material with a size of 60 × 60 cm. Due to the practicality of such an industrial-matured "coating-curing" manufacturing process, the scaling up production of the HCF material is feasible. Taking the unique flexibility performance of the textile fabric, the HCF could tolerate large bending, folding, rolling, and twisting deformations without any fracture, as demonstrated in Figure 5.2b. The surface morphology of the HCFs could be easily controlled by adjusting the concentration of the polymer coating solution. As demonstrated in Figure 5.2c, after coated with PVA-co-PE-g-DAM polymer, HCF-x showed rough surfaces compared with the pristine DMH-g-Cotton fabric. With the concentration increase of the coating polymer, HCFs exhibited both increased roughness on the fiber surfaces and increased size of fiber diameter. Additionally, the textures of the cotton fabrics of HCF-5 and HCF-7.5 were fully covered by the polymer coating layer with a reduced specific surface area.

5.3.2 Structural characterization and properties of HCF

The coexistence of hydantoin and melamine halamine precursors was confirmed by the Fourier-transform infrared spectra (FTIR). As shown in Figure 5.2d, the characteristic peaks at 1720 cm^{-1} could be attributed to the vibration of carbonyl groups in the hydantoin ring, which has been fully demonstrated in previous work.[23] Moreover, the peak at 1544 cm^{-1} is assigned to the vibration triazines ring in the DAM compounds.[32]

Physiochemical performances of the HCF, including wettability, air permeability, and mechanical properties, were evaluated to justify the serviceability as a potential food-contact material. The DMH-g-Cotton fabric exhibited a great moisture absorption performance with a wicking distance of 9.0 cm. Proper hydrophilicity of the composite materials benefits the good surface contact with

microorganisms and high biocidal efficiency. Both the fabric and the polymer are hydrophilic and contain hydroxyl groups, which ensure the formed composite materials with strong interaction and compatibility as a composite. After coating with the PVA-co-PE-g-DAM polymer, the HCF-x could still maintain the good surface hydrophilicity of the material but with reduced moisture absorption and the capillary effect of the cotton substance. As shown in Figure 5.2e, the wicking distance gradually decreased as the concentration of PVA-co-PE-g-DAM was raised in the composites. Air permeability was employed to evaluate the porosity of the HCF-x (Figure 5.2e). Without the coating, the DMH-g-Cotton exhibited a high air permeability of 45 cubic feet per minute (CFM). After the coating treatment, the PVA-co-PE-g-DAM polymer could fill the gaps among the cotton fibers or even yarns, reducing the porosity of the HCF materials. Specifically, the air permeabilities of the HCF-5 and the HCF-7.5 were nearly zero, indicating that PVA-co-PE-g-DAM fully covered the fabric surface and generated the dense protective layer. Such results are consistent with the SEM images of the HCF samples.

Moreover, the mechanical property is one of the critical features of the composite materials. The results of abrasion resistance tests revealed a good protective function of the polymeric coating layer. As shown in Figure 5.2f, with the thicker coating layer embedded in the fabrics, more abrasion cycles they can survive. The HCF-2.5 could tolerate nearly 1000 cycles of the abrasive head motion, which indicated a nearly 12-fold increase compared with the untreated fabric. Figure 5.3 shows the optical images of the relevant fabrics after 200 abrasion cycles. Figure 5.2g depicts the tensile stress-strain curves of HCF-x. The samples of DMH-g-Cotton, HCF-1, HCF-2.5, and HCF-5 exhibited similar patterns with robust Young's moduli (> 10000 Mpa). The HCF-7.5, with the highest breaking tensile stress of 22500 Mpa, showed a two-stages pattern due to the thick layer of PVA-co-PE-g-DAM. The beginning stage could be assigned to the mechanical

performance of the coating layer, which was broken at a tensile strain of 15%, and then the reinforced fabric revealed the resistance to the tensile force.

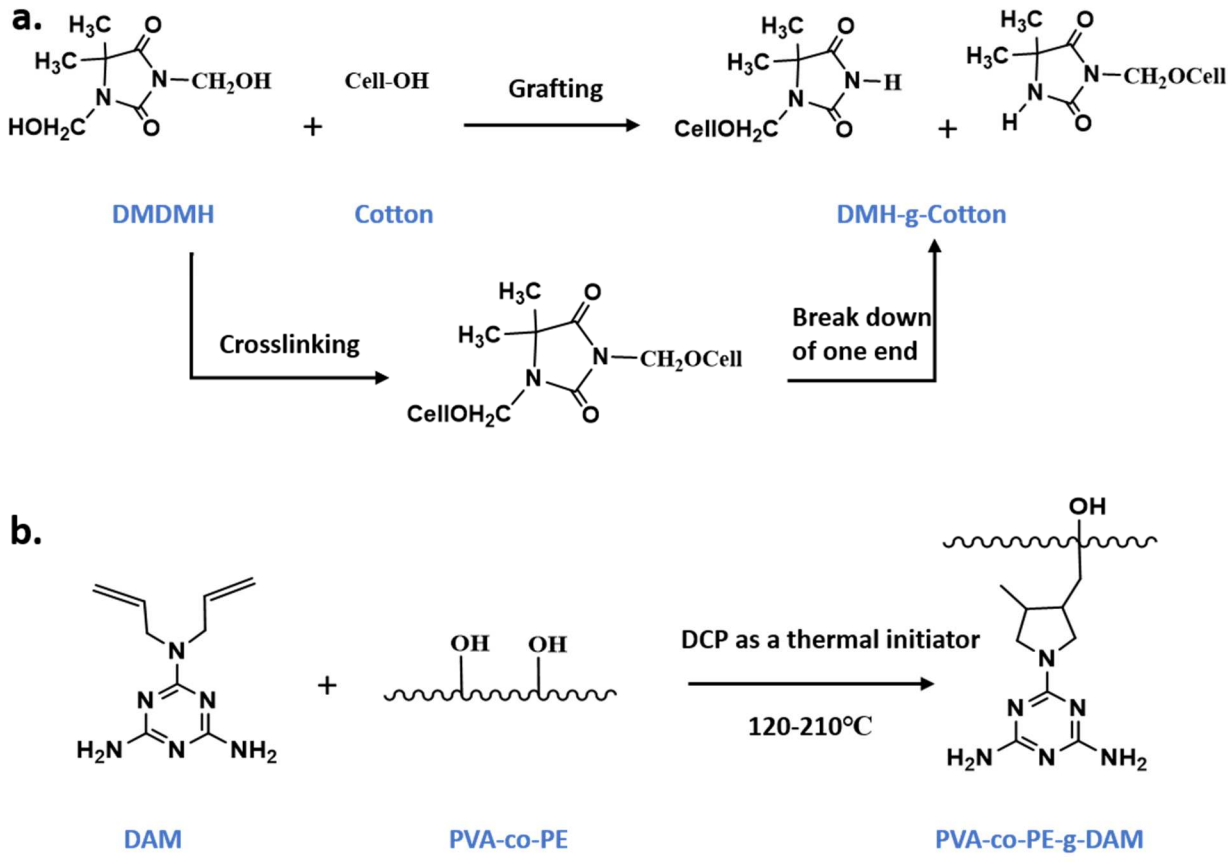

Figure 5.1. (a) Potential grafting reaction pathways of DMDMH to Cotton fabric, and the (b) graft polymerization reaction of PVA-co-PE with DAM; DCP is dicumyl peroxide.

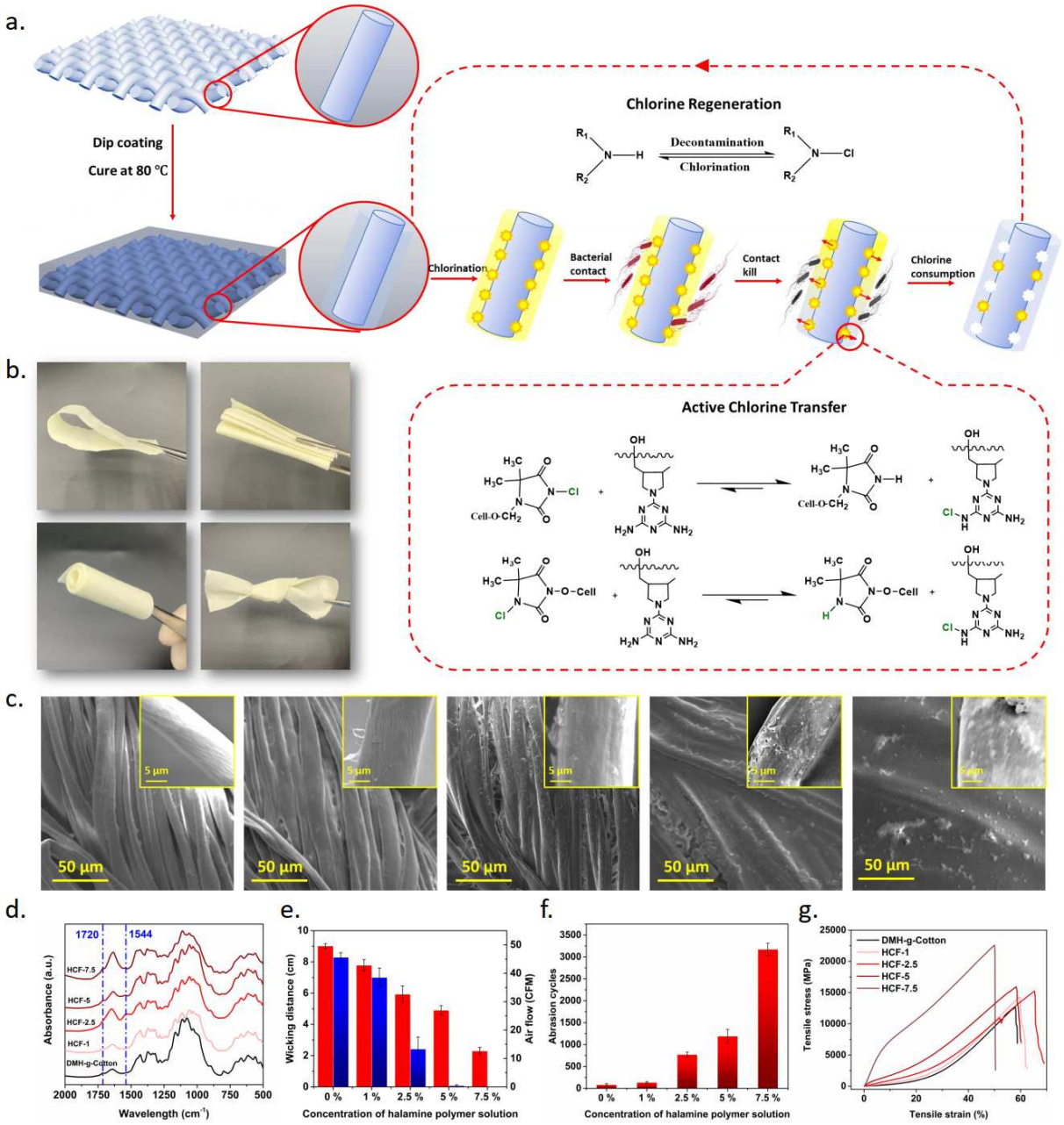

Figure 5.2. (a) Scheme of the design, processing, and rechargeable biocidal function of the halamine compositive fabric. The top inset image shows chlorination of N-halamine precursors and decontamination of N-halamine structures, and the bottom inset image exhibits the potential active chlorine transfer among imide-, amide, and amine-halamine structures. (b) Optical images of an HCF-2.5 fabric after bending, folding, rolling, and twisting. (c) SEM images of cotton fabrics

coated with i) 0 %, ii)1%, iii) 2.5%, iv) 5%, and v) 7.5% of halamine polymer solutions. (d) FT-IR spectra, (e) wicking properties and air permeabilities, (f) abrasion performances, and (g) tensile stress-strain curves of the halamine composite fabrics.

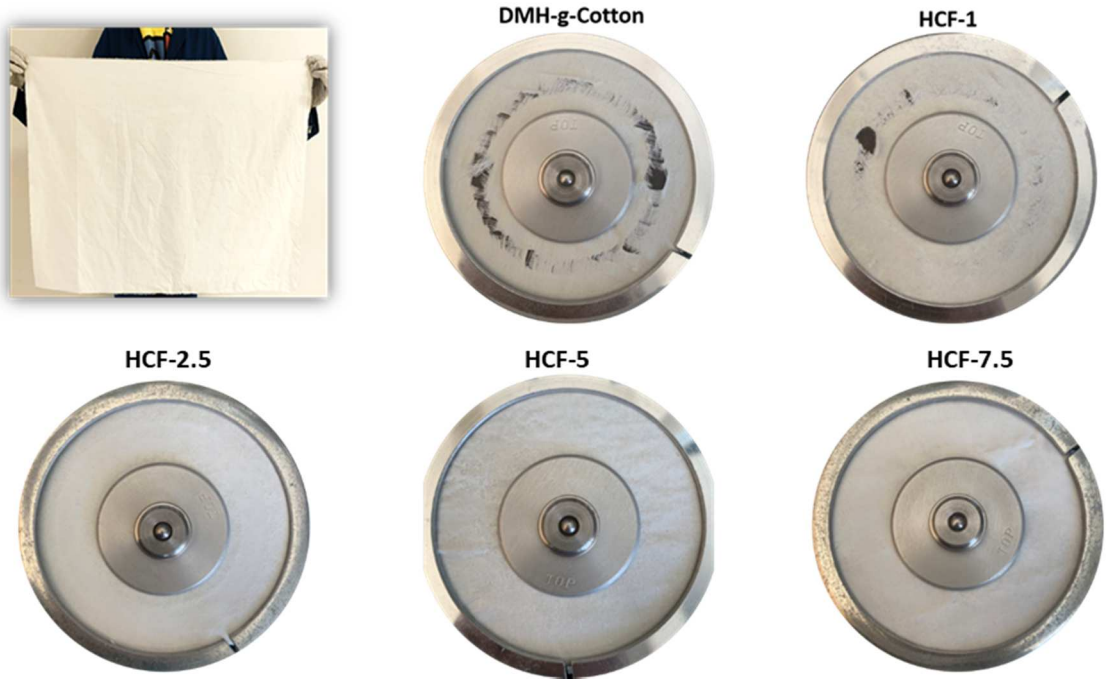

Figure 5.3. Optical image of an HCF-2.5 fabric in a size of 60 × 60 cm, and optical image of the DMH-g-Cotton, HCF-1, HCF-2.5, HCF-5, and HCF-7.5 after 200 abrasion cycles.

5.3.3 Rechargeable chlorination of HCF

The HCF-x possesses rechargeable antimicrobial activities, demonstrated by simply soaking in a diluted chlorination solution with active chlorine of 1 wt%, and the active chlorine contents of the chlorinated HCF-x were measured by an established iodometric titration method.[7, 8] As shown in Figure 5.4a, the active chlorine contents of the chlorinated HCF-x were highly pH-dependent with a maximum value achieved under a neutral condition. Under acidic conditions, the amine, amide, or imide groups could be protonated and can not convert to active halamine structures. However, at high pH conditions, most of the hypochlorous acid (HOCl) is converted to OCl^-, which exhibits

relatively lower chlorination efficiency. Besides the pH value of the chlorination solution, the specific surface area is the other factor, which could affect the active chlorine contents of the HCF-x. The active chlorine contents of the HCF-5 and the HCF-7.5 with the reduced specific surface area were slightly lower than the HCF-2.5 due to full coverage of the fabric by the coating polymer (Figure 5.2c iv), v), and Figure 5.2e).

Therefore, we selected HCF-2.5 with the highest active chlorine content as an example to conduct the following experiments. Figure 5.4b demonstrated the active chlorine content as a function of chlorination time. With the increase of the chlorination time, a two-characteristic reaction region could be found on both the DMH-g-Cotton and the HCF-2.5: a linear growth region at the first 1-hour chlorination and then a saturation region with nearly constant active chlorine contents. The maximum active chlorine content of the HCF-2.5 is about 600 ppm at an optimized pH condition for 1 hour, which is almost 200 ppm higher than that of the DMH-g-Cotton.

Long-term stability is another practical concern for antimicrobial food-contact materials. The coated PVA-co-PE-g-DAM layer could serve as a physical barrier to reduce the moisture uptake by the cotton substance, thereby slowing down the chlorine dissociation rate of the inside halamine structure. Additionally, the consumed active chlorine in PVA-co-PE-g-DAM could be replenished by the internal halamine structures to provide a long-lasting biocidal function. As shown in Figure 5.4c, after 14 days of storage, about 68 % of the active chlorine could be retained by HCF-2.5. In contrast, without an amine-halamine polymer coating layer, the DMH-g-Cotton lost almost 54 % of the active chlorine under the same condition. Moreover, the HCF-2.5 and the DMH-g-Cotton demonstrated a robust rechargeability of the N-halamine structures. For each cycle, the DMH-g-Cotton and the HCF-2.5 were chlorinated for 1 h (pH = 7), and then was quenched by an excess amount of $Na_2S_2O_3$ solution. Afterward, the samples were rinsed over DI-water to remove any

residual $Na_2S_2O_3$. As shown in Figure 5.4d, after five times charging/ quenching cycles, the active chlorine contents of both the DMH-g-Cotton and the HCF-2.5 exhibited a slight decrease, possibly due to dissociation of the connected hydantoin rings and loss of the coated halamine polymer. However, the total active chlorine contents on both materials were still high enough to provide desired biocidal activity against bacteria.

Overall, the active chlorine contents of the HCF-x were influenced by two parameters: the amount of loaded halamine polymer and specific surface area. Figure 5.4e demonstrated the relationship between active chlorine contents and washing times of the HCF-x. For the DMH-g-Cotton, the HCF-1, and the HCF-2.5, the active chlorine contents gradually decreased as the washing time increased due to the loss of the coated halamine polymer. Interestingly, the active chlorine content of the HCF-5 increased from 540 to 600 ppm after the first time washing. The coated halamine polymers on the HCF-5 could be washed off, and the blocked fabric texture could be exposed, increasing the specific surface area of such composite material. However, a further increase in the coating polymer on the composite (HCF-7.5) could not show such an effect. In order to quantify the integration effects of these two factors, the weight changes of each HCF-x before and after washing treatments were recorded. As shown in Figure 5.4f, the maximum active chlorine content of 633 ppm could be achieved when the weight ratio of the coating polymer versus the fabric was at 109 wt%.

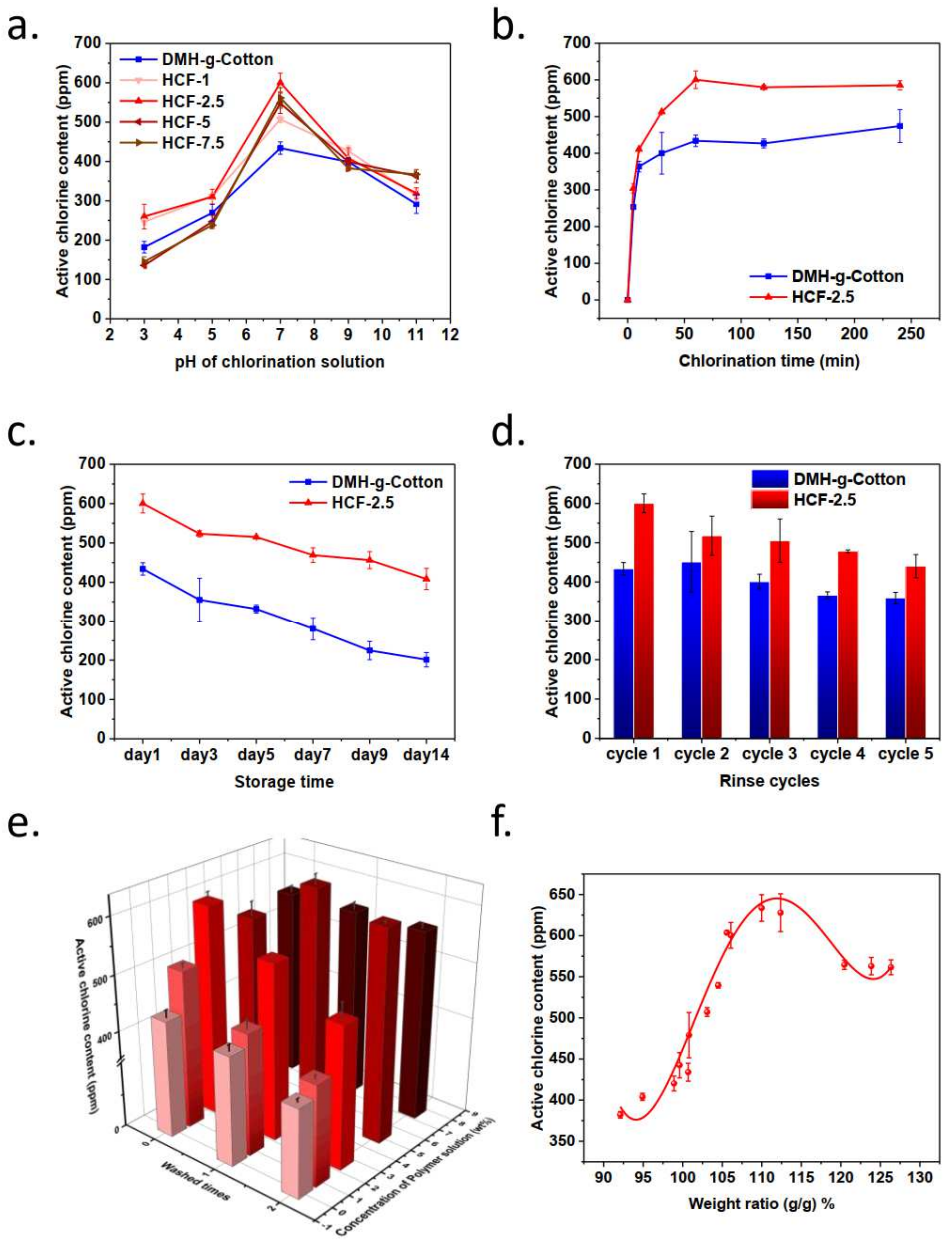

Figure 5.4. Active chlorine contents of the halamine compositive fabrics as a function of (a) pH values of chlorination solution and (b) chlorination time. Active chlorine contents of the DMH-g-Cotton and HCF-2.5 versus (c) storage times and (d) chlorine charging/ quenching cycles. (e) Summary of the active chlorine contents of various washing cycles coated with different

concentrations of halamine polymer solution, and (f) the relationship between active chlorine content and the weight ratio of coating polymer over the fabric.

5.3.4 Antimicrobial activity against *E. coli* and *L. innocua*

Two typical foodborne pathogenic bacteria, Gram-negative *E. coli* and Gram-positive *L. innocua* were applied to evaluate the antimicrobial properties of the chlorinated HCF-2.5. An appropriate diluted nutrient broth solution was employed to simulate the chemical oxygen demand (COD) on the food surfaces or potentially leaked juices from spoiled foods. Figures 5.5a-d display the time-dependent antimicrobial profiles of the chlorinated HCF-2.5 and the unchlorinated HCF-2.5 (control) against *E. coli* and *L. innocua* with COD = 0 and 1000, respectively. Less than 1 log of bacteria reduction could be observed in all the control groups. In contrast, the chlorinated HCF-2.5 exhibited a rapid and robust killing performance for both *E. coli* and *L. innocua*, achieving nearly 5 log of bacteria reduction after 10 min of contact at both non-COD and high COD conditions. Additionally, the chlorinated HCF-2.5 is also responsible for the robust regenerable antimicrobial performance. As shown in Figure 5.5e, the biocidal activity of the chlorinated HCF-2.5 was almost constant with more than 4 log bacteria reductions of both *E. coli* and *L. innocua* within 10 min of contact (COD = 0) after repeated exposure cycles.

The coated protective amine halamine polymer layer ensured the HCF-2.5 with promising long-term stability. As shown in Figure 5.5f, g, after 14 days of storage, the chlorinate HCF- 2.5 exhibited promising durable bacterial contact-killing efficiency against both *E. coli* and *L. innocua*, with nearly 5 log of bacteria reduction within 10 min of contact. In sharp contrast, the biocidal activity of the chlorinated DMH-g-Cotton gradually decreased, achieving only 3 log of bacterial reduction within 10 min after 14 days of storage. These antimicrobial results were consistent with the results of the active chlorine stability tests (Figure 5.4c), highlighting that the PVA-co-PE-g-

DAM composite coating layer could effectively reduce the loss of the active chlorine and maintain the high biocidal activity of the composite after long time storage.

As proposed before, the microorganisms should firstly consume the amine-halamine located on the outside surface, then the active chlorine transfer from internal halamine to the outside amine structures. Both PVA-co-PE-g-DAM (sample) and PVA-co-PE (control) polymers were coated with the same amount of 7.5%wt onto the chlorinated DMH-g-Cotton fabrics. As shown in Figure 5.5h, the dense polymeric coating layer physically blocked the direct contact between the chlorinated DMH-g-Cotton fabrics and the microorganisms. Interestingly, with only active chlorine located inside the fabrics, the control polymer coated sample revealed a 3 log of bacterial reduction after 30 min of contact, caused by the diffusion and migration of active chlorine from the fabrics to the surfaces. However, with the existence of the amine structures in the coating polymer serving as a chlorine conductive transfer media, the sample group exhibited a significantly higher biocidal activity with more than 6 log of bacterial reduction achieved within 30 min of contact. These results confirmed the chlorine transfer from inside to the outside of composite materials and concerted durable and refreshable biocidal functions of the halamine system.

The chlorinated HCF-2.5 inactivates the bacteria via destroying the cellular structures, leading to the leakage of nucleic acids, which could be quantified by measuring the absorbance intensity of the bacterial supernatants (obtained by centrifuge the bacterial suspension of a concentration of 10^6 CFU/ mL) at 260 nm. As shown in Figure 5.6, nearly no nucleic acid was detected on both of the living bacterial supernatants and the bacterial supernatants after contacting with the unchlorinated HCF-2.5. However, significant absorbance at 260 nm was observed for both *E. coli* and *L. innocua* supernatants after contacting with the chlorinated HCF-2.5, implying the lethal damage of the cell structures and the leakage of the nucleic acids. An observation of the bacterial

morphology change in contact with the chlorinated HCF-2.5 further confirmed the bactericidal mechanism of the chlorinated HCF-2.5. As shown in Figure 5.5i, k, both *E. coli* and *L. innocua* cells retained intact cell structures with smooth cell membranes after 1-hour contact with the unchlorinated HCF-2.5. However, the cellular deformation and the surface collapse of the *E. coli* and the *L. innocua* could be clearly observed after exposure to the chlorinated HCF-2.5 for 1 hour (Figure 5.5j, l).

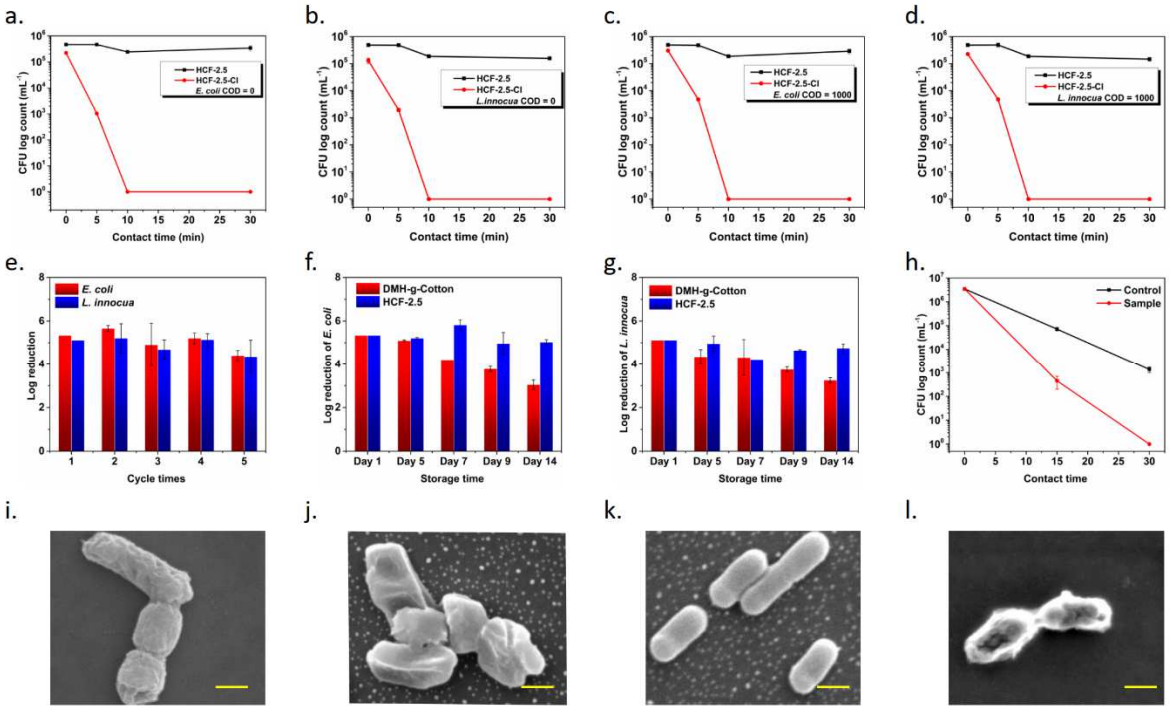

Figure 5.5. Biocidal activity of chlorinated HCF-2.5 against *E. coli* ((a) COD = 0 and (c) COD = 1000 and *L. innocua* ((b) COD = 0 and (d) COD = 1000). (e) Five cycle antimicrobial tests of chlorinated HCF-2.5 against *E. coli* and *L. innocua* and the biocidal activity of the chlorinated DMH-g-Cotton and the chlorinated HCF-2.5 against *E. coli* (f) and *L. innocua* (g) as a function of storage time. (h) Antimicrobial behaviors of the chlorinated DMH-g-Cotton after coating with 7.5 wt% of PVA-co-PE (control) and PVA-co-PE-g-DAM (sample) polymers. SEM images of the (i,

j) *E. coli* and (k, l) *L. innocua* after exposing to the (i, k) unchlorinated and the (k, l) chlorinated HCF-2.5 (scale bar = 500 nm).

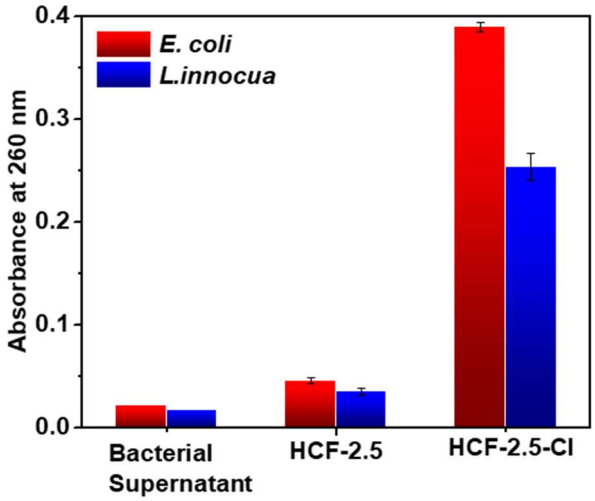

Figure 5.6. Measurement of the leakage of nucleic acid from *E. coli* and *L. innocua*.

5.3.5 Bacteria transfer via stimulated leaf-to-leaf cross-contamination

The bacterial cross-contamination from a contaminated item to a non-contaminated item is a rapid and highly efficient process, resulting in the spread of the bacteria during food processing and accelerating the spoilage of the food during storage. [30,31,33]A cross-contamination experiment was designed and conducted, and the process is demonstrated in Figure 5.7a. Bacteria could transfer from a contaminated leaf A (wetted surface) to relevant fabrics, and finally, transfer to a clean leaf B (dry surface). The population of the transferred bacteria on the relevant fabrics and the leaf Bs was assessed by a plate counting method. As shown in Figure 5.7b, after chlorination, both DMH-g-Cotton and HCF-2.5, (denoted as DMH-g-Cotton-Cl and HCF-2.5-Cl, respectively), could immediately kill any attached bacteria and cut off the bacterial transformation pathway. Therefore, no living bacteria could be detected on the chlorinated fabrics and the leaf Bs, and the overall bacteria transfer efficiency ($BTE_{overall}$) of both DMH-g-Cotton-Cl and HCF-2.5-Cl is 0.

Interestingly, the $BTE_{overall}$ of the unchlorinated HCF ($BTE_{overall}$ = 0.15 %) with additional hydrophilic polymeric coating layer is lower than that of the unchlorinated DMH-g-Cotton ($BTE_{overall}$ =0.28 %). At the first step, more bacteria distributed on the wet leaf A transferred to the unchlorinated DMH-g-Cotton due to the capillary effect of the unique fabric texture (BTE_1 of DMH-g-Cotton = 12.7 % > BTE_1 of HCF = 4.9 %). However, at the second step, the contaminated DMH-g-Cotton contact with the dry leaf B. Most of the bacteria was trapped inside the cotton fabric, thereby, only 2.2% of the bacteria could transfer to the leaf B. In contrast, with a polymeric coating layer, the capillary effect of the fabric significantly reduced with a wicking distance of 5.9 cm, fewer bacteria could be transferred to the HCF-2.5 on a wet condition, and the attached bacteria could mainly distribute on the top surface, resulting in an easier bacteria transfer to the dry leaf B with BTE_2 = 3.0 %. Overall, HCF-2.5 could reduce cross-contamination via two mechanisms: (1) inactivation of the microorganisms, considered as a majority pathway, and (2) decrease of the bacterial transfer from the wetted contaminated surfaces (BTE_1).

5.3.6 Food-contact application of HCF

To prove the expected antimicrobial and food preservation efficiency of the chlorinated HCF and potential practical food applications, we designed a simple strawberry storage experiment. As shown in Figure 5.7c, the chlorinated HCF-2.5 was placed inside the plastic food packaging box and directly contacted with the fresh strawberries. Similarly, the control groups were placed with pristine cotton fabric, and these strawberries were stored at 4 □. After 14 days, the strawberries contacted with the chlorinated HCF-2.5 exhibited slight spoilage and became softer compared with the fresh one. However, some white molds could be found on the strawberries of the control groups, and some juices were leaked out from the spoiled strawberries. These findings implied that the

chlorinated HCF-2.5 exhibited a significant potential of acting as a food-contact material to prolong the lifetime of the foods via inactive a broad-spectrum of bacteria.

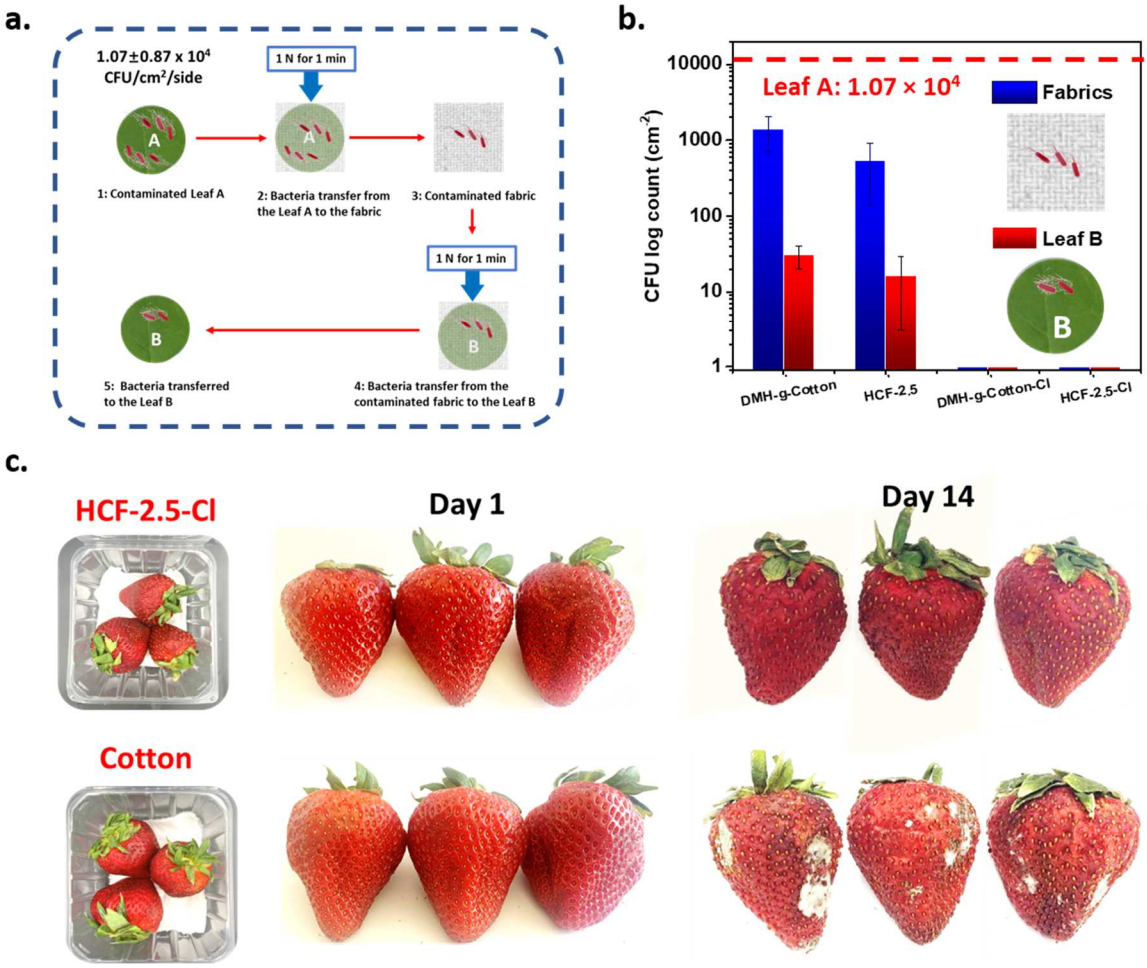

Figure 5.7. (a) Scheme of the experimental process for stimulating leaf-to-leaf cross-contamination. (b) The population of the living bacteria transferred from leaf As to relevant fabrics and leaf Bs. (c) Optical photographs showing the spoilage process of the strawberries by using the cotton fabric and the HCF-2.5-Cl as the packaging pads.

5.4 Conclusions

We demonstrated a scalable process for the fabrication of a rechargeable antimicrobial composite material by coating the amine-halamine polymers onto halamine cotton fabrics, serving as

reinforcement substances. Benefiting from the robust amine-halamine coating layer, the chlorinated composite (HCF-2.5) exhibited high active chlorine contents of over 600 ppm with improved storage stability and proper mechanical properties to serve as food packaging and processing materials. Additionally, the as-prepared composite could achieve 5 log of *E. coli* and *L. innocua* reductions within 10 min of contact time even under high COD condition. The integration of robust biocidal performances and the controllable manufacturing process enable the HCF to be considered as a potential active food-contact material that could effectively reduce the cross-contamination, prolong the food lifetime, decrease food spoilage, and ensure food safety.

5.5 References

1. Bourdichon, F.; Rouzeau, K. Microbial Food Spoilage: A major concern for food business operators. *New Food* **2012,** 54.
2. Gram, L.; Ravn, L.; Rasch, M.; Bruhn, J. B.; Christensen, A. B.; Givskov, M., Food spoilage—interactions between food spoilage bacteria. *International Journal of Food Microbiology* **2002,** *78* (1-2), 79-97.
3. Wu, H.; Teng, C.; Liu, B.; Tian, H.; Wang, J., Characterization and long term antimicrobial activity of the nisin anchored cellulose films. *International journal of biological macromolecules* **2018,** *113*, 487-493.
4. Wu, H.; Tian, H.; Li, S.; Wang, Y.; Ma, Z.; Song, Z.; Wang, J., Preparation, characterization and long-term antibacterial activity of nisin anchored magnetic cellulose beads. *Cellulose* **2020,** *27* (1), 357-367.
5. Buzby, J. C.; Wells, H. F.; Bentley, J. ERS's food loss data help inform the food waste discussion; **2013,** 1490-2016-128488.
6. Irwansyah, I.; Li, Y. Q.; Shi, W.; Qi, D.; Leow, W. R.; Tang, M. B.; Li, S.; Chen, X., Gram-positive antimicrobial activity of amino acid-based hydrogels. *Advanced Materials* **2015,** *27* (4), 648-654.
7. Si, Y.; Cossu, A.; Nitin, N.; Ma, Y.; Zhao, C.; Chiou, B. s.; Cao, T.; Wang, D.; Sun, G., Mechanically robust and transparent N-halamine grafted PVA-co-PE films with renewable antimicrobial activity. *Macromolecular Bioscience* **2017,** *17* (3), 1600304.

8. Ma, Y.; Li, J.; Si, Y.; Huang, K.; Nitin, N.; Sun, G., Rechargeable antibacterial N-halamine films with antifouling function for food packaging applications. *ACS applied materials & interfaces* **2019,** *11* (19), 17814-17822.
9. Qiao, M.; Liu, Q.; Yong, Y.; Pardo, Y.; Worobo, R.; Liu, Z.; Jiang, S.; Ma, M., Scalable and rechargeable antimicrobial coating for food safety applications. *Journal of Agricultural and Food Chemistry* **2018,** *66* (43), 11441-11450.
10. Scallan, E.; Hoekstra, R. M.; Angulo, F. J.; Tauxe, R. V.; Widdowson, M.-A.; Roy, S. L.; Jones, J. L.; Griffin, P. M., Foodborne illness acquired in the United States—major pathogens. *Emerging Infectious Diseases* **2011,** *17* (1), 7.
11. Kinsinger, N. M.; Mayton, H. M.; Luth, M. R.; Walker, S. L., Efficacy of post-harvest rinsing and bleach disinfection of *E. coli O157: H7* on spinach leaf surfaces. *Food Microbiology* **2017,** *62*, 212-220.
12. Qiao, M.; Huang, T.-S., Potential applications of N-halamines in food production, processing and packaging for improving food safety. *Food Safety Magazine* **2016,** 34-8.
13. Larsen, M. H.; Dalmasso, M.; Ingmer, H.; Langsrud, S.; Malakauskas, M.; Mader, A.; Møretrø, T.; Možina, S. S.; Rychli, K.; Wagner, M., Persistence of foodborne pathogens and their control in primary and secondary food production chains. *Food Control* **2014,** *44*, 92-109.
14. Muhterem-Uyar, M.; Dalmasso, M.; Bolocan, A. S.; Hernandez, M.; Kapetanakou, A. E.; Kuchta, T.; Manios, S. G.; Melero, B.; Minarovičová, J.; Nicolau, A. I., Environmental sampling for Listeria monocytogenes control in food processing facilities reveals three contamination scenarios. *Food Control* **2015,** *51,* 94-107.
15. Barbosa, J.; Albano, H.; Silva, C.; Teixeira, P., Microbiological contamination of reusable plastic bags for food transportation. *Food Control* **2019,** *99,* 158-163.

16. Nerin, C.; Aznar, M.; Carrizo, D., Food contamination during food process. *Trends in Food Science & Technology* **2016,** *48,* 63-68.

17. Ren, T.; Hayden, M.; Qiao, M.; Huang, T.-S.; Ren, X.; Weese, J., Absorbent pads containing N-halamine compound for potential antimicrobial use for chicken breast and ground chicken. *Journal of Agricultural and Food Chemistry* **2018,** *66* (8), 1941-1948.

18. Wang, H.; Chen, M.; Jin, C.; Niu, B.; Jiang, S.; Li, X.; Jiang, S., Antibacterial [2-(methacryloyloxy) ethyl] trimethylammonium chloride functionalized reduced graphene oxide/poly (ethylene-co-vinyl alcohol) multilayer barrier film for food packaging. *Journal of Agricultural and Food Chemistry* **2018,** *66* (3), 732-739.

19. Liu, M.; Wang, F.; Liang, M.; Si, Y.; Yu, J.; Ding, B., In situ green synthesis of rechargeable antibacterial N-halamine grafted poly (vinyl alcohol) nanofibrous membranes for food packaging applications. *Composites Communications* **2020,** *17*, 147-153.

20. Huang, C.; Chen, Y.; Sun, G.; Yan, K., Disinfectant performance of a chlorine regenerable antibacterial microfiber fabric as a reusable wiper. *Materials* **2019,** *12* (1), 127.

21. Tian, H.; Zhai, Y.; Xu, C.; Liang, J., Durable antibacterial cotton fabrics containing stable acyclic N-halamine groups. *Industrial & Engineering Chemistry Research* **2017,** *56* (28), 7902-7909.

22. Sun, G.; Xu, X.; Bickett, J. R.; Williams, J. F., Durable and regenerable antibacterial finishing of fabrics with a new hydantoin derivative. *Industrial & Engineering Chemistry Research* **2001,** *40* (4), 1016-1021.

23. Hui, F.; Debiemme-Chouvy, C., Antimicrobial N-halamine polymers and coatings: a review of their synthesis, characterization, and applications. *Biomacromolecules* **2013,** *14* (3), 585-601.

24. Qian, L.; Sun, G., Durable and regenerable antimicrobial textiles: Synthesis and applications of 3-methylol-2, 2, 5, 5-tetramethyl-imidazolidin-4-one (MTMIO). *Journal of Applied Polymer Science* **2003,** *89* (9), 2418-2425.
25. Qian, L.; Sun, G., Durable and regenerable antimicrobial textiles: Improving efficacy and durability of biocidal functions. *Journal of Applied Polymer Science* **2004,** *91* (4), 2588-2593.
26. Save, N. S.; Jassal, M.; Agrawal, A. K., Polyacrylamide based breathable coating for cotton fabric. *Journal of Industrial Textiles* **2002,** *32* (2), 119-138.
27. Qian, L.; Sun, G., Durable and regenerable antimicrobial textiles: Chlorine transfer among halamine structures. *Industrial & Engineering Chemistry Research* **2005,** *44* (4), 852-856.
28. Si, Y.; Li, J.; Zhao, C.; Deng, Y.; Ma, Y.; Wang, D.; Sun, G., Biocidal and rechargeable N-halamine nanofibrous membranes for highly efficient water disinfection. *ACS Biomaterials Science & Engineering* **2017,** *3* (5), 854-862.
29. Dabral, M.; Francis, L.; Scriven, L., Drying process paths of ternary polymer solution coating. *AIChE journal* **2002,** *48* (1), 25-37.
30. Flores, R. A.; Tamplin, M. L.; Marmer, B. S.; Phillips, J. G.; Cooke, P. H., Transfer coefficient models for *Escherichia coli O157: H7* on contacts between beef tissue and high-density polyethylene surfaces. *Journal of Food Protection* **2006,** *69* (6), 1248-1255.
31. Yi, J.; Huang, K.; Young, G. M.; Nitin, N., Quantitative analysis and influences of contact dynamics on bacterial cross-contamination from contaminated fresh produce. *Journal of Food Engineering* **2020,** *270*, 109771.
32. Padgett, W. M.; Hamner, W., The infrared spectra of some derivatives of 1, 3, 5-triazine. *Journal of the American Chemical Society* **1958,** *80* (4), 803-808.

33. Wachtel, M. R.; Charkowski, A. O., Cross-contamination of lettuce with *Escherichia coli O157: H7*. *Journal of Food Protection* **2002,** *65* (3), 465-470.

Chapter 6. Executive Conclusion

In this dissertation, three types of rechargeable biocidal and antifouling functional materials have been developed, which exhibited great potentials in applications in food packaging, water filtration, and medical areas. A dual functional structure was initially proposed: the biocidal moieties immobilized at the inner layer, and the antifouling moieties served as a protective layer located on the outside of the surface. With such a unique multifunctional surface structure, once the microorganisms are approaching the designed surfaces, (i) the antifouling moieties could reduce the non-specific adsorption of the microorganisms and make them difficult to adhere; (ii) any live bacteria attached on the surface could be immediately killed by the incorporated biocidal moieties; (iii) any resulting cell debris and other biofoulants could be easily washed off with mild hydrodynamic force applied; furthermore, (iv) the consumed biocidal activity could be regenerated by either chlorination or photoirradiation.

Initial investigations began with a proof of the proposed concept. A chlorine rechargeable biocidal poly(vinyl alcohol-co-ethylene) film (SBMA@HAF film) with the antifouling function was successfully developed via chemically incorporating both N-halamine (HAF) and zwitterionic (SBMA) moieties. Both functional moieties worked independently, and constructed concerted microbial resisting, killing, and releasing functions to reduce microbial contamination and prevent biofilm formation. The resulting SBMA@HAF films exhibited integrated properties of high transparency, robust mechanical property, great hydrophilicity, ease of chlorine recharging (>250 ppm), long-term stability, high biocidal efficacy (>99.9999% via contact killing), and promising antifouling functions, enabling the SBMA@HAF films to serve as an ideal biocidal material for food packaging applications. More importantly, with the existence of the superhydrophilic

zwitterion moieties, the chlorinated SBMA@HAF films exhibited faster biocidal performance due to the better contact between the films and microbes.

Nanofibrous membrane with the superhigh specific surface area, which could effectively magnify the interfacial effect, was selected as an ideal substance to investigate the antifouling mechanisms of the zwitterions with the existence of the halamine moieties. A rechargeable biocidal PVA-co-PE-g-DAM nanofibrous membrane (BNF membrane) was prepared by applying the electrospinning technique, and a zwitterionic polymer (PEI-S), serving as an antifouling agent, was introduced onto the BNF membrane through an optimized chemical crosslink process. The final product, named PEI-S@BNF membrane, was tested by the same evaluation system of the SBMA@HAF film, including active chlorine contents, antimicrobial efficiency, microbial resisting/releasing performance, and other physicochemical properties. Additionally, BSA protein was employed as a model probe to evaluate the resisting and releasing properties of the PEI-S@BNF membrane. The kinetics of the BSA adsorption can be described as a pseudo-first-order process, and the isothermal adsorption behaviors of the nanofibrous membranes matched well with the monolayer Langmuir model. With the presence of zwitterionic polymer, the PEI-S@BNF membrane exhibited lower K_a and C_s values, which could be attributed to the generation of the electro-induced hydration layer, thereby reducing the affinity with the BSA protein and the overall adsorption capacity. Depending on the different positions of the BSA protein, the releasing behavior could be divided into three stages, which was fully explained by a Ritger-Peppas model. Specifically, at the second stage, the superhydrophilic zwitterion moieties, with the strong interaction with surrounding water molecules, allows the formation of a hydration layer, leading to a faster release of the protein located near the membrane surface. These biocidal and antifouling

functions enabled the PEI-S@BNF-2h nanofibrous membrane to effectively disinfect the microbe-contaminated water in high fluxes while maintaining itself clean for a long-term application.

Besides the N-halamine structure, the proposed antibiofilm strategy should also work for other biocidal matrixes. Instead of N-halamine structure, a photosensitizer, benzophenonetetracarboxylic dianhydride (BPTCD), which could produce reactive oxygen species (ROS) under photoirradiation conditions, was incorporated onto the PVA-co-PE nanofibrous membrane, serving as a biocidal component. After the combination of the antifouling moieties, the resulted product, SBMA@EVOH nanofibrous membranes were also tested by the established evaluation system. This photo-induced bifunctional material proved the universality of such proposed double-layer surface with the antimicrobial moieties locating in the inner layer while the antifouling moieties locating in the outside layer and extended the potential application areas.

Finally, a rechargeable antimicrobial composite fabric (HCF) was fabricated via industrial scalable dip-coating method to combine amine-halamine polymer (PVA-co-PE-g-DAM) with an imide/amide-halamine grafted cotton fabric (DMH-g-Cotton). The DMH-g-cotton served as a reinforcement component and a reservoir of active chlorine, and an amine halamine polymer (PVA-co-PE-g-DAM) as a coating component could reduce the loss of active chlorine the realize long-term killing performance. The integration of robust biocidal performances and the controllable manufacturing process enable the designed HCF could be considered as a potential active food-contact material that could effectively reduce the cross-contamination, prolong the food lifetime, decrease food spoilage, and ensure food safety.